

AD-A147 426

(12)

## CLUSTERS OF DEFECTS IN SEMICONDUCTORS

J.P. Baukus

Hughes Research Laboratories  
3011 Malibu Canyon Road  
Malibu, CA 90265

August 1984

ARPA Order No. 4174  
N00014-81-C-0285  
Final Report  
1 February 1981 through 14 July 1983

OFFICE OF NAVAL RESEARCH  
800 No. Quincy Street  
Arlington, VA 22217

DTIC  
ELECTE  
NOV 14 1984  
A

DTIC FILE COPY

This document has been approved  
for public release and sale; its  
distribution is unlimited.

The views and conclusions contained in this document are those of the authors and should not be interpreted as necessarily representing the official policies, either expressed or implied, of the Defense Advanced Research Projects Agency or the U.S. Government.

84 10 12 201

UNCLASSIFIED

SECURITY CLASSIFICATION OF THIS PAGE

## REPORT DOCUMENTATION PAGE

1a. REPORT SECURITY CLASSIFICATION Unclassified		1b. RESTRICTIVE MARKINGS	
2a. SECURITY CLASSIFICATION AUTHORITY		3. DISTRIBUTION/AVAILABILITY OF REPORT	
2b. DECLASSIFICATION/DOWNGRADING SCHEDULE			
4. PERFORMING ORGANIZATION REPORT NUMBER(S)		5. MONITORING ORGANIZATION REPORT NUMBER(S) N00014-81-C-0285	
6a. NAME OF PERFORMING ORGANIZATION Hughes Research Laboratories	6b. OFFICE SYMBOL (If applicable)	7a. NAME OF MONITORING ORGANIZATION Office of Naval Research	
6c. ADDRESS (City, State and ZIP Code) 3011 Malibu Canyon Road Malibu, CA 90265		7b. ADDRESS (City, State and ZIP Code) 800 N. Quincy Street Arlington, VA 22217	
8a. NAME OF FUNDING/SPONSORING ORGANIZATION Office of Naval Research	8b. OFFICE SYMBOL (If applicable)	9. PROCUREMENT INSTRUMENT IDENTIFICATION NUMBER NR 322-101/12-12-80 (427)	
8c. ADDRESS (City, State and ZIP Code) 800 N. Quincy Street Arlington, VA 22217		10. SOURCE OF FUNDING NOS.	
11. TITLE (Include Security Classification) Clusters of Defects in Semiconductors (U)		PROGRAM ELEMENT NO.	PROJECT NO.
12. PERSONAL AUTHOR(S) J.P. Baukus		TASK NO.	WORK UNIT NO.
13a. TYPE OF REPORT Final	13b. TIME COVERED FROM 1 Feb 81 to 14 Jul 83	14. DATE OF REPORT (Yr., Mo., Day) August 1984	
15. PAGE COUNT 115		16. SUPPLEMENTARY NOTATION	
17. COSATI CODES		18. SUBJECT TERMS (Continue on reverse if necessary and identify by block number)	
FIELD	GROUP	SUB. GR.	
19. ABSTRACT (Continue on reverse if necessary and identify by block number)			
<p>The purpose of this program was to study the clustering of defects in semiconductors. This area is becoming increasingly important in semiconductor technology as the understanding of these defects grows. It has become apparent that a number of effects in materials and devices are in fact due to clusters of defects. The program was a cooperative effort between Hughes Research Laboratories (HRL), the California Institute of Technology (Cal Tech) and Atom Sciences, Incorporated.</p> <p>HRL grew, characterized and delivered samples to the subcontractors for subsequent analyses. Silicon crystals were grown by the Czochralski and floating-zone techniques; GaAs was grown by the liquid-encapsulated Czochralski method. Characterization methods included Hall effect, infrared transmission, photoluminescence, neutron activation analysis, and charged particle activation analysis.</p>			
20. DISTRIBUTION/AVAILABILITY OF ABSTRACT UNCLASSIFIED/UNLIMITED <input type="checkbox"/> SAME AS RPT. <input type="checkbox"/> DTIC USERS <input type="checkbox"/>		21. ABSTRACT SECURITY CLASSIFICATION Unclassified	
22a. NAME OF RESPONSIBLE INDIVIDUAL J.P. Baukus		22b. TELEPHONE NUMBER (Include Area Code) (213) 317-5336	22c. OFFICE SYMBOL

DD FORM 1473, 83 APR

EDITION OF 1 JAN 73 IS OBSOLETE.

UNCLASSIFIED

SECURITY CLASSIFICATION OF THIS PAGE

UNCLASSIFIED

SECURITY CLASSIFICATION OF THIS PAGE

Cal Tech studied the defect associated with the PQR luminescence lines that they discovered in In-doped Si. The defect associated with the PQR lines was undoubtedly made up of more than just a single point and hence was a good candidate to study of the phenomenon of defect clustering. Their experimental and theoretical program was aimed at first determining the chemical species that participate in the formation of the defect and then to study the formation and breakup of the defect under a number of experimentally varied conditions. The program to identify the defect consisted of selectively introducing various chemical species and studying the resulting increases or decreases in the concentration of the defect level, and then introducing isotopes of the chemical species to study the changes induced in the local phonon modes. In connection with this experimental program, theoretical calculations of the local mode spectrum of possible defects were carried out to make positive identification possible.

Atom Sciences demonstrated the technique of Sputter Initiated Resonance Ionization Spectroscopy (SIRIS) for the detection of impurity atoms in silicon. Specifically, In, Al, and Ga were measured in samples of silicon supplied by Hughes. In addition, the concentrations of Al and V were determined in certified samples of stainless steel, supplied by the National Bureau of Standards. Atom Sciences demonstrated that their SIRIS apparatus and technique are sensitive to 5 parts in  $10^9$ , and have shown that current technology will permit the desired sensitivity of 1 part in  $10^{10}$  to be achieved. Diagnostic testing of the apparatus has been completed and specific improvements to be made have been identified. The present sensitivity has been well demonstrated using the known standards supplied by Hughes Research Laboratories and the National Bureau of Standards.



UNCLASSIFIED

SECURITY CLASSIFICATION OF THIS PAGE

## TABLE OF CONTENTS

CHAPTER		PAGE
1	INTRODUCTION.....	1
2	HUGHES RESEARCH LABORATORIES.....	3
	A. Crystal Growth.....	3
	B. Characterization.....	3
	C. Samples Delivered.....	9
3	CALIFORNIA INSTITUTE OF TECHNOLOGY.....	11
	A. Introduction.....	11
	B. Chemical Species Responsible for the PQR Luminescence.....	11
	C. Pair Formation and Breakup.....	13
	D. Diffusion of Transition Metal from Silicide into Silicon.....	13
	Publication List.....	14
	References.....	15
4	ATOM SCIENCES.....	17
	A. Introduction.....	17
	B. Research and Development Performance.....	18
	C. Summary.....	22
APPENDICES		
A	FIVEFOLD SPLITTING OF THE $C_{As}$ LOCAL VIBRATIONAL MODE BY Ga ISOTOPES IN GaAs.....	23
B	MEASUREMENTS OF Fe CONCENTRATIONS IN Si:In BY CHARGED PARTICLE ACTIVATION ANALYSIS.....	39
C	ROLE OF Fe IN NEW LUMINESCENCE LINES IN Si:Ti and Si:In.....	45

## APPENDICES

## PAGE

D	ISOTOPE SHIFTS FOR THE P, Q, R LINES IN INDIUM-DOPED SILICON.....	47
E	LOCAL PHONON MODE CALCULATIONS FOR POINT DEFECTS IN Si.....	51
F	ISOTOPE SHIFTS OF THE P,Q,R LINES IN INDIUM-DOPED SILICON.....	61
G	ISOTOPE-SHIFT EXPERIMENTS ON LUMINESCENCE ATTRIBUTED TO (Fe,B) PAIRS IN SILICON.....	71
H	PHOTOLUMINESCENCE OF Si-RICH Si-Ge ALLOYS.....	73
I	PLATINUM DIFFUSION INTO SILICON FROM PtSi.....	87
J	SPUTTER-INITIATED RESONANCE IONIZATION SPECTROSCOPY.....	91
K	ULTRASENSITIVE ELEMENTAL ANALYSIS OF SOLIDS BY SPUTTER INITIATED RESONANCE IONIZATION SPECTROSCOPY.....	101
	INTRUCTIONS FOR DISTRIBUTION.....	111

## CHAPTER 1

### INTRODUCTION

The purpose of this program was to study the clustering of defects in semiconductors. This area is becoming increasingly important in semiconductor technology as the understanding of defect clusters grows. It is becoming more apparent that a number of effects in materials and devices are in fact due to such defects. For example, the so called "thermal donor" in Czochralski-grown silicon (Si), the fine structure observed in the local vibrational modes of carbon (C) in gallium arsenide (GaAs), and the "PQR" lines in indium-doped Si (Si:In) are all attributable to defect clusters.

This program began on 1 February 1981 as a cooperative effort between Hughes Research Laboratories (HRL) and the California Institute of Technology (Cal Tech). HRL was the prime contractor. Atom Sciences, Incorporated became a subcontractor, effective 15 March 1982, to explore the capabilities of the sputter initiated resonance ionization spectroscopy (SIRIS) technique, apply it to semiconductors, and then evaluate it as a diagnostic tool.

This report is organized into chapters representing and written by each of the participating organizations. Chapter 2 describes HRL's contribution, Chapter 3 details Cal Tech's work, and Chapter 4 presents the results of the effort at Atom Sciences. Since the chapters were written by different authors, each contains its own table, figure, and reference numbering. The Appendices contain further details of some of the work and reprints of published papers reporting work supported by this contract.

## CHAPTER 2

### HUGHES RESEARCH LABORATORIES

#### A. CRYSTAL GROWTH

In order to facilitate the study of defect clusters HRL grew a number of crystals with controlled amounts of multiple dopants. It was intended that this would provide a range of concentrations of dopant pairs for study. A total of six Si crystals and one GaAs crystal were grown specifically for this program. The Si crystals, along with the results of Hall effect measurements made on samples from them, are described in Table 1.

Crystals C120 and C126 were designed to have a relatively large indium (In) concentration and widely different boron (B) concentrations. Crystals C125 and C131 were grown with different amounts of In and P (Phosphorous) to form In-P pairs in different concentrations. The P-doping dominated the In-doping in crystal C131, resulting in an n-type sample. Crystal C123 was grown to produce samples with Ga (Gallium)-B pairs. A floating zone crystal, Z244, was grown to study the effect of carbon (C) on the Si:In x-level concentration and anneal dependence.

A carbon (C)-doped liquid encapsulated Czochralski (LEC) GaAs crystal, M045, was grown in order to study the splitting of the C local phonon line. The results of the growth were disappointing in that the carbon concentration was only  $7 \times 10^{15} \text{ cm}^{-3}$ . Much higher concentrations were desired in order to obtain strong infrared absorption lines.

#### B. CHARACTERIZATION

Because of the complex nature of these defects, it was extremely important to start with well characterized samples in order to make unambiguous conclusions based on the sophisticated measurements applied in this program. A number of characterization methods were applied at HRL, including Hall effect, IR transmission and several others.

Hall effect measurement is the principal tool used at HRL to determine the concentration of electrical active impurities in semiconductors. When crystals such as those listed in Table 1 are evaluated van der Pauw samples are taken from slices from various places along the ingot. Carrier concentration and resistivity are measured as a function of temperature. Carrier concentration is then iteratively fitted to the charge balance equation to determine dopant concentration, ionization energy, and g-factor.

In a previous program\* samples from floating-zone (FZ) refined and Czochralski (Czo) crystals were subjected to a sequence of anneals at various temperatures; Hall-effect measurements versus temperature were made after each anneal. The purpose of the study was to determine the thermal equilibrium concentration of a defect known as the X-level, believed to result from indium-carbon pairs, as a function of anneal temperature and compare it with the relationship predicted by the mass-action law. The Czo samples exhibited the inverse temperature relationship predicted by the mass-action law which should hold for the indium-carbon pair model. However, the X-level concentration in the FZ samples was independent of annealing temperature! We believe that this phenomenon resulted from the In-C pairs not reaching their equilibrium distribution and that the diffusion of C in Czo material is greatly enhanced relative to that in FZ material, perhaps by the presence of O.

The FZ samples in that work were all from the same crystal, Z008. In order to verify that the observed temperature independence was not just an artifact of that particular crystal, we have investigated samples from another crystal, Z038, in this program. The crystal had similar amounts of In, X level, and net donors:  $6. \times 10^{16}$ ,  $2. \times 10^{14}$ , and  $3. \times 10^{13} \text{ cm}^{-3}$ , respectively, to those in the crystal investigated previously. These new results are shown in Figure 1, where the X-level concentration is plotted as a function of the reciprocal anneal temperature. The

---

\*Characterization and Analysis of Indium-doped Silicon Extrinsic Detector Material, Final Report, Contract No. DAAK-77-C-0082.

Table 1. Crystals Grown for the Clusters Program

(all units in  $\text{cm}^{-3}$ )

CRYSTAL	POS.	N(In or Ga)	N(B)	N(donors)
C120InB	seed		$8.2 \times 10^{16}$	$6.2 \times 10^{13}$
	tang	$4.7 \times 10^{16}$	$8.4 \times 10^{16}$	$7.4 \times 10^{13}$
C123GaB	seed	$5.0 \times 10^{16}$	$2.1 \times 10^{16}$	$6.7 \times 10^{14}$
	tang	$6.6 \times 10^{16}$	$2.2 \times 10^{16}$	$5.5 \times 10^{14}$
C125InP	seed	$4.4 \times 10^{16}$		$1.8 \times 10^{16}$
	tang	$6.5 \times 10^{16}$		$2.4 \times 10^{16}$
C126InB	seed	$3.0 \times 10^{16}$	$1.5 \times 10^{15}$	$2.5 \times 10^{13}$
	tang	$3.5 \times 10^{16}$	$1.6 \times 10^{15}$	$3.1 \times 10^{13}$
C131InP	seed	$1.4 \times 10^{15}$		$4.8 \times 10^{15}$
	tang	$1.8 \times 10^{15}$		$5.7 \times 10^{15}$
Z244InC	seed	$7.4 \times 10^{13}$	$2.3 \times 10^{13}$	$4.9 \times 10^{15}$
	mid	$1.4 \times 10^{17}$	$3.7 \times 10^{13}$	$8.3 \times 10^{12}$
	tang	$1.6 \times 10^{17}$	$2.0 \times 10^{13}$	$7.3 \times 10^{12}$

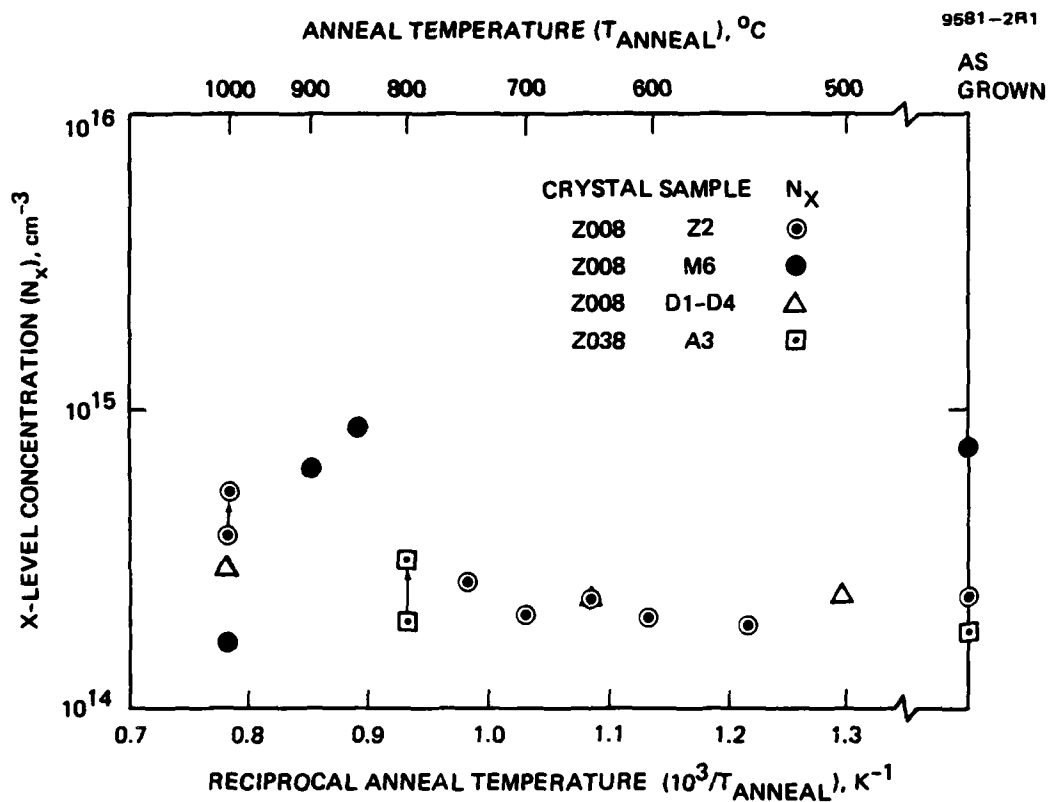


Figure 1. X-level and donor concentrations as functions of anneal temperature for FZ Si:In crystals.

points from crystal 2008 were obtained in the previous program and the points for 2038 are from this program. The points connected by arrow are due to subsequent anneals at the same temperature. In both cases the X-level concentration went up with further annealing, not down as would be expected. These results verify the previous conclusion that the X-level concentration does not depend on annealing conditions in FZ samples.

Infrared spectroscopic analyses were performed to investigate the local vibrational modes (LVMs) of carbon in GaAs and to search for phonon modes of iron-related pairs in Si and of carbon in GaAs in the far-infrared. Measurements were made on a Bomen model Da2.01 Interferometric Spectrophotometer, which has a wavelength range from the visible to millimeters, a resolution better than  $0.02\text{ cm}^{-1}$ , and specified photometric accuracy and spectrum reproducibility of 0.1%. The instrument provides for selection of source, optical and digital filtering, optical aperture, and detector, as well as interchangeable beamsplitters so that the signal-to-noise ratio can be optimized for the wavelength range of interest in a given experiment.

The instrument, it should be noted, arrived shortly after this program began and was a very early version of the model; it exhibited a number of problems which forced us to expend a considerable amount of manpower in their diagnosis and correction. The instrument still does not meet some of its specifications and we are continuing to work with the manufacturer to bring the instrument's performance up to our needs. While none of the intentional diagnoses and none of the repair work was charged to this contract, a considerable amount of time was lost in attempting experiments which did not work and in delays caused by instrument problems.

The  $582\text{ cm}^{-1}$  LVM of C in GaAs was measured at high resolution ( $0.05\text{ cm}^{-1}$ ) at HRL and compared with Green's-function and defect-cluster calculations performed at Cal Tech. Five spectral peaks were observed in agreement with the theory. The results verify that the C sits substitutionally on the As site

in the GaAs lattice and that the C-Ga bond-bending force constant is affected more than the bond-stretching force when compared to the undisturbed lattice. This work is summarized in Appendix A.

We have also recorded spectra of GaAs and Si in the far-infrared range below 10 meV photon energy to look for transverse acoustic phonon modes, but we have not observed them. Photoluminescence studies at Cal Tech and elsewhere indicate the presence of these phonon modes of Fe and B in Si samples containing clusters of Fe or Cu and In or B. Also, calculations at Cal Tech indicated the possibility of a similar phonon mode in GaAs:C. Since none of these modes were observed in the far-infrared, we were unable to verify their existence.

Cal Tech attributed the "R" line which they observed in PL to Fe-In pairs. They saw dramatic increases in the intensity of this line after diffusion of Fe into the samples. This increase in the "R-line" was verified by PL measurements at HRL. Since the presence of Fe could not be verified by far-infrared measurements, several other techniques were tried. Scanning Auger microprobe measurements were made at HRL to see if Fe was accumulating at the surface of the samples. Once Fe was diffused into the samples they were kept at liquid nitrogen temperature to prevent out-diffusion of the Fe. The Auger measurements were taken to ensure that this was not happening. However, no Fe was detected to a level of about 1% which is the detectability level of the measurement.

Samples were then sent to Prof. Ron Hart at Texas A&M University for neutron activation analysis (NAA) and charged particle activation analysis (CPAA) to determine their Fe concentrations. Seven samples were measured, four by NAA and three by CPAA. The results are given in Table 2. Details of the CPAA measurements are provided in Appendix B. Even though Fe was detected in only one sample, the group at Cal Tech feels that Fe could exist in these crystals at levels below the detection limits and still produce PL lines of the observed intensity.

Table 2. Fe Concentrations in Si:In by NAA and CPAA

Sample	Pos	Technique	Concentration (Fe/cm <sup>3</sup> )
C008IN	tang	NAA	$< 7 \times 10^{14}$
C014INC	seed	NAA	$< 1 \times 10^{14}$
C025IN	seed	NAA	$< 2 \times 10^{14}$
Z008IN	tang	NAA	$< 6 \times 10^{14}$
C1121INB	mid	CPAA	$1.2 + .4 \times 10^{15}$
C70401IN	tang	CPAA	$< 6.5 \times 10^{13}$
C117IN	tang	CPAA	$< 3.9 \times 10^{13}$

(Note: the < indicates the detection limit for the measurement.  
Fe was not detected in these samples.)

### C. SAMPLES DELIVERED

A large part of the HRL effort in this program was expended in preparing and characterizing samples for use at Cal Tech and Atom Sciences, as well as at HRL. Samples from the crystals listed in Table 1, as well as other characterized samples from crystals grown on HRL IR&D projects, were delivered to Cal Tech for the experiments reported in this program.

Well characterized samples were very important to the Atom Sciences program since their technique was to be calibrated and the minimum detectable concentrations of impurities were to be determined. Samples and Hall-effect characterizations from HRL were provided for this aspect of the Atom Sciences program.

Silicon samples doped with Ga, Al, and In, as well as undoped samples, were provided. Ga-implanted samples were delivered to provide calibration points at concentrations higher than those which can be incorporated during crystal growth. All samples were evaluated by Hall effect. In cases where infrared results for O and C concentration were available, these

values were also given. Impurity concentration ranges were  $1 \times 10^{15}$  to  $5 \times 10^{18} \text{ cm}^{-3}$  for Ga,  $2 \times 10^{16}$  to  $1 \times 10^{18} \text{ cm}^{-3}$  for Al, and  $2 \times 10^{14}$  to  $4 \times 10^{17} \text{ cm}^{-3}$  for In. The results of Hall analyses versus temperature of some of these samples are presented in Table 3. In all, more than 50 samples were delivered to Atom Sciences.

Table 3. Hall Results of Some Si:Ga Samples Delivered to Atom Sciences

(All concentrations are in atoms/cm<sup>3</sup>)

Crystal	Samp	N <sub>Ga or Al</sub>	N <sub>B</sub>	N <sub>net donors</sub>
Z20801AL	G50	$3.0 \times 10^{16}$	$1.0 \times 10^{13}$	$1.2 \times 10^{13}$
	C60	$2.8 \times 10^{16}$	$1.2 \times 10^{13}$	$1.3 \times 10^{13}$
10517GA	B00	$4.8 \times 10^{15}$	$6.5 \times 10^{13}$	$6.8 \times 10^{13}$
	200	$2.5 \times 10^{15}$	$3.5 \times 10^{13}$	$3.3 \times 10^{13}$
Z20104GA	C50	$6.7 \times 10^{16}$	$6.6 \times 10^{12}$	$1.2 \times 10^{13}$
	N30	$7.1 \times 10^{16}$	$7.1 \times 10^{12}$	$1.4 \times 10^{13}$
Z096	X40	$1.9 \times 10^{16}$	$3.3 \times 10^{13}$	$1.5 \times 10^{13}$
Z277AL	430	$2.1 \times 10^{18}$		$1.3 \times 10^{14}$

## CHAPTER 3

### CALIFORNIA INSTITUTE OF TECHNOLOGY

#### A. INTRODUCTION

The basic goal of this program was to study the clustering of defects in semiconductors. While the clustering of defects is of scientific interest in all technologically viable semiconductors, we chose to study this phenomenon in Si where the defects are the best characterized. In particular, we chose to study the defect associated with the PQR luminescence lines that we discovered in In-doped Si.<sup>1</sup> These luminescence lines have been the subject of numerous experimental investigations and hence are reasonably well characterized. The defect associated with the PQR lines is undoubtedly made up of more than just a single point and hence is a good candidate for our study of the phenomenon of defect clustering.

Our experimental and theoretical program was aimed at first determining the chemical species that participate in the formation of the defect and then to study the formation and breakup of the defect under a number of experimentally varied parameters. The program to identify the defect consisted of selectively introducing various chemical species and studying the increases or decreases in the concentration of the defect level, and then introducing isotopes of the chemical species to study the induced changes in the local phonon modes to make positive identification possible. In connection with this experimental program, theoretical calculations of the local mode spectrum of possible defects were carried out to make positive identification possible.

#### B. CHEMICAL SPECIES RESPONSIBLE FOR THE PQR LUMINESCENCE

As noted above, the first step to our program was to identify the chemical species responsible for the PQR luminescence.

We found that the introduction of Fe into In-doped Si did produce a striking increase in the intensity of the PQR luminescence. Control samples that were subjected to the same procedure did not show the same increase in photoluminescence. Studies with the deep-level-transient spectrometer (DLTS) on the samples in which Fe had been introduced produced results that indicate that Fe had, in fact, been incorporated into the sample. The first paper sponsored by this contract (see Paper No. 1 in the list of publications) reported the results of this study.

To ensure that our results were not purely accidental, we decided to carry out a further test on these lines. Some of the lines appear to be phonon replicas of others and are thought to be produced by a local mode related to the Fe at about 9 meV. Hence, if we introduced an isotope of Fe into the sample and measured the isotope shift of the phonon replica, this would be strong evidence that the PQR lines were Fe-related.

Three isotopically pure samples of Fe were purchased from Oak Ridge; these had isotopic masses of 54, 56, and 57 and were introduced into samples of In-doped Si. Photoluminescence spectra showed no evidence of an isotope shift. The results of this study are presented in Papers 2 and 3 in the list of published papers.

Theoretical calculations were undertaken to see if it was possible to have a local mode about the Fe which would not show substantial isotope shift. The results of that study are presented in Paper No. 4 in the list of published papers.

Because of the failure to see the isotope shift in what was thought to be (Fe, In) pairs, we decided to study the phenomenon in a much more characterized system of (Fe,B) pairs in Si.<sup>2</sup> Again, we performed isotope shift experiments on the luminescence that has been attributed to (Fe,B) pairs and again we found little or no isotope shift. To check the validity of this experimental approach, we conducted similar isotope shift experiments on (Cu,Cu) pairs using isotopes 63 and 65. The

luminescence features show a local phonon mode at 7 meV. In this case we observed an isotope shift similar to that observed by other investigators.<sup>3</sup> This study is described in Paper No. 5 in the list of published papers.

The lack of a clear connection between the chemical species of Fe and the defect producing the PQR luminescence made it difficult to continue the study. However, we were able to continue to explore some of the phenomena governing cluster formation and breakup without identifying the origin of the levels.

#### C. PAIR FORMATION AND BREAKUP

The defect responsible for the PQR luminescence exhibits extraordinary temperature dependence. The pairs appear to breakup even at room temperature. After the introduction of Fe in the samples, the PQR luminescence is observed to decay with time, with a time constant on the order of days at room temperature. With the sample at 4.2K, the PQR lines are observed to decrease with time when the sample is irradiated with a laser. This decrease could be due to sample heating or could be the results of photo-induced pair breakup, a phenomenon we previously observed in (Zn,O) pairs in GaP.<sup>4</sup> After numerous experimental attempts, we were unable to disconnect these two phenomenon and hence could not be assured which one was responsible for the observations in the case of the PQR lines.

#### D. DIFFUSION OF TRANSITION METAL FROM SILICIDE INTO SILICON

The poisoning of silicon by the diffusion of transition metal atoms from the silicide into the silicon during various processing steps is of great importance technically. Under this contract we initiated a study of the diffusion of Pt and Si during the anneal of samples consisting of silicon substrates with a layer of PtSi. We found that the Pt could in fact diffuse into the Si for processing at temperatures < 700C. The results of this study were published in Applied Physics Letters and is listed in publication 7.

## E. STATISTICS

The funds from this contract were used to support the research of four graduate students. The four students, their citizenship and current positions are listed in the table below.

Student	Citizenship	Current Position
R.J. Hauenstein	US	Completing Ph.D.
T.E. Schlesinger	Canadian	Completing Ph.D.
S. Hetzler	US	Completing Ph.D.
A. Prabhakar	US	Completing Ph.D.

## PUBLICATION LIST

The following papers were published by the Cal Tech group. Reprints of these papers are included as appendices to this report. The letter at the front of each title is the appendix designation.

- C. T.E. Schlesinger and T.C. McGill, "The Role of Fe in New Luminescence Lines in Si:Tl and Si:In", Physical Review B25, 7850 (1982).
- D. T.E. Schlesinger, R.J. Hauenstein, R.M. Feenstra, T.C. McGill, "Isotope Shifts for the PQR Lines in Indium-Doped Silicon", Solid State Communications 46, 321 (1983).
- E. R.J. Hauenstein, T.C. McGill and R.M. Feenstra, "Local Phonon Mode Calculations in Si", Proceedings of the Electrochemical Society Meeting, San Francisco, edited by W.M. Bullis and L.C. Kimerling, (1983).
- F. T.E. Schlesinger and T.C. McGill, "Isotope Shift of the P, Q, R Lines in Indium-doped Silicon", Proceedings of the Symposium on Defects in Silicon, San Francisco Meeting of the Electrochemical Society, edited by W.M. Bullis and L.C. Kimerling, (1983).
- G. T.E. Schlesinger and T.C. McGill, "Isotope Shift Experiments on Luminescence Attributed to (Fe,B) Pairs in Si", Physical Review B28, 3643 (1983).

- H. G.S. Mitchard and T.C. McGill, "Photoluminescence of Si-Rich Si-Ge Alloys", Physical Review B25, 5351 (1982).
- I. A. Prabhakar, T.C. McGill, and M-A. Nicolet, "Platinum Diffusion into Silicon from PtSi", Applied Physics Letters 43, 1118 (1983).

#### REFERENCES

- 1. G.S. Mitchard, S.A. Lyon, K.R. Elliott and T.C. McGill, "Observation of Long Life-time Lines in Photoluminescence from Si<sup>+</sup>In", Solid State Communications 29, 425 (1979).
- 2. L.C. Kimerling and J.L. Benton, "Electronically Controlled Reactions of Interstitial Iron in Silicon", Proceedings of the 12th International Conference on Defects in Semiconductors, Amsterdam, 1982.
- 3. R. Sauer and J. Weber, "Photoluminescence Characterization of Deep Defects in Silicon", Proceedings of the 12th International Conference on Defects in Semiconductors, Amsterdam, 1982.
- 4. R.M. Feenstra and T.C. McGill, "Defect Reactions in GaP:(Zn,O)", Physical Review Letters 47, 925 (1981).

## CHAPTER 4

### ATOM SCIENCES

#### A. INTRODUCTION

Work performed for the "Development of a RIS Technique for the Analysis of Impurities in Electronic Grade Silicon", under contract with Hughes Research Laboratories, has been completed by Atom Sciences. Atom Sciences' objectives for this contract were:

1. To select and demonstrate resonance ionization spectroscopy (RIS) schemes to selectively ionize impurity atoms of interest.
2. To develop the technique of SIRIS whereby atoms such as O, C, B, P, In, and Mn liberated from silicon by ion beam sputtering may be selectively ionized and detected using RIS.
3. To demonstrate that SIRIS is sensitive to levels of impurities of better than 1 part in  $10^{10}$  by calibrating the apparatus using first principles and making comparisons with known and unknown samples supplied by Hughes Research Laboratories.
4. To collaborate with Hughes Research Laboratories in working toward a program of performing routine analyses to investigate the infusion of impurities in the manufacturing process of silicon devices from raw materials to final product.

During the course of this work, RIS schemes were selected for nearly every atom in the periodic chart. The schemes for selected elements were demonstrated and used for obtaining the results in the work reported here. In addition, alternative RIS schemes were determined and demonstrated. Much of this work was performed before Atom Sciences had its SIRIS apparatus in place.

Atom Sciences demonstrated the technique of Sputter Initiated Resonance Ionization Spectroscopy (SIRIS) for the

detection of impurity atoms in silicon. Specifically, In, Al, and Ga were measured in samples of silicon supplied by Hughes. In addition, the concentration of Al and V were determined in certified samples of stainless steel supplied by the National Bureau of Standards.

Atom Sciences has now demonstrated that its SIRIS apparatus and technique are sensitive to 5 parts in  $10^9$ , and it has shown that current technology will permit the desired sensitivity of 1 part in  $10^{10}$  to be achieved. Diagnostic testing of the apparatus has been completed and specific improvements to be made have been identified. The present sensitivity has been well demonstrated with the known standards supplied by Hughes Research Laboratories and the National Bureau of Standards.

Atom Sciences and Hughes Research Laboratories established a collaborative working relationship which was indeed productive in establishing SIRIS as a viable technique for surface and bulk analysis for the semiconductor industry. The participation of Hughes personnel in this work was greatly appreciated and is gratefully acknowledged.

This work is an important step toward making possible the inclusion of SIRIS measurements into the manufacturing and/or quality control processes for the manufacture of more reliable, cost-effective devices.

#### B. RESEARCH AND DEVELOPMENT PERFORMANCE

The R&D effort to develop a RIS technique for the analysis of impurities in electronic grade silicon centered around the development of the technique of Sputter Initiated Resonance Ionization Spectroscopy (SIRIS). SIRIS combines ion beam sputtering and resonance ionization spectroscopy to provide a new method for the analysis of solids. Sensitivities as great as 1 part in  $10^{10}$  should be possible in routine analyses, and greater sensitivities should be possible in special cases.

RIS uses high power tunable dye lasers to selectively excite and ionize the atoms of a specific element among a host of undesired atoms of other elements. Besides being selective, the process is efficient. In SIRIS an energetic ion beam is used to sputter out the constituents of a solid sample so that a vapor "cloud" of ions and neutral atoms is formed above the sample located in vacuum. An RIS laser beam then probes the vapor cloud to selectively ionize the atoms of a given element. Ionized atoms of the selected element are then directed to an ion detector and counted. In a more practical form a mass spectrometer is added to the detection system to confirm the elemental identity of the ionized atom and/or to add isotopic.

The RIS and SIRIS processes, together with Atom Sciences' apparatus for the SIRIS technique, are described in a paper presented at the International Conference on Metallurgical Coatings, April 18-22, 1983 in San Diego, Ca. The paper was also published in the journal, Thin Solid Films\*, and is included in this report as Appendix J. The SIRIS process is fully described and the specifications of the apparatus are listed and explained. The SIRIS system is shown in Figure 1 of this report. Some performance data are given. The early results presented in that paper are mostly qualitative in nature. The RIS scheme for gallium is described and illustrated. A typical wavelength scan of the apparatus while tuned to gallium impurity atoms found in silicon is shown to demonstrate the selectivity of the RIS process. Magnetic field scans of the mass spectrometer are shown for a sample of silicon containing 100 ppm gallium. Spectra are shown for comparison, with the apparatus operated as a SIMS instrument and as a SIRIS instrument.

---

\*J.E. Parks, H.W. Schmitt, G.S. Hurst, and W.M. Fairbank, Jr., Thin Solid Films, 108 (1983) 69.

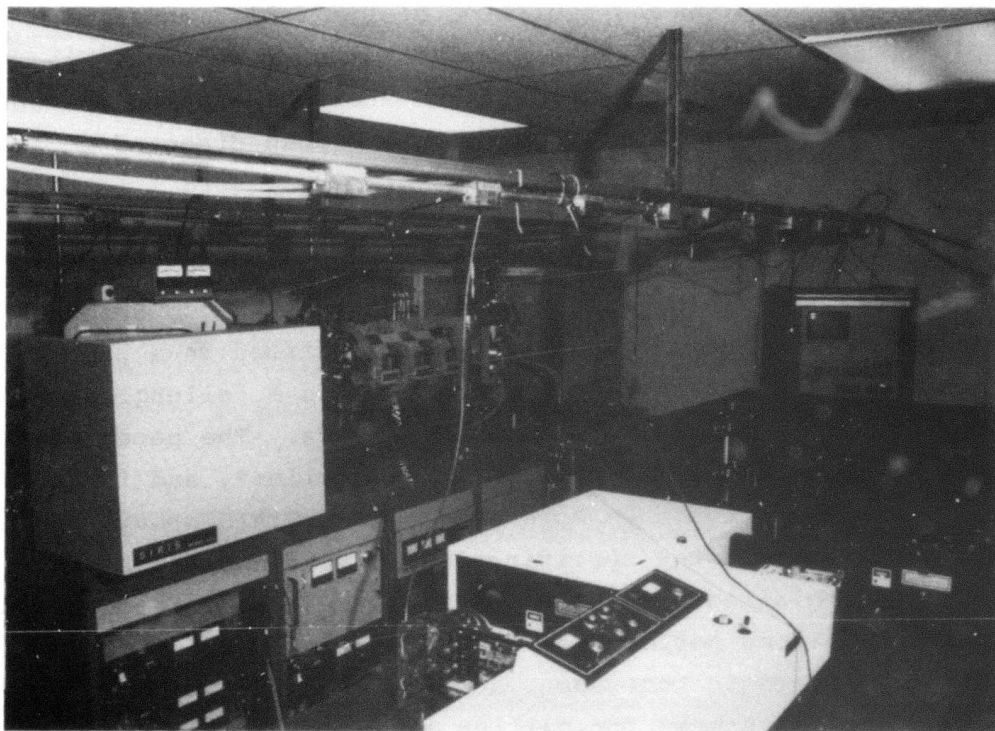


Figure 1. Photograph of SIRIS Facility.

The present state of development of Atom Sciences' SIRIS technology and the work for this contract have been described in a paper presented at the SPIE's 27th Annual International Technical Symposium and Instrument Display in San Diego, CA, August 21-26, 1983. This invited talk was published in Volume 426 of the Proceedings of SPIE\* and a copy is included with this report as Appendix K.

The present sensitivity and capabilities of the system are well documented quantitatively in that paper; well characterized reference samples were supplied by Hughes and certified samples of standard reference materials were supplied by the National Bureau of Standards. The SIRIS results are correlated with the known standard values supplied with the samples. Results are presented for gallium and indium in silicon and for aluminum and vanadium in stainless steel.

The detection limit at the time that paper was written was about 0.1 ppm; presently, the detection limit is 5 parts in  $10^9$ . Two areas remain in the apparatus where we may realize significant potential gains in sensitivity. One is in the ion beam current on target and the other is transmission through the mass spectrometer.

Our desired beam current on target is 1 mA; the data for the work presented in the paper were taken with only 50 mA on target. This is a factor of 20 too small; the sensitivity of the technique is directly proportional to the beam current.

The second deficiency in overall sensitivity is in the transmission of the mass spectrometer. The design of the mass spectrometer incorporates the latest technology and has not been fully optimized. Recently, diagnostic test of the mass spectrometer have been completed. These tests indicate that only about

---

\*J.E. Parks, H.W. Schmitt, G.S. Hurst, and W.M. Fairbank, Jr., "Ultrasensitive Elemental Analysis of Solids by Sputter Initiated Resonance Ionization Spectroscopy," Laser-based Ultrasensitive Spectroscopy and Detection V, Richard A. Keller, Editor, Proc. SPIE 426, 32-39 (1983).

2% of the RIS ions produced from the sputtered neutrals arrive at the detector. Correction of this deficiency should permit at least 80% of those ions to be transmitted through the system; a factor of 40 in improvement is expected.

#### C. SUMMARY

The desired sensitivity limit of 1 part in  $10^{10}$  is referenced to a 5 minute counting period in which 100 atoms are detected. At this time we have a sensitivity limit of 5 parts in  $10^9$ , and have identified specific improvements to be made in the apparatus which will lead to the sensitivity limit we desire.

Sputter Initiated Resonance Ionization Spectroscopy (SIRIS) is under active development and has yet to be established as a routine method for the sensitive analysis of materials. The validation of the SIRIS technique will require collaborative measurements with other established researchers and techniques. In due time SIRIS will be recognized as possibly the best technique for making accurate quantitative measurements of impurities in solids and will set the standards of the industry.

APPENDIX A  
Fivefold splitting of the  $CA_s$  local vibrational mode  
by Ga isotopes in GaAs

*R. J. Hauenstein*

*California Institute of Technology  
Pasadena, California 91125*

*and*

*J. P. Baukus*

*Hughes Research Laboratories  
Malibu, California 90265*

*and*

*R. M. Feenstra\* and T. C. McGill  
California Institute of Technology  
Pasadena, California 91125*

## ABSTRACT

The  $582\text{ cm}^{-1}$  localized vibrational mode (LVM) of the  $\text{C}_{\text{As}}$  defect in GaAs has been reexamined. High resolution ( $0.05\text{ cm}^{-1}$ ) Fourier transform IR absorption measurements indicate the presence of *five* peaks in the LVM spectrum. Green's-function and defect-cluster calculations predict nine localized modes (previously reported to be four) which broaden into five peaks, in good agreement with experiment. Results from a nearest-neighbor-interaction model indicate a much larger fractional variation in the C-Ga bond-bending than bond-stretching force constants, relative to bulk As-Ga values.

## I INTRODUCTION

Substitutional carbon impurities in GaAs have recently been shown to reside on the As sublattice.<sup>1</sup> This site has been deduced from the observed splitting of the localized vibrational mode (LVM) of the carbon defect, the splitting being attributed to isotopic variation among the four nearest-neighbor Ga atoms. However, the number of peaks (four or five) into which the  $C_{As}$  LVM is split is not clear from the original data, and, furthermore, the number of peaks predicted theoretically from a simple valence-force model has been incorrectly reported to be four.<sup>1,2</sup> In this paper, we reexamine the  $C_{As}$  LVM, both experimentally, through high resolution, Fourier transform IR absorption measurements, and theoretically, through Green's-function and "molecular" defect-cluster calculations. Our theoretical analysis makes use of a two-parameter nearest-neighbor-interaction model<sup>3</sup> to describe the bulk (As-Ga) and defect (C-Ga) interactions, and simple group-theoretic considerations to predict the splittings. We find that group theory predicts a rigorous splitting of the  $C_{As}$  LVM into nine distinct localized modes, which after broadening, merge into five bands, which we observe experimentally. Reasonably good agreement between theory and experiment for the peak frequencies and relative intensities is obtained, confirming the observation of Theis, Bajaj, Litton, and Spitzer<sup>1</sup> that substitutional carbon occupies the arsenic site in GaAs. The parameters required to fit the observed splittings indicate that the fractional variation between defect and bulk bond-bending interactions is much larger than for bond-stretching interactions for the  $C_{As}$  defect.

## II. EXPERIMENTAL DETAILS

We have made liquid-nitrogen-temperature IR transmission measurements on the band of local vibrational modes occurring in GaAs near  $582\text{ cm}^{-1}$ . The measurements were made using a BOMEM Model DA3.01 Interferometric Spectrophotometer. The source used was a globar, the beamsplitter was Ge-coated KCl, the detector was narrow bandpass ( $14\text{--}18\text{ }\mu\text{m}$ ) cold-filtered Ge:Zn operated at liquid helium temperature, and the instrument was evacuated. The data were numerically filtered to a free spectral range of  $510\text{ to }764\text{ cm}^{-1}$ . The results presented here are from a  $0.298\text{ cm}$ -thick sample from near the tang end of a carbon-doped, liquid encapsulated Czochralski crystal grown at the Hughes Research Laboratories (HRL). Low resolution ( $0.5\text{ cm}^{-1}$ ) IR data yield an integrated area of  $0.34\text{ cm}^{-2}$  for the  $582\text{ cm}^{-1}$  line in this sample. A calibration factor from area to concentration of  $1.1 \times 10^{16}\text{ cm}^{-1}$  has been established at HRL based on low temperature Hall effect and IR measurements of *p*-type GaAs material.<sup>4</sup> Thus we estimate the carbon concentration of the sample to be  $3.7 \times 10^{15}\text{ cm}^{-3}$ . The previously accepted calibration factor<sup>5</sup> was  $2.4 \times 10^{16}\text{ cm}^{-1}$  which would yield a carbon concentration of  $7 \times 10^{15}\text{ cm}^{-3}$ .

High resolution transmission data are shown in Fig. 1a. Five clearly resolved peaks were observed. The instrumental resolution was  $0.05\text{ cm}^{-1}$  and the measured linewidths were about  $0.08\text{ cm}^{-1}$ . The presented data were unapodized. That is, sharp lines would have the instrument lineshape:  $\sin x/x$ . Various smoothing functions were applied to the data to verify that none of the five

observed peaks was a secondary peak of a  $\sin x/x$  distribution. The observed peak positions and relative amplitudes are tabulated in Table I. The amplitudes given in the table are peak heights relative to the baseline shown in Fig. 1.

### III. THEORETICAL CONSIDERATIONS

The  $C_{As}$  localized mode consists mostly of carbon atom motion, but because a small fraction of the motion ( $\sim 6-7\%$  of the total energy) involves the nearest-neighbor-Ga shell, the vibrational frequency of the mode has a slight dependence on these Ga masses. The splitting of the  $C_{As}$  LVM band due to the mass variation of Ga isotopes in the nearest-neighbor shell can be readily predicted with the aid of group theory. There are two Ga isotopes,  $^{69}\text{Ga}$  and  $^{71}\text{Ga}$ , with natural abundances of 60.4% and 39.6%, and masses of 68.925574 and 70.924706 amu, respectively.<sup>6</sup> Hence, there are five possible nearest-neighbor-shell configurations of the Ga isotopes, which we label  $l = 0, \dots, 4$ , where  $l$  denotes the number of light ( $^{69}\text{Ga}$ ) nearest-neighbor atoms. Assuming that the  $C_{As}$  defect is accurately substitutional on the As site, each nearest-neighbor configuration is associated with a point-group:  $T_d$  for the  $l = 0$  and  $l = 4$  configurations,  $C_{3v}$  for  $l = 1$  and  $l = 3$ , and  $C_{2v}$  for  $l = 2$ . For  $T_d$  symmetry, the LVM is a triply degenerate, IR-active  $T_2$  mode. Upon lowering the symmetry to  $C_{3v}$ , the  $T_d$  irreducible representation,  $T_2$ , decomposes according to  $T_2 \rightarrow A_1 \oplus E$ , splitting the  $C_{As}$  LVM into two modes. Similarly, for the case of  $C_{2v}$  symmetry we have  $T_2 \rightarrow A_1 \oplus B_1 \oplus B_2$ , resulting in a threefold splitting of the LVM. Now, we simply

enumerate the possible nearest-neighbor-shell configurations: for the cases,  $l = 0, \dots, 4$ , we obtain 1, 2, 3, 2, and 1 peak(s) in the LVM spectrum, respectively, giving a total of nine peaks for natural Ga isotopic abundances, all of which are IR-active.<sup>7</sup>

To examine the LVM splitting quantitatively, we have made both Green's-function and defect-cluster calculations<sup>3</sup> for the  $^{12}\text{C}_{\text{As}}$  defect in GaAs for the five nearest-neighbor configurations,  $l = 0, \dots, 4$ . In our Green's-function calculations, the complete defect consists of a (known) mass perturbation at the substitutional and nearest-neighbor-Ga sites, and a (fitted) perturbation in the nearest-neighbor interactions involving the defect site. To describe lattice dynamics of bulk GaAs, we have used a general nearest-neighbor-interaction model<sup>3</sup> whose two parameters may be chosen to physically correspond to nearest-neighbor bond-stretching ( $f_1$ ) and bond-bending ( $f_2$ ) force constants. By fitting the bulk GaAs  $\text{TO}_\Gamma$  and  $\text{TA}_X$  phonon frequencies<sup>8</sup> we obtain the values,  $f_1 = 6.31 \text{ eV}/\text{\AA}^2$  and  $f_2 = 0.414 \text{ eV}/\text{\AA}^2$ . The C-Ga force constants ( $f'_1$  and  $f'_2$ ) have been allowed to independently vary from these bulk values, and the same C-Ga force constants are assumed for all five nearest-neighbor configurations. For our cluster calculations, we use the same interaction scheme, but instead solve for the normal modes of the carbon atom and its nearest-neighbor-Ga shell vibrating in an immovable lattice.

#### IV. RESULTS AND DISCUSSION

The results of our Green's-function calculations are presented in Fig. 1b.

As expected, the calculations predict nine localized modes. The relative intensities of these lines have been computed from the nearest-neighbor-configuration probability, weighted by the degeneracy of each mode. Since the localized modes from the Green's-function calculations are  $\delta$  functions in  $\omega^2$  [Ref. 3], we simulate the physical and instrumental broadening effects by using weighted Lorentzian curves<sup>2</sup> centered at the nine LVM frequencies, each identically broadened so that agreement with experimental linewidths is achieved. Upon broadening, we see from Fig. 1 that the nine lines become five peaks whose relative intensities are in reasonably good agreement with experiment.

The results of the Green's-function calculations are indistinguishable (on the scale shown in Fig. 1) from the simpler, defect-cluster results, indicating that to a very good approximation, the LVM motion can be considered completely restricted to the carbon and its Ga nearest-neighbor's. First, let us consider the results of the cluster calculation for the case,  $l = 0$ . We find that the LVM has energy  $E_0 = E(^{71}\text{Ga}) = 72.170$  meV, and that we can write the components of an eigenvector for this mode as

$$\begin{aligned} c_a &= 0.0895 \\ c_b &= 0.239 \\ c_c &= 0.967, \end{aligned} \tag{1}$$

where  $c_c$  corresponds to carbon motion,  $c_a$  to Ga-shell bond-bending motion, and  $c_b$  to Ga-shell bond-stretching motion.<sup>3</sup> From this result we can obtain approximate energies for the eight remaining LVM lines. To first order in the mass perturbation,  $\epsilon = 1 - (m_{69}/m_{71})$ , the expressions for the energy shifts  $\delta E$  of the eight remaining LVM's are

$$(\delta E)_{A_1}^{l=1} = \frac{3}{8}c_b^2\epsilon E_0 \quad (2a)$$

$$(\delta E)_E^{l=1} = \frac{3}{16}c_a^2\epsilon E_0 \quad (2b)$$

$$(\delta E)_{A_1}^{l=2} = \frac{1}{4}(c_a^2 + c_b^2)\epsilon E_0 \quad (3a)$$

$$(\delta E)_{B_1}^{l=2} = \frac{1}{8}(c_a^2 + 4c_b^2)\epsilon E_0 \quad (3b)$$

$$(\delta E)_{B_2}^{l=2} = \frac{3}{8}c_a^2\epsilon E_0 \quad (3c)$$

$$(\delta E)_{A_1}^{l=3} = \frac{1}{8}(4c_a^2 + c_b^2)\epsilon E_0 \quad (4a)$$

$$(\delta E)_E^{l=3} = \frac{1}{16}(5c_a^2 + 8c_b^2)\epsilon E_0 \quad (4b)$$

$$(\delta E)_{T_2}^{l=4} = \frac{1}{2}(c_a^2 + c_b^2)\epsilon E_0. \quad (5)$$

The energy shifts predicted by Eqs. (2)–(5) differ from those computed directly (from both Green's-function and defect-cluster calculations) by less than 3%, showing that the LVM splittings are well described by first order perturbation theory.

In Fig. 1 we compare the results of the Green's-function calculations with the observed LVM spectrum. These results are also summarized in Table I. We see from Eqs. (2a), (3a), and (4a) that the three center peaks in Fig. 1 should be equally spaced, and that the entire spectrum should be symmetric in frequency with respect to the center peak [Eq. (3a)]. From Fig. 1, we see that this is indeed the case for the theoretical peaks, and also appears to be nearly true for the experimental spectrum, though all five theoretical peaks do not line up exactly with their experimental counterparts. For this work, we have arbitrarily chosen to fit our theory to the outer peaks. Alternatively, we could have fit the three middle peaks. In the latter case, the outer peaks would then be spread too far

apart in our simple nearest-neighbor-interaction model. However, more realistic models, which include second-nearest-neighbor and long-range Coulomb effects, would probably tend to reduce the fraction of nearest-neighbor-Ga motion, i.e., the magnitudes of  $c_a$  and  $c_b$  in Eq. (1), and thereby pull in the outer peaks. In deriving Eqs. (2)–(5) no special assumptions were made other than the on-site geometry of the carbon defect; in particular, these equations remain valid (as first order equations) in the presence of more complicated interactions. Hence, so long as values for  $c_a$  and  $c_b$  can be found that accurately, with the aid of Eqs. (2)–(5), predict all five peaks (which seems likely given the symmetry of the observed spectra), we may identify the Ga isotopic fluctuation as the source of the LVM splitting. The lack of exact quantitative agreement with experiment for all five peaks in our Green's-function and cluster calculations is then only a consequence of the simplicity of our model.

The calculated results presented here have made use of a two parameter description of the C-Ga interactions. These two parameters (bond-stretching and bond-bending C-Ga force constants) were determined by fitting the two outer peaks. In our model we found it necessary to fractionally increase the C-Ga bond-bending much more than the bond-stretching force constants, relative to the bulk, to avoid significantly ( $> 50\%$ ) overestimating the outer peak-to-peak splitting, as Theis *et al.* have done using a monatomic, linear chain, defect model.<sup>1</sup> For our Green's-function calculations, we fit the outer peaks with the defect force constants,  $f'_1 = (1.0965)f_1$  and  $f'_2 = (4.25)f_2$ . As argued in the preceding paragraph, the nearest-neighbor-interaction model assumed here is evidently too

simple for this last result to be *quantitatively* meaningful, though it may remain qualitatively correct in the context of more elaborate models.

## V. CONCLUSION

We have made Green's-function and defect-cluster calculations on the local vibrational modes of the substitutional  $^{12}\text{C}_{\text{As}}$  defect in GaAs. We have shown from group theoretic considerations that, at the natural abundances of the Ga isotopes, the LVM band consists of nine discrete localized modes which, after suitable broadening, form *five* bands. The results of high resolution measurements confirm the prediction of five LVM peaks. Reasonably good agreement between theoretically predicted and experimentally observed peak frequencies and relative amplitudes are obtained. We have derived approximate expressions for the energy splittings which should remain valid for more complex models than the simple, nearest-neighbor-interaction model considered here. Qualitative predictions from these approximate expressions are consistent with experimentally observed features, further supporting the identification of Ga isotopic variation as the source of the LVM splitting. Thus, our results confirm in detail the observation of Theis *et al.*<sup>1</sup> that the carbon defect is substitutional for As in GaAs. Finally, the parameters required to fit the observed LVM spectra indicate that there is a much larger fractional variation in the bond-bending than the bond-stretching C-Ga force constants, relative to the values for bulk GaAs.

## **ACKNOWLEDGEMENTS**

We acknowledge the support of H. Olson for sample preparation and R. Wong Quen for her untiring efforts in the IR spectroscopy. The authors also gratefully acknowledge the support of the Defense Advanced Research Projects Agency and the Office of Naval Research under contract number N00014-81-C-0285.

## REFERENCES

\*Present Address: IBM Thomas J. Watson Research Center, Yorktown Heights,  
New York 10598

<sup>1</sup>W. M. Theis, K. K. Bajaj, C. W. Litton, and W. G. Spitzer, *Appl. Phys. Lett.*  
41 (1), 70 (1982).

<sup>2</sup>W. M. Theis, K. K. Bajaj, C. W. Litton, and W. G. Spitzer, in *Physics of Semiconductors*, edited by M. Averous (North-Holland, Amsterdam, 1983), p. 116.

<sup>3</sup>For a description of the Green's-function and cluster calculations and the nearest-neighbor-interaction model used, see R. M. Feenstra, R. J. Hauenstein, and T. C. McGill, *Phys. Rev. B* 28, 5793 (1983).

<sup>4</sup>A. T. Hunter, H. Kimura, J. P. Baukus, H. V. Winston, and O. J. Marsh, *Appl. Phys. Lett.* (to be published).

<sup>5</sup>M. R. Brozel, J. B. Clegg, and R. C. Newman, *J. Phys. D* 11, 70 (1978).

<sup>6</sup>P. A. Tipler, *Foundations of Modern Physics* (Worth, New York, 1969), p. 496.

<sup>7</sup>G. Herzberg, *Molecular Spectra and Molecular Structure* (Van Nostrand, Princeton, 1968), Vol. 2, ch. 3.

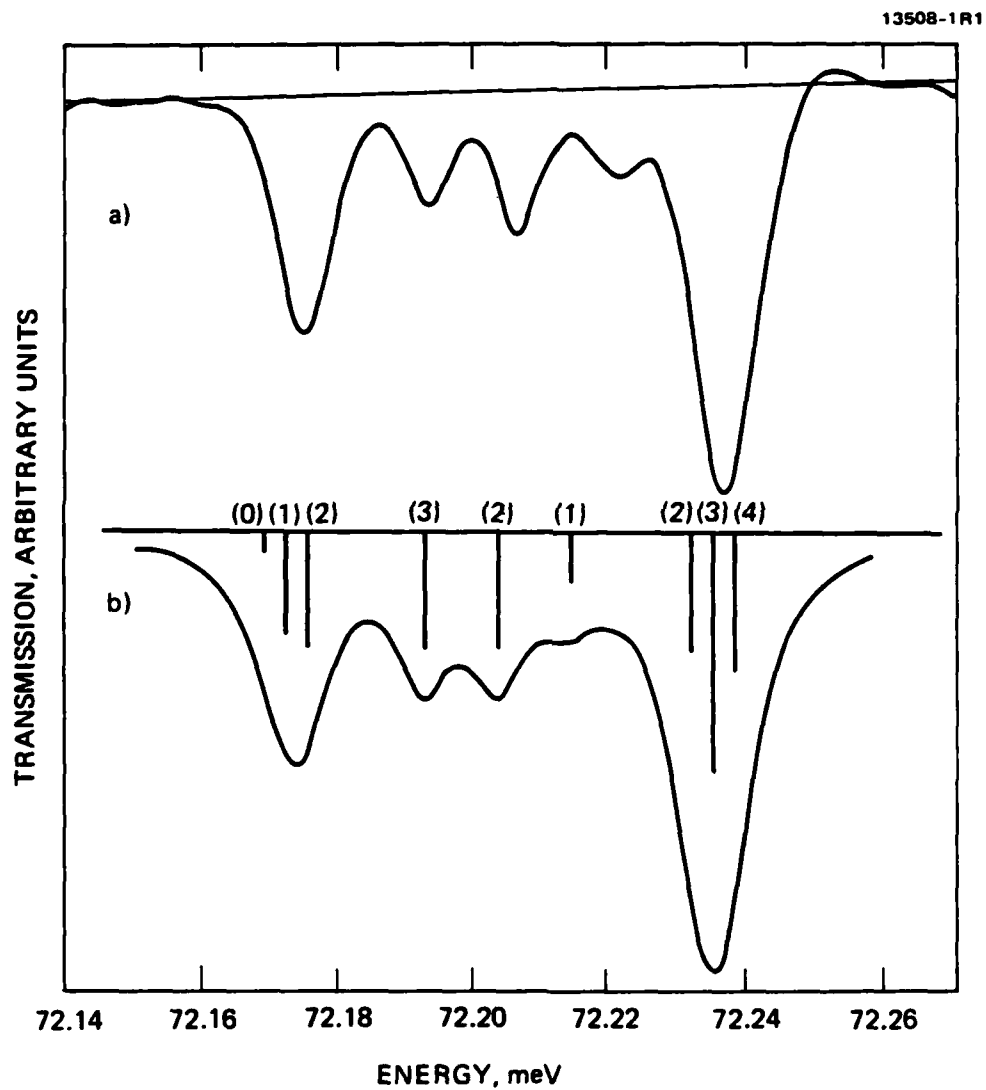
<sup>8</sup>J. L. T. Waugh and G. Dolling, *Phys. Rev.* **132**, 2410 (1963).

TABLE I. Comparison of observed and calculated LVM peak frequencies ( $\nu$ ) and relative intensities ( $I$ ) for the  $C_{A_8}$  defect. The relative intensities were obtained from the amplitudes of the deconvoluted peaks.

Peak	$\nu_{(exp)} (cm^{-1})$	$\nu_{(calc)} (cm^{-1})$	$I_{(exp)}$	$I_{(calc)}$
1	582.12	582.12	0.59	0.50
2	582.27	582.28	0.27	0.28
3	582.37	582.36	0.35	0.28
4	582.48	582.45	0.14	0.12
5	582.61	582.61	1.00	1.00

## FIGURE CAPTIONS

**FIG. 1.** (a) High resolution, Fourier transform IR absorption measurement of the localized vibrational mode (LVM) band of  $^{12}\text{C}_{\text{As}}$  in GaAs. At a resolution of  $0.05\text{ cm}^{-1}$ , we see five peaks in the LVM spectrum. (b) Calculated LVM spectrum, before and after broadening, based on a Green's-function computation. The values in parentheses indicate the number of light ( $^{69}\text{Ga}$ ) atoms coordinating the defect for the particular mode. The baselines used in determining peak heights are also shown.



APPENDIX B

MEASUREMENTS OF Fe CONCENTRATIONS IN Si:In BY  
CHARGED PARTICLE ACTIVATION ANALYSIS

R.R. Hart  
and  
S. Lee

Texas A & M University  
College Station, Texas 77843

High sensitivity determinations of trace Fe concentrations in heavily doped Si(In) samples were carried out using charged particle activation analysis (CPAA). Use of the  $^{56}\text{Fe}(p,n)^{56}\text{Co}$  reaction minimized the production of long-lived radioisotopes from the In doping, allowing selective activation and determination of Fe.  $^{56}\text{Co}$  activities, produced by proton irradiations of the Si(In) samples as well as a high-purity Fe standard, allowed determination of Fe concentrations in the Si(In) using a comparative technique. The experimental procedure consisted of activation of the samples and standard using a high energy proton beam, chemical etching of the samples to remove possible surface and recoil  $^{56}\text{Co}$  contamination, and counting of the samples and standard to determine relative  $^{56}\text{Co}$   $\gamma$ -ray activities.

Irradiations were carried out at the Texas A&M variable energy cyclotron using a 20.31 MeV extracted proton beam. The samples and standard were individually irradiated for 2-75 minutes using beams of 0.5-1.5  $\mu\text{A}$  in intensity. The target chamber apparatus has been thoroughly described elsewhere.<sup>1</sup> In short, it provided: collimation of the analysis beam to 0.5 or 1.0  $\text{cm}^2$ , a working vacuum of  $< 1 \times 10^{-4}$  Torr, a water-cooled target holder, and on-line beam monitoring and viewing. During each Si(In) irradiation a foil stack, consisting of one 23.2  $\mu\text{m}$  thick Fe foil and several 36.1  $\mu\text{m}$  thick Al foils, was placed at the front of the polished sample. The  $^{56}\text{Co}$  activity induced in the Fe foil served as a relative beam current monitor during each irradiation. The Al foils degraded beam energy to 11-15 MeV depending on the Al thickness used. The Fe standard consisted of a stack of 40, 23.2  $\mu\text{m}$  thick, 99.99% pure Fe foils.

Following irradiation, the samples were etched in three steps using a planar silicon etch ( $3\text{HNO}_3:1\text{CH}_3\text{COOH}:0.4\text{HF}$ ). A nominal thickness of  $10\text{ }\mu\text{m}$  was removed from the irradiated face of each sample. Using the kinematics of an elastic two-body collision and tabulated range data,<sup>2</sup> the maximum recoil depth of  $^{56}\text{Co}$  produced from possible Fe contamination of the sample surface was estimated to be  $1\text{ }\mu\text{m}$ . Thus, the conservatively deep, multistep, post-irradiation etch assured that only bulk Fe was measured.

Several weeks elapsed between irradiation and counting of the samples. The remaining long-lived ( $T_{1/2} = 78.5\text{ d}$ ) activity of  $^{56}\text{Co}$  was determined by measurements of the  $846.7\text{ keV}$  photopeak using ordinary  $\gamma$ -ray spectroscopy. All samples were counted at the face of a Ge(Li) detector with a resolution of  $2.0\text{ keV FWHM}$  at  $847\text{ keV}$ . For the counting geometry used the absolute photopeak detection efficiency was  $1.2\%$  at  $847\text{ keV}$ . Samples were counted for times ranging from 58-761 hours. Standard foils were counted in the same fashion except that a counting time of 1000 seconds was used.

In an attempt to improve the detection limits of the measurements a coincidence counting technique employing a  $3\times 3$  in NaI(Tl) detector opposite the above Ge(Li) detector was used in the collection of coincidence spectra. Unfortunately, the improvement in signal to noise ratio obtained was essentially offset by an accompanying decrease in efficiency yielding only marginal improvement in the detection limit. The positive result of this effort is that Fe determinations and detection limits calculated using both the coincidence and ordinary  $\gamma$ -ray spectra agree well.

Fe concentrations in the samples were calculated using the average cross section method described by Ricci.<sup>3</sup> As noted earlier, activities induced in the Fe beam monitor foils yielded the relative beam intensities required in the calculations. Needed range-energy relationships for protons in Si, Al and Fe were obtained through numerical integration of the stopping powers of Andersen and Ziegler.<sup>4</sup>

The Fe concentration detection limit for each sample was determined by estimating the detection limit of the photopeak at 847 keV. The detection limit of the photopeak area was calculated by applying the well known blank case of Currie<sup>5</sup> to the spectrum background underlying the 847 KeV photopeak region. The background signal required in the calculation was defined to be the background counts which would underlie 95% of the photopeak area of a gaussian photopeak centered at 847 KeV with a 2.0 KeV FWHM. Currie's methodology provides a consistent statistical definition for the detection limit as it is used here.

Since very low concentrations of Fe were of interest, the major source of uncertainty in the results was due to the statistical error associated with the small Co<sup>56</sup> photopeaks. Other sources of error due to uncertainties in the final bombardment energy, the stopping power data used, and the counting geometry were negligible when compared to the counting uncertainties. Thus, the error reported below for the Fe concentration is the standard error due to  $\gamma$ -ray counting statistics.

Results for the determination of the Fe concentration in each of the Si(In) samples are given in Table 1.

Table 1. Fe Concentrations in Si(In)

Sample	Description	CPAA Fe Concentration (cm <sup>-3</sup> )
C112.M	Si(In,B), Fe diffused	$1.2 \pm .4 \times 10^{15}$
C70401	Si(In), as grown tang slice	$< 6.5 \times 10^{14}$
C117IN	Si(In), as grown tang slice	$< 3.9 \times 10^{13}$

Since the solid solubility and the diffusion coefficient for Fe in Si<sup>6,7</sup> are known for the conditions under which the Fe diffusion of sample C112.M was performed,<sup>8</sup> the depth profile of the Fe was estimated at the time of sample quenching using a simple 1-d model. In order to compare this profile to the CPAA result, the inherent depth sensitivity of CPAA must be accounted for by folding in the Fe activation cross section. This calculation gives a CPAA Fe concentration of  $1.5 \times 10^{15}$  cm<sup>-3</sup>. The agreement between the measured and calculated results for the Fe diffused sample indicates that the Fe was largely retained in the sample bulk following quenching and room temperature storage for several weeks prior to analysis by CPAA.

Analysis of the as grown Si(In) detected no bulk Fe at the concentration detection limits shown in Table 1. The improvement in detection limits from sample C70401 to sample C117IN resulted from a concerted effort where beam current, irradiation time, beam energy and counting time were increased for the analysis of sample C117IN.

## References

1. Rook, H.L., Ph.D. Dissertation, Texas A&M University, College Station, Texas (1969).
2. Northcliffe, L.C. and Schilling, R.F., Nuclear Data Tables, A7 (1970) 233.
3. Ricci, E., Advances in Activation Analysis, Vol. 2, (New York, Academic Press, 1972) 221-263.
4. Andersen, H.H. and Ziegler, J.F., Hydrogen - Stopping Powers and Ranges in All Elements, (New York, Pergamon Press, 1977).
5. Currie, L.A., Anal.Chem., 40 (1968) 586-593.
6. Graff, K. and Pieper, H., J. Electrochem. Soc., 188 (1981) 669-674.
7. Struthers, J.D., J. Appl. Phys., 27 (1956) 1560.
8. Schlesinger, T.E. and McGill, T.C., Phys. Rev. B, 25 (1982) 7850.

## Role of Fe in new luminescence lines in Si:Tl and Si:In

T. E. Schlesinger and T. C. McGill

California Institute of Technology, Pasadena, California 91125

(Received 28 December 1981)

We report on the experimental results which indicate that complexes of Fe with Tl are likely to be the origin of the recently observed A, B, C lines. We have also confirmed that diffusion of Fe produces substantial increase in similar lines, labeled P, Q, R, observed in Si:In.

The luminescence spectra of Si:In have been studied in much detail.<sup>1-4</sup> In particular long-lived lines were observed in the work of Lightowers and Vouk<sup>2</sup> and by Mitchard *et al.*,<sup>5</sup> who labeled these lines P, Q, R. Weber *et al.* suggested that these lines were a result of an Fe-In complex with a (100) axial symmetry.<sup>6</sup> More recently a similar set of luminescence lines were observed by Thewalt *et al.* in Si:Tl.<sup>7</sup> In this Report we present evidence that the luminescence observed by Thewalt *et al.* in Si:Tl is created by the introduction of Fe into Tl-doped Si samples. We confirm the observations of Weber *et al.* that the long-lived lines observed in Si:In are also enhanced upon the introduction of Fe into those samples.

Iron is introduced into the samples as follows. A layer of iron is evaporated onto the surface of the sample after it has been cleaned using a chemical etch (3HNO<sub>3</sub>:1CH<sub>3</sub>COOH:0.4HF). The iron is then diffused into the sample by annealing it at 1100°C for 1 h and then quickly quenching the sample in distilled water. The surface is then cleaned again using the same chemical etch. We estimate that this procedure results in an iron concentration of 10<sup>15</sup> cm<sup>-3</sup>.<sup>8</sup> The photoluminescence spectra were obtained using a Coherent Model CR 3000 K krypton-ion laser for above-band-gap excitation. The laser was operated in cw mode at a peak output power of 4 W. The luminescence was then collected from the edge of the sample and directed through the entrance slits of a Spex Model 1404 spectrometer and measured with a Ge detector.

In Fig. 1, we present the spectrum of Si:Tl before (upper panel) and after (lower panel) Fe diffusion. The spectra were taken at 4.2 K and are labeled with the notation used by Thewalt *et al.* The spectrum in the top half of Fig. 1 is plotted on a different arbitrary intensity scale than that in the lower panel. The large peak is the thallium

bound-exciton line and the smaller peaks at lower energies are probably due to donor-acceptor luminescence resulting from the unintentional presence of P in the samples. This same spectrum is presented in the bottom half of the figure along with the spectrum from the sample diffused with iron. To indicate the intensities of the various lines relative to the bound-exciton line for Si:Tl, the two spectra in this panel have been scaled so that the Tl bound-exciton line is of the same intensity in both.<sup>9</sup> These spectra show that after the

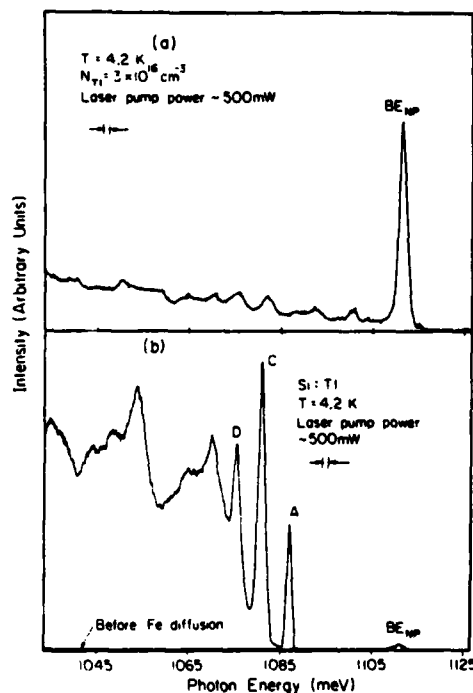


FIG. 1. (a) Photoluminescence spectrum of Si:Tl (a) before Fe diffusion, and (b) after Fe diffusion at 4.2 K taken using a Ge detector. The line labeled BE is the Tl bound-exciton line.

diffusion of Fe the *A, C, D* lines in Si:Ti are increased in intensity from not being observable in the spectra before diffusion to dominating the spectrum after diffusion. When some care was taken not to contaminate the samples and when we subjected them to the same cleaning and annealing procedure without iron this luminescence did appear. The luminescence was, however, more than an order of magnitude less intense relative to the Ti bound-exciton line than in samples into which iron was diffused. We attribute the appearance of the luminescence to the presence of iron in the as-grown material or to slight contamination during the processing. This result is consistent with the work of Mitchard *et al.*<sup>5</sup> in Si:In in which *P, Q, R* luminescence was observed without intentionally introducing iron into their samples.

In Fig. 2 we present the spectrum of Si:In before and after iron diffusion and following the labeling scheme of Mitchard *et al.*<sup>5</sup> Again the spectra were taken at 4.2 K and are presented so that the In bound-exciton line has the same intensity in both. The spectra show that after the diffusion of Fe the *P, Q, R* lines in Si:In are increased in intensity from being barely observable to dominating the spectra. We have also observed in the case of Si:In that the luminescence can be diminished by annealing the samples at high temperatures (1100°C) and allowing them to cool slowly. This can be attributed to the iron precipitating out of the samples.<sup>8</sup>

In summary, we have shown that the introduction of Fe in Si:Ti produces the luminescence reported by Thewalt *et al.*, implying that this luminescence is due to an Fe-Ti complex. We have also made observations which confirm the conclusions

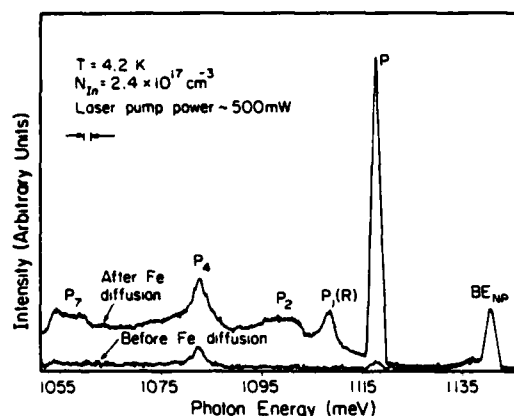


FIG. 2. Photoluminescence spectra of Si:In before and after Fe diffusion (as labeled) at 4.2 K taken using a Ge detector. The line labeled BE is the In bound-exciton line.

of Weber *et al.*<sup>6</sup> that the *P, Q, R* luminescence observed in Si:In is due to an Fe-In complex.

The authors are pleased to acknowledge useful technical discussions with R. M. Feenstra and thank J. Weber for providing copies of unpublished work reporting the results at Stuttgart. Measurements of the carrier concentration were carried out at Hughes Research Laboratories where H. Kumura and F. Harvey have provided us with the samples. This work was supported in part by Office of Naval Research under Contract No. NO0014-81-C-0285. One of us (T.E.S.) received financial assistance from the Natural Sciences and Engineering Research Council of Canada.

<sup>1</sup>P. J. Dean, J. R. Haynes, and W. F. Flood, *Phys. Rev.* **161**, 711 (1967).

<sup>2</sup>M. A. Vouk and E. C. Lightowers, *J. Lumin.* **15**, 357 (1977).

<sup>3</sup>M. A. Vouk and E. C. Lightowers, *Proceedings of the Thirteenth International Conference on the Physics of Semiconductors, Rome, 1976*, edited by F. G. Fumi (Tipografia Marves, Rome, 1977), p. 1098.

<sup>4</sup>S. A. Lyon, D. L. Smith, and T. C. McGill, *Phys. Rev. B* **17**, 2620 (1978).

<sup>5</sup>G. S. Mitchard, S. A. Lyon, K. R. Elliott, and T. C. McGill, *Solid State Commun.* **29**, 425 (1979).

<sup>6</sup>J. Weber, R. Sauer, and P. Wagner, in *Proceedings of the International Conference on Luminescence, Berlin, 1981*, edited by I. Broser (North-Holland, Amsterdam, 1981).

<sup>7</sup>M. L. W. Thewalt, U. O. Ziemelis, and R. R. Parsons, *Phys. Rev. B* **24**, 3655 (1981).

<sup>8</sup>K. Graff and H. Pieper, *J. Electrochem. Soc.* **128**, 669 (1981).

<sup>9</sup>The process of introducing Fe into the Si is not likely to result in any change in the Ti concentration since Ti is such a large atom that diffusion is unlikely at the temperature used in the Fe diffusion.



## APPENDIX D

### ISOTOPE SHIFTS FOR THE P, Q, R LINES IN INDIUM-DOPED SILICON

T. E. Schlesinger, R. J. Hauenstein, R. M. Feenstra,\* and T. C. McGill  
California Institute of Technology  
Pasadena, California 91125

(Received 14 November 1982 by H. Suhl)

We have measured the isotope shift of the P and R luminescence lines in Si doped with In and diffused with isotopically enriched Fe. We find no measurable shift in the R line. Similar experiments on the luminescence lines attributed to an isolated Fe complex show no shift in the previously identified "phonon replicas." Theoretical calculations of defect phonon resonances near 9 meV for interstitial and substitutional Fe predict an isotope shift of 0.17 meV for  $^{56}\text{Fe}$  and  $^{54}\text{Fe}$ . This value is in disagreement with the observed lack of a shift.

The properties of transition metal impurities in Si have been the subject of many studies recently.<sup>1</sup> In particular, the photoluminescence spectrum of Si diffused with Fe has been of interest.<sup>1-5</sup> A number of luminescence features have been tentatively identified as being due to (Fe,In),<sup>1,3,5</sup> (Fe,Tl),<sup>3</sup> and (Fe,B)<sup>1,4</sup> pairs while some features have been related to an isolated Fe complex alone.<sup>4</sup> These luminescence features are seen to be greatly enhanced upon the deliberate introduction of Fe into the samples.<sup>3-5</sup> Also, these spectra usually consist of one or two sharp lines identified as no-phonon transitions followed at lower energies by lines identified as local "phonon replicas" of the no-phonon line.<sup>1,4,6</sup> It is thought that the local phonon mode involves some motion of the Fe atom with a characteristic energy of about 9 meV.<sup>4,5</sup> To identify conclusively that certain spectra are indeed due to the presence of Fe in the sample, we have conducted experiments to measure shifts in those lines previously identified as being due to local vibrational modes of the Fe as a function of the isotope of the Fe introduced into the sample.

We first looked at the so-called P,Q,R luminescence in Si:In.<sup>2</sup> It has been thought that this luminescence is due to (Fe,In) pairs.<sup>1,3,5</sup> The R line has been identified as a phonon replica of the P line.<sup>5,7</sup> This phonon mode is supposed to be a local vibrational mode of the Fe. This seemed to be an ideal case for measuring an isotope shift to verify this assertion.

Two isotopes of Fe,  $^{56}\text{Fe}$  (99.93%-enriched) and  $^{54}\text{Fe}$  (97.08%-enriched), were obtained as oxide ( $\text{Fe}_2\text{O}_3$ ) from Oak Ridge National Laboratories. The oxide was subsequently reduced at 700°C for one hour in an atmosphere consisting of 12%  $\text{H}_2$  with the balance made up of He. We used float-zone Si:In samples with In concentration  $2.8 \times 10^{16} \text{ cm}^{-3}$  and Si:P samples with resistivity of  $12 \Omega\text{-cm}$  for the luminescence experiments. The iron was evaporated onto the surface of the samples and then

diffused in at 1100°C, using the method described in Ref. 3. Particular care was taken during the diffusion and quench to prevent the introduction of iron from undesired sources.

All of the spectra presented here were obtained at 4.2 K, with the samples mounted in a Janis variable temperature dewar and using a Spectra Physics model 166 argon ion laser for above band gap excitation. The laser was operated in the CW mode at a peak output power of 1 W. The luminescence was then collected from the edge of the sample and directed through the entrance slits of a Spex model 1269 spectrometer and measured with an RCA model 7102 photomultiplier tube cooled to liquid nitrogen temperatures in the case of the Si:In and measured with an InAs or Ge detector in the case of the Si:P.

The resulting spectra of the P and R lines for  $^{56}\text{Fe}$  and  $^{54}\text{Fe}$  are shown in Fig. 1. The spectra shown here are the result of extensive signal averaging which has resulted in much increased signal-to-noise ratio and also provided us with a greater sensitivity in determining relative line positions. As can be seen, there is no shift in the position of the R line to at least 0.2 Å. In the spectra of the R line for both isotopes, we see that the width of the peak is the same in both cases, and a broad feature at about  $1.1192 \mu\text{m}$  has been reproduced. We also observe no shift in the position of that feature of the spectrum that has been labeled P7.<sup>5</sup> In the case of the P line, the no-phonon line, we see what seems to be a very small shift of about 0.1 Å. However, we attribute this apparent shift to the limitations in repeatability of our apparatus.

We have also investigated the isotope shifts of some other luminescence lines that have been observed in both n- and p-type Si at about  $1.7 \mu\text{m}$ . These lines show the 9.0 meV phonon replica and are thought to be related to an isolated Fe complex.<sup>4</sup> In Fig. 2 we show this luminescence spectrum in Si:P after it has been diffused with Fe. The line at  $1.687 \mu\text{m}$  has been

\* Present address: T. J. Watson Research Center,  
Yorktown Heights, New York 10598

identified as actually consisting of two no-phonon lines. The lines at 1.704  $\mu\text{m}$  and 1.709  $\mu\text{m}$  have been identified as phonon replicas.<sup>4</sup> The 9 meV phonon replica was a partial basis for the identification of the R line as being a local phonon mode of the iron in the case of P,Q,R luminescence. To observe any isotope shift in these lines we once again used <sup>54</sup>Fe and <sup>56</sup>Fe. We did not, however, apply the signal averaging technique here. The data show no shift in the no-phonon lines or in the phonon replicas to at least 0.5 Å, and, in general, the line shapes remain unchanged.

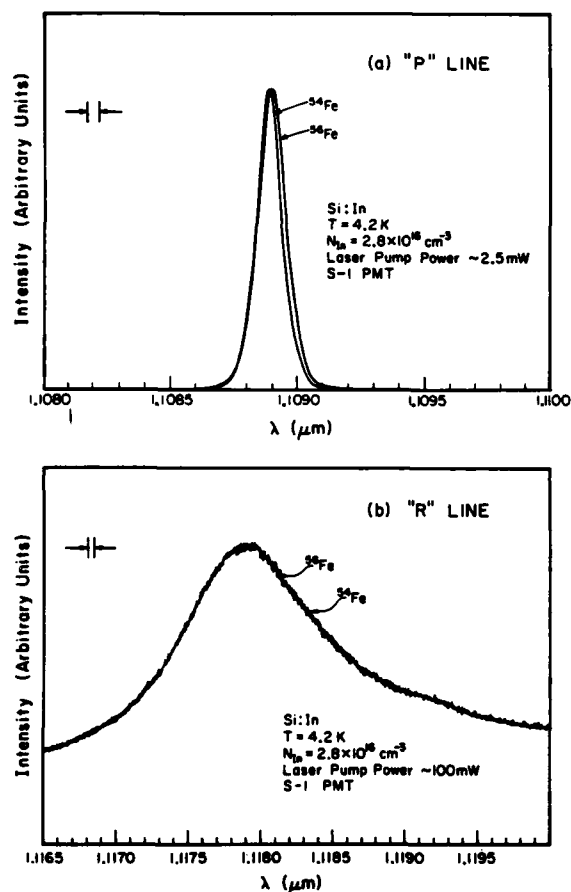


Fig. 1. The spectrum of Si:In after diffusion of <sup>56</sup>Fe and <sup>54</sup>Fe. (a) is the P line presented for both isotopes and (b) is the R line presented for both isotopes.

To ensure that our samples were not contaminated with iron initially, we carried out DLTS measurements on them before any treatment, after annealing them but without evaporating iron on the surface, and after iron evaporation and diffusion. We have found that the as-grown samples and those that were annealed but did not have iron evaporated onto the surface showed no iron related deep levels to a concentration of less than  $10^{13} \text{ cm}^{-3}$ . Samples that did have iron deliberately introduced did show iron related deep levels which have been identified previously.<sup>8</sup>

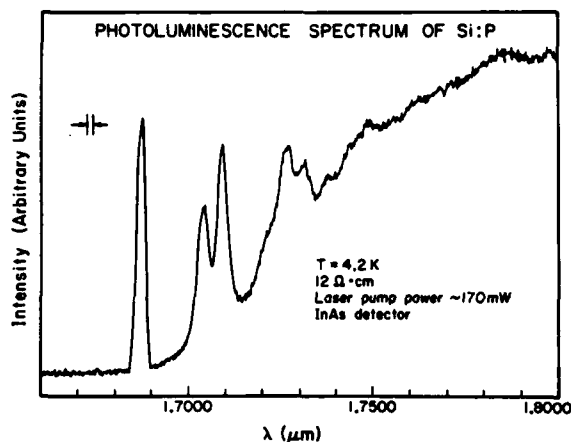


Fig. 2. The spectrum of Si:P after diffusion of natural Fe. The line at about 1.687  $\mu\text{m}$  actually consisting of two no-phonon lines followed by phonon replicas at about 1.704  $\mu\text{m}$  and 1.709  $\mu\text{m}$ .

The questions then are: Should one expect an isotope shift for an interstitial Fe, and, if so, what is the magnitude of this shift? These questions have been addressed by calculation of the local mode frequencies of these defects.

We have developed a numerical method for determining the local phonon modes associated with the introduction of point defects into a general zinc blende lattice, which we here specialize to the case of interstitial Fe in Si. This method is based on the Green's function formalism described by Maradudin et al.<sup>9</sup> We essentially first calculate the Green's functions for the unperturbed system in that subspace of the bulk crystal affected by the perturbation and then combine this information with the perturbation itself to yield the defect mode frequencies. We present an extensive discussion of the theoretical and computational details elsewhere,<sup>10</sup> limiting ourselves here to a description of the major features of this work.

For the present numerical calculations we have considered all interactions to occur only between nearest neighbors. In the perfect crystal it is readily shown that, as a consequence of the point-group symmetry,  $T_d$ , there are then only two independent parameters, the appropriate linear combinations of which can be directly interpreted as "bond-stretching" and "bond-bending" spring constants,  $f_1$  and  $f_2$ , respectively, which connect each Si atom to its nearest neighbors. To treat the problem of an interstitial Fe atom in the lattice we consider the center of a fcc conventional unit cell as the defect site. This site has the full point-group symmetry ( $T_d$ ) of the crystal. The bulk-defect coupling is then modeled by connecting the Fe atom to each of its four Si nearest neighbors with bond-stretching and bond-bending "defect springs,"  $f'_1$  and  $f'_2$ .

By using group-theoretic techniques we maximally exploit the defect-site symmetry to both simplify the calculations and to provide a natural classification scheme

for the defect modes. The bulk subspace affected by the perturbation is spanned by 12 coordinates, the three coordinates of each of the four nearest-neighbor Si atoms. These coordinates form the basis for a reducible representation,  $\Gamma$ , of the point group  $T_d$ , which is decomposed into irreducible representations as

$$\Gamma = A_1 \oplus E \oplus T_1 \oplus 2T_2. \quad (1)$$

Maradudin<sup>11</sup> has shown, for frequencies imbedded within the quasicontinuous band of eigenfrequencies of the bulk crystal, that the "resonance mode" frequencies are given by

$$\text{Re} \left[ \det [1 - g_0^{(s)}(\omega^2) \delta l^{(s)}(\omega^2)] \right] = 0, \quad (2)$$

where  $(s)$  labels the various irreducible representations, and  $\delta l^{(s)}$  is the appropriate perturbation. For the two-parameter model we have obtained the following results for the perturbation,  $\delta l^{(s)}$ :

$$(\delta l^{(s)})^{A_1} = \frac{f'_1}{m_{Si}} \quad (3a)$$

$$(\delta l^{(s)})^E = (\delta l^{(s)})^{T_1} = \frac{f'_2}{m_{Si}} \quad (3b)$$

$$(\delta l^{(s)})^{T_2} = \frac{f'_2}{m_{Si}} + \frac{8}{3} \left( \frac{f'_2}{m_{Si}} \right)^2 L^{-1}(\omega^2) \quad (3c)$$

$$(\delta l^{(s)})^{T_2} = \frac{f'_1}{m_{Si}} + \frac{4}{3} \left( \frac{f'_1}{m_{Si}} \right)^2 L^{-1}(\omega^2) \quad (3d)$$

$$(\delta l^{(s)})^{T_2} = \frac{4\sqrt{2}}{3m_{Si}^2} f'_1 f'_2 L^{-1}(\omega^2), \quad (3e)$$

where

$$L(\omega^2) = \left( \frac{m_{Fe}}{m_{Si}} \right) \omega^2 - \frac{4}{3m_{Si}} (f'_1 + 2f'_2). \quad (4)$$

Here we have placed the mass dependence in  $\delta l^{(s)}$  rather than in  $g_0$ . This amounts to a trivial redefinition of these matrices and does not alter any of the numerical results to follow. The Green's function itself was calculated using standard techniques.

The results of the local mode calculations are summarized in Fig. 3. There we plot defect mode energy,  $E = \hbar\omega$ , for those values of  $\omega^2$  which satisfy Eq. (2), as a function defect spring strength. For simplicity, we have considered defects of the form,  $f'_1/f_1 = f'_2/f_2 = \alpha$ , where  $\alpha$  is varied from 0 to 2. The modes are labeled by the irreducible representation of  $T_d$  according to which their associated displacement vectors transform. Also presented for comparison are the results of a five-atom "molecular" calculation in which the Fe and its four neighboring Si atoms move in the presence of a lattice which is elsewhere stationary.

The relevant feature of these results for the present work is that a 9 meV resonant mode, having width

1.2 meV and  $T_2$  symmetry, is obtained for a spring constant ratio,  $\alpha$ , of 0.11. The width calculated here is in close agreement with the width of the R lines shown in Fig. 1b. Now, modes with  $T_2$  symmetry involve motion of the four Si atoms and the Fe atom. Calculations for the two isotopes,  $^{54}\text{Fe}$  and  $^{56}\text{Fe}$ , made at  $\alpha = 0.11$  reveal an energy difference of 0.17 meV, or, in terms of the expected wavelength shift of the R line, of about 1.7 Å. The energy difference is due to the fact that the Fe atom moves in this mode.

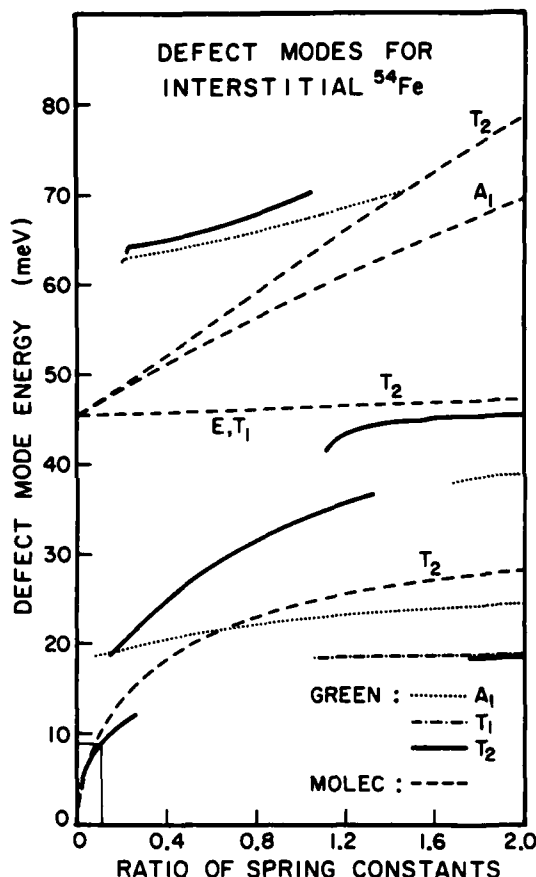


Fig. 3. The energy and symmetry of defect modes for interstitial  $^{54}\text{Fe}$  as a function of the defect spring constants. The results of the Green's function and molecular calculations are described in the text. The defect spring constant ratio indicated for the 9.0 meV mode is 0.11.

Indeed, in the limit of vanishing defect spring constants, the motion in the lowest-energy  $T_2$  mode becomes increasingly that of Fe alone, the actual limit corresponding to free translation of the Fe in a rigid lattice. We expect the dependence on  $m_{Fe}$  of the lowest-energy mode in the weak-perturbation limit to also be characteristic of more elaborate models in which, for example, second-nearest-neighbor interactions are included, or site symmetry is lowered. For comparison we have made similar calculations for substitutional Fe isotopes in Si, recovering approximately the same numeri-

cal result for the energy shift as well as the same limiting behavior of the Fe atom.

As a test of our theoretical techniques, we have made calculations on interstitial Cu in Si for comparison with other experimental data. Weber et al. have identified resonant phonon modes of energies 6.96 meV and 7.03 meV for the isotopes,  $^{65}\text{Cu}$  and  $^{63}\text{Cu}$ , respectively.<sup>12</sup> The results of our calculations made near 7.0 meV predict an isotopic energy shift of about 0.11 meV. Apart from obvious refinements that could be made on our model, this value is in quite reasonable agreement with experiment.

From the above discussion it appears that there is a basic disagreement between the theoretical predictions and the experimental results for Fe in Si. It may be possible to draw a number of conclusions from this disagreement. We might conclude that neither the P,Q,R

lines nor the lines ascribed to an isolated Fe complex are in fact related to Fe after all. This would then mean that the other pieces of evidence that led to the identification of these lines as involving Fe would have to be re-examined and explained in some other way. Finally, it may be that these luminescence spectra do involve Fe and that the so-called "phonon replicas" are in fact electronic excited states of the Fe.

**Acknowledgement**—We would like to gratefully acknowledge the support of the Office of Naval Research and Defense Advanced Research Projects Agency under Contract No. NO0014-81-C-0285. Further, two of us (T. E. S. and R. M. F.) received financial assistance from the Natural Sciences and Engineering Research Council of Canada. The samples were provided by Hughes Research laboratories (J. P. Baukus and O. J. Marsh).

### References

1. R. Sauer and J. Weber, "Photoluminescence Characterization of Deep Defects in Silicon" in *Proceedings of the 12th International Conference on Defects in Semiconductors*, Amsterdam, August 31–September 3, 1982, and the references contained therein.
2. G.S. Mitchard, S.A. Lyon, K.R. Elliott, and T.C. McGill, *Solid State Commun.* **29**, 425 (1979).
3. T. E. Schlesinger and T. C. McGill, *Phys. Rev.* **B25**, 7850 (1982).
4. J. Weber and P. Wagner, *J. Phys. Soc. Jap.* **49**, 263 (1980).
5. J. Weber, R. Sauer, and P. Wagner, *J. of Lumin.* **24/25**, 155 (1981).
6. M. L. W. Thewalt, U. O. Ziemelis, and R. R. Parsons, *Solid State Commun.* **39**, 27 (1981).
7. M. L. W. Thewalt, U. O. Ziemelis, and R. R. Parsons, *Phys. Rev.* **B24**, 3655 (1981).
8. K. Wunstel and P. Wagner, *Solid State Commun.* **40**, 797 (1981).
9. A. A. Maradudin, E. W. Montroll, G. H. Weiss, and I. P. Ipatova, *Solid State Physics*, Suppl. 3, 2nd ed. (Academic Press, New York, 1971), ch. 8.
10. R. J. Hauenstein, R. M. Feenstra, and T. C. McGill (to be published).
11. Maradudin et al., *ibid.*, p. 424.
12. J. Weber, H. Bauch, and R. Sauer, *Phys. Rev.* **B25**, 7688 (1982).

## LOCAL PHONON MODE CALCULATIONS FOR POINT DEFECTS IN Si

R. J. Hauenstein, T. C. McGill, and R. M. Feenstra\*

*California Institute of Technology*

*Pasadena, California 91125*

*and*

*\*IBM Thomas J. Watson Research Center*

*Yorktown Heights, New York 10598*

Localized and resonant phonon modes have been calculated, using the Green's function technique for substitutional and  $T_d$ -interstitial defects in Si. Energies and symmetries are presented as a function of the defect-bulk interaction for Fe and Cu defect modes. In all cases a single defect-mass-dependent, low energy  $T_2$  mode is predicted. An isotope shift of 0.16 meV of the 9 meV photoluminescence feature is calculated for interstitial Fe upon the substitution,  $^{54}\text{Fe}$  for  $^{56}\text{Fe}$ . No shift is observed experimentally. It is concluded that the observed 9 meV feature is not a vibrational excitation of an Fe defect complex in Si.

## 1. Introduction

The properties of transition-metal impurities in Si, because of their tendency to form deep-level defect complexes which may drastically alter electronic properties, have been actively investigated.<sup>1</sup> The technique of photoluminescence is particularly useful in determining the nature of the defect. The photoluminescence spectra are informatively structured, often containing features attributed to local vibrational modes of the defect. One type of local vibrational mode which may occur is a "resonant" mode. Resonant modes occur at bulk lattice frequencies and involve large amplitudes of vibration near the defect and smaller but non-vanishing amplitudes away from the defect site over some small frequency range. Identification of local modes provides information on the strength of the defect-bulk interaction, site symmetry, and local lattice relaxation and provides a consistency check in the identification of defects.

In this paper we use the Green's function technique to calculate the local vibrational modes due to substitutional and  $T_d$ -interstitial Fe and Cu atoms in Si. We shall show that in all cases we should expect a shift in the local mode energy due to isotopic replacement of the defect species. We shall see that our calculations are consistent with the 7 meV feature seen in Cu photoluminescence but not with the

9 meV Fe satellite. Finally, we shall argue that the 9 meV Fe satellite, if properly a feature of an Fe defect complex, cannot be an Fe local phonon.

We consider a model of the Si lattice in which only nearest-neighbor (NN) interactions are present. There are then only two parameters required to describe the lattice dynamics.<sup>2</sup> The appropriate linear combinations of these parameters represent "bond-stretching" and "bond-bending" spring constants,  $f_1$  and  $f_2$ , respectively. Bond-stretching and -bending springs provide a restoring force for displacements along and perpendicular to the equilibrium bond direction, respectively. In this model, the bond-bending springs provide the  $k$ -dependence of the transverse-acoustic (TA) and transverse-optical (TO) branches of the bulk-phonon spectrum.

## 2. Computational Method

The Green's function method was used to determine the local vibrational modes for Fe and Cu impurities in Si. It can be shown<sup>3</sup> that the local mode frequencies  $\omega$  satisfy

$$\text{Re}(\det[1 - G^0(\omega^2)\delta L(\omega^2)]) = 0. \quad (1)$$

In this expression,  $G^0$  is the Green's function matrix of the host Si lattice, and  $\delta L$  is the perturbation matrix which contains the mass and spring constant defect. The substitutional defects considered in this paper consist of a mass defect at the substitutional site and a NN-interaction defect with the four surrounding sites. In this case,  $G^0$  and  $\delta L$  are 15 by 15 matrices determined in the space of coordinates,  $x_1, y_1, z_1, \dots, z_5$ , of the five lattice sites directly affected by the defect.

For interstitial defects, we extend Eq. (1) to include the extra degrees of freedom due to the interstitial by defining

$$\hat{G}^0 \equiv \begin{pmatrix} G^0 & 0 \\ 0 & g \end{pmatrix} \quad \delta \hat{L} \equiv \begin{pmatrix} \delta L & A \\ A^\dagger & \delta L \end{pmatrix}, \quad (2)$$

where  $G^0$  and  $g$  are Green's functions for the bulk and a (general) interstitial defect complex isolated from each other. The bulk-defect coupling occurs through  $A$ , and  $\delta L$  and  $\delta L$  contain the resultant perturbations on the respective isolated systems. The interstitial defect modes are then found by using  $\hat{G}^0$  and  $\delta \hat{L}$  in Eq. (1). For the interstitial point-defect considered in this paper, four Si sites are affected by the perturbation; hence,  $G^0$  and  $\delta L$  are 12 by 12, and  $\hat{G}^0$  and  $\delta \hat{L}$  15 by 15 matrices, respectively.

All the point-defects treated here lie at positions having  $T_d$  symmetry. This is clearly true for a substitutional site. The  $T_d$ -interstitial site lies at the center of the fcc conventional unit cell coordinated by four Si atoms. The perturbations  $\delta\mathbf{L}$  and  $\delta\hat{\mathbf{L}}$  are chosen to preserve the  $T_d$  symmetry. Accordingly, we decompose the five-atom, 15-dimensional representation of  $T_d$  into its irreducible representations as

$$\Gamma = A_1 \oplus E \oplus T_1 \oplus 3T_2. \quad (3)$$

The matrices  $\mathbf{G}^0$  and  $\delta\mathbf{L}$  (or  $\hat{\mathbf{G}}^0$  and  $\delta\hat{\mathbf{L}}$ ) are block-diagonalized when expressed in the basis of "collective coordinates" which transform according to these irreducible representations. The form of the block-diagonalization and the collective coordinates are reported elsewhere.<sup>4</sup> Here, we simply observe that the independent, non-zero matrix elements are labeled by the representation ( $A_1, \dots, T_2$ ) and occurrence (1, ..., 3). There are nine independent elements to evaluate for each matrix.

The bulk Green's function matrix is evaluated from the two-parameter model discussed above. We obtain the bond-stretching and -bending spring constants,  $f_1 = 9.33 \text{ eV}/\text{\AA}^2$  and  $f_2 = 0.544 \text{ eV}/\text{\AA}^2$ , by fitting the experimental values,<sup>5,6</sup>  $\hbar\omega_{\text{LOF}} = 64.3 \text{ meV}$  and  $\hbar\omega_{\text{TAx}} = 18 \text{ meV}$ , for bulk Si exactly. From this, the eigenvalues and eigenvectors of the dynamical matrix are used to determine  $\mathbf{G}^n(\omega^2)$  numerically using standard techniques.<sup>4</sup> In the present calculations, a scheme was devised to achieve even energy binning in  $\omega$  rather than  $\omega^2$ , as in previous work.<sup>4,7</sup> The energy bin size of  $\hbar(\Delta\omega) = 0.03215 \text{ meV}$  thereby obtained results in greater precision at low energies. Note that this number is *not* the limit of precision of the defect mode energies but simply the interval spacing at which  $\mathbf{G}^0$  is evaluated. The isolated interstitial Green's function is given by  $\mathcal{G} = (1/\omega^2)\mathbf{1}$  where, here,  $\mathbf{1}$  is the three by three unit matrix.

The perturbation  $\delta\mathbf{L}$  for the substitutional defect consists of a mass perturbation,  $\Delta m = m_{\text{sub}} - m_{\text{Si}}$ , and a perturbation in the defect-Si spring constants,  $f'_i = f_i + \Delta f_i$ ,  $i = 1, 2$ . In order to satisfy the infinitesimal rotation-invariance condition,<sup>8</sup> it is sufficient to connect 2NN bond bending springs  $\mu$  among the four NN Si atoms. It is easily shown that we must have  $\mu = -(\Delta f_2)/4$ . In practice, the addition of the springs  $\mu$  to the five-atom complex has negligible effect on local mode energies, but their inclusion allows variation of  $\Delta f_2$  which would otherwise be forbidden. Because the effective spring constant for the substitutional defect is  $4(f'_1 + 2f'_2)/3$ , the weak spring limit can now be considered in a reasonable way.  $\delta\mathbf{L}$  is given explicitly as

$$(\delta L)_{A_1} = \frac{\Delta f_1}{m_{Si}} \quad (4a)$$

$$(\delta L)_E = \frac{\Delta f_2}{4m_{Si}} \quad (4b)$$

$$(\delta L)_{T_1} = 0 \quad (4c)$$

$$(\delta L)_{T_2}^{11} = \frac{5}{6} \left( \frac{\Delta f_2}{m_{Si}} \right) \quad (4d)$$

$$(\delta L)_{T_2}^{22} = \frac{1}{m_{Si}} \left( \Delta f_1 - \frac{1}{3} \Delta f_2 \right) \quad (4e)$$

$$(\delta L)_{T_2}^{33} = \frac{4}{3m_x} (\Delta f_1 + 2\Delta f_2) - \frac{\Delta m}{m_{Si}} \omega^2 \quad (4f)$$

$$(\delta L)_{T_2}^{12} = \frac{\sqrt{2}}{6} \left( \frac{\Delta f_2}{m_{Si}} \right) \quad (4g)$$

$$(\delta L)_{T_2}^{13} = \sqrt{\frac{8}{3m_{Si}m_x}} (\Delta f_2) \quad (4h)$$

$$(\delta L)_{T_2}^{23} = \sqrt{\frac{4}{3m_{Si}m_x}} (\Delta f_1), \quad (4i)$$

where  $m_x = m_{Si}$  for substitutional defects.

The perturbation  $\delta \hat{L}$  for the interstitial case consists of connecting the interstitial atom of mass  $m_x$  to its four Si neighbors with defect stretching springs,  $f'_1$ . We could have, in addition, included defect bond-bending springs,  $f'_2$ , in analogy with the substitutional case just described. However, we are interested in the weak spring limit for Fe and Cu defects. In the substitutional calculation it is necessary to weaken  $f'_2$  to zero to reach this limit. In the interstitial case, we are adding springs. Further, we shall see that the weak spring limit involves motion of the defect atom only, so that adding the (small) springs  $f_2$  has little effect.  $\delta \hat{L}$  can be obtained from Eq. (4) with the substitutions,

$$\delta L \rightarrow \delta \hat{L} \quad \Delta f_1 \rightarrow f'_1 \quad \Delta f_2 \rightarrow 0 \quad \Delta m \rightarrow 0.$$

### 3. Results and Discussion

The lattice-dynamical results for bulk Si, as calculated from the two parameter model, are summarized in Figs. 1 and 2. In Fig. 1, we show the bulk dispersion curves and in Fig. 2 the bulk density-of-states (BDOS). The calculated X-point phonon energies are  $\hbar\omega_{LA,LOX} = 45.5$  meV and  $\hbar\omega_{TOX} = 61.7$  meV, compared to the respective experimental values,<sup>5</sup> 49.2 meV and 58.7 meV. In the units shown

in Fig. 2, the BDOS integrates to the value, 5.997, in comparison with the exact value of 6. Integrals over  $\text{Im} [G^0(\omega^2)]$  show comparable relative numerical precision. Hence, we expect that our calculated local phonon energies are good (with respect to computational error) to at least three significant figures.

In Fig. 3, we show the local modes calculated from Eq. (1) as a function of the parameter,  $\alpha = f'_1/f_1$ , for interstitial  $^{56}\text{Fe}$ . The local modes are labeled by the irreducible representations ( $A_1$ - $T_2$ ) of the symmetry group of the defect. In the figure, we see that the Green's function computation produces only  $A_1$  and  $T_2$  modes.  $A_1$  modes consist of "breathing" motion of the four Si neighbors and do not involve motion of the defect.  $T_2$  modes, on the other hand, are the only modes which couple defect-atom motion to Si-atom motion. Also, included in Fig. 3 are the results of a "molecular-defect-cluster" calculation in which the Fe and four Si atoms vibrate in a lattice which is immovable elsewhere. The molecular calculation is useful as a check on the Green's function computation for defect modes with strong spatial localization. This is the case in the lower left corner of Fig. 3 where, in the weak spring limit, the motion approaches that of Fe alone.

Photoluminescence spectra from certain Fe defect complexes in Si show a characteristic satellite about 9 meV below the principal line.<sup>9,10,11</sup> This satellite has been thought to be a local phonon mode involving Fe.<sup>10,11</sup> From Fig. 3, we see that a single  $T_2$  mode is predicted for  $^{56}\text{Fe}$  at a defect spring constant,  $f'_1 = (14.1\%)f_1$ . The calculated 9 meV mode involves significant Fe motion and undergoes a shift in energy of  $\hbar(\Delta\omega) = 0.16$  meV upon the isotopic replacement,  $^{56}\text{Fe} \rightarrow ^{54}\text{Fe}$  (see Fig. 5). We have carried out similar calculations for substitutional Fe, in which case, we compute an isotope shift of 0.17 meV. However, recent experiments, reported in these *Proceedings*, observe the lack of an isotope shift of the 9 meV feature.<sup>7</sup>

To test our theoretical technique, we have made local mode calculations for substitutional and interstitial Cu isotopes, for which an isotope shift has been observed.<sup>12</sup> Results similar to those shown in Fig. 3 were obtained for Cu; the weak spring results for all of our local mode calculations are presented in Fig. 4. There, we plot defect mode energy vs.  $\alpha$  where  $\alpha = f'_1/f_1 = f'_2/f_2$  for the substitutional defects. Experimentally, local phonon replicas at 6.96 meV and 7.03 meV, attributed to a Cu-pair complex, have been reported for  $^{65}\text{Cu}$  and  $^{63}\text{Cu}$ , respectively, by Weber et al.<sup>12</sup> We compute a shift of 0.11 meV, for both interstitial and substitutional Cu isotopes, in reasonable agreement with experiment, considering that our calculation was made for single-atom defects.

The Fe and Cu isotope shifts of the low energy  $T_2$  resonant modes are apparent in the local density-of-states (LDOS) shown in Fig. 5. The LDOS is given by

$-(1/\pi)\text{Tr}[(1 - G^0\delta L)^{-1}G^0]$ , where the trace sums over  $T_2$  matrix elements in this case. Strong resonances appear as sharp Lorentzian peaks in the LDOS. From Fig. 5, we see that the width of the resonances is greater for Fe ( $\sim 2$  meV) than for the more weakly bound Cu ( $\sim 0.7$  meV). We also note that the 2 meV resonance width is of comparable magnitude to the spectral width of the R-line observed in the Fe-In luminescence seen by Schlesinger *et al.*<sup>7,13</sup> It is worth noting here that we have also obtained a 9 meV local  $T_2$  mode of width  $\sim 2$  meV for substitutional In at a spring constant ratio,  $\alpha = 0.53$ .

#### 4. Conclusion

Our calculations of Fe local modes in Si show that a 9 meV phonon should involve appreciable Fe motion and should consequently undergo a shift in energy upon isotopic substitution. Although our calculations treated the highest symmetry case with a particularly simple phenomenological model, we expect this statement to remain valid in more general cases. First, Fe is a heavy defect and will likely participate in any observed low energy local vibration. Secondly, the effect of reducing site symmetry will alter labels (such as  $T_2$ ) but not the participation of Fe in low energy modes, which will, in general, be split by the symmetry-breaking. And finally, even in more complicated phenomenological interaction schemes, the strongest effects are short range, and these are the most important to the motion of a single atom (Fe).

Given this assertion, our calculations imply that if the 9 meV feature is an Fe phonon, it should undergo an isotope shift. However, measurements with different Fe isotopes show the expected shift not to occur (although certain experiments suggest that the 9 meV satellite might be an Fe feature). Also, no prominent phonon feature associated with bulk Si occurs near 9 meV. We conclude that the 9 meV feature is not a vibrational excitation of an Fe defect complex in Si.

**Acknowledgement**—We would like to gratefully acknowledge the support of the Office of Naval Research and Defense Advanced Research Projects Agency under Contract No. N00014-81-C-0285. We also thank T. E. Schlesinger for thoughtful discussion of his experimental results.

#### REFERENCES

1. R. Sauer and J. Weber, "Photoluminescence Characterization of Deep Defects in Silicon," in *Proceedings of the 12th International Conference on Defects in Semiconductors*, Amsterdam, August 31–September 3, 1982, and the references contained therein.
2. A. Grimm, A. A. Maradudin, I. P. Ipatova, and A. V. Subashiev, *J. Phys.*

*Chem. Solids* **33**, 775 (1972).

3. A. A. Maradudin, E. W. Montroll, G. H. Weiss, and I. P. Ipatova, *Solid State Physics*, Suppl. 3, 2nd ed. (Academic Press, New York, 1971), ch. 8.
4. R. M. Feenstra and T. C. McGill (submitted for publication in *Phys. Rev. B*).
5. B. N. Brockhouse, *Phys. Rev. Lett.* **2**, 256 (1959).
6. K. Kunc, M. Balkanski, and M. A. Nusimovici, *Phys. Stat. Sol.* **72**, 229 (1975).
7. T. E. Schlesinger and T. C. McGill, "Isotope Shifts of the P,Q,R Lines in In-Doped Si," in *Proceedings of the 163rd Meeting of the Electrochemical Society*, San Francisco, May 8-13, 1983.
8. Maradudin et al., *ibid.*, ch. 2.
9. T. E. Schlesinger and T. C. McGill, *Phys. Rev. B* **25**, 7850 (1982).
10. J. Weber and P. Wagner, *J. Phys. Soc. Jap.* **49**, 263 (1980).
11. J. Weber, R. Sauer, and P. Wagner, *J. of Lumin.* **24/25**, 155 (1981).
12. J. Weber, H. Bauch, and R. Sauer, *Phys. Rev. B* **25**, 7688 (1982).
13. T. E. Schlesinger, R. J. Hauenstein, R. M. Feenstra, and T. C. McGill, *Solid State Commun.* Vol. **46**, No. **4**, 321 (1983).

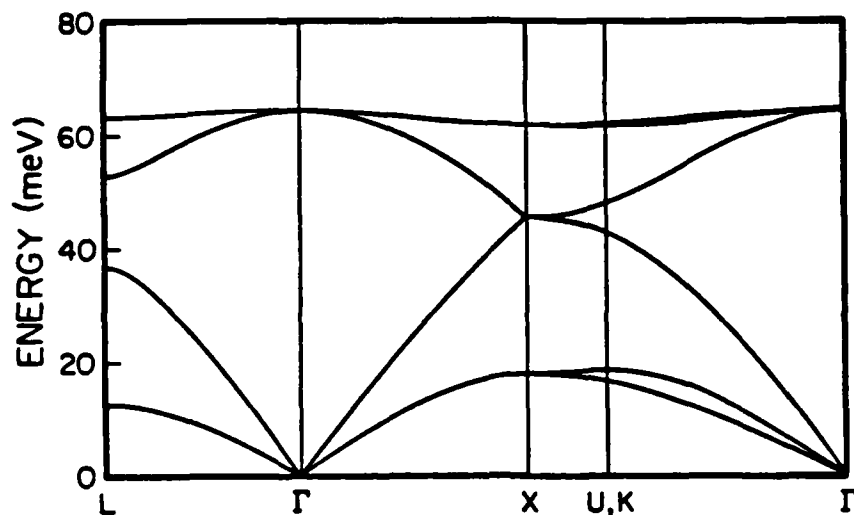


Fig. 1. The phonon dispersion curves for bulk Si as calculated from the two-parameter model discussed in the text. The spring constants  $f_1$  and  $f_2$  were determined by fitting the points,  $LO_\Gamma$  and  $TA_X$ , exactly.

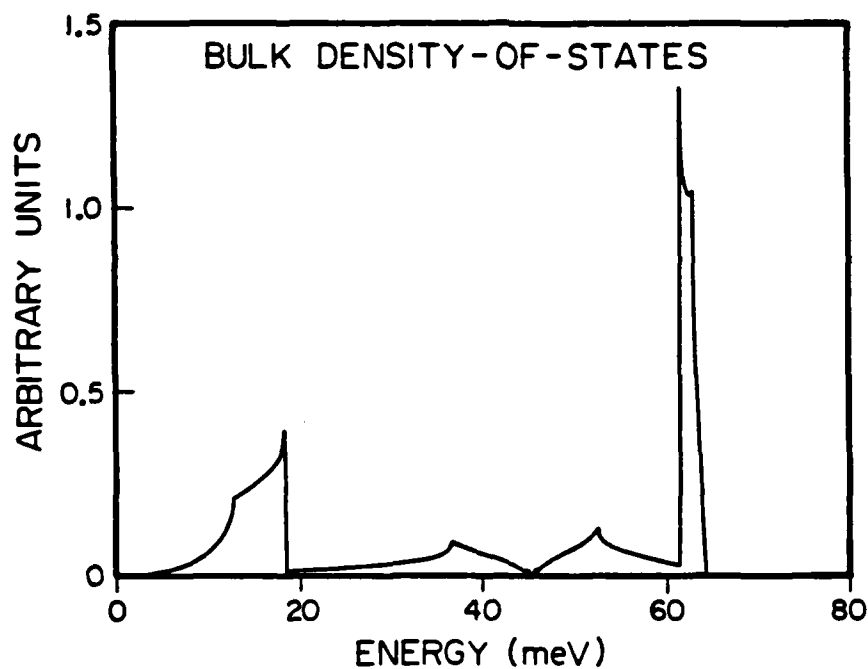


Fig. 2. The BDOS as calculated from the two-parameter model. The energy resolution is 0.03215 meV. In the units shown, the actual area under the curve is 5.997, compared to the exact value, 6.

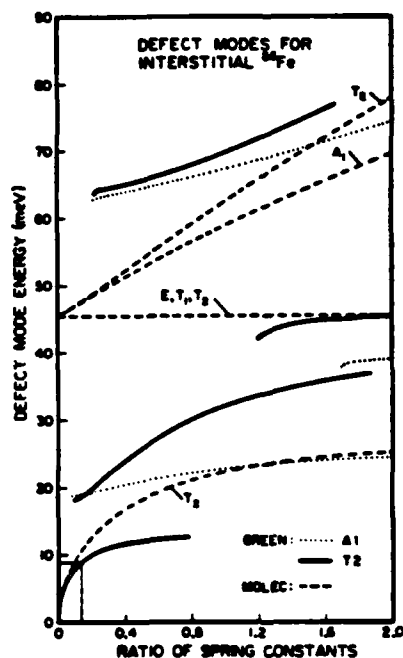


Fig. 3. The energy and symmetry of defect modes for interstitial  $^{56}\text{Fe}$  as a function of the parameter,  $\alpha$ , described in the text. The results of a molecular calculation are included for comparison with the Green's function results. For the 9 meV mode,  $\alpha = 14.1\%$ .

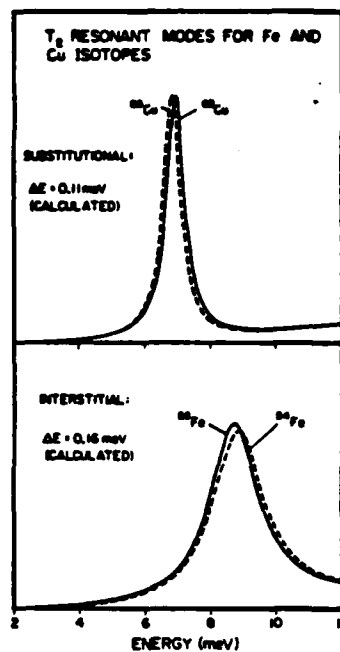


Fig. 5. The  $T_2$  LDOS showing the resonant character of the low energy Fe and Cu local modes. The local-mode energies calculated from Eq. (1) are 9.00 and 9.16 meV for  $^{56}\text{Fe}$  and  $^{54}\text{Fe}$ , and 6.89 and 7.00 meV for  $^{65}\text{Cu}$  and  $^{63}\text{Cu}$ , respectively.

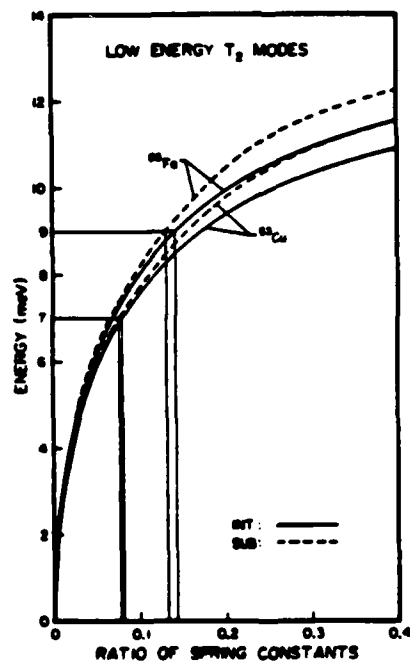


Fig. 4. The low energy  $T_2$  modes for  $T_2$ -interstitial and substitutional  $^{56}\text{Fe}$  and  $^{63}\text{Cu}$ , vs. the parameter,  $\alpha$ . For the 9 meV Fe mode,  $\alpha = 14.1\%$  and  $13.0\%$ , respectively. For the 7 meV Cu mode,  $\alpha = 7.88\%$  and  $7.64\%$ .

## APPENDIX F

### Isotope Shifts of the P,Q,R Lines in Indium-Doped Silicon

*T. E. Schlesinger and T. C. McGill*

*California Institute of Technology*

*Pasadena, California 91125*

We have measured the isotopic shifts of lines identified as local vibrational modes of Fe in Si. Two sets of lines were studied, the P,Q,R luminescence lines in Si:In ascribed to (Fe,In) pairs, and lines at about  $1.7\ \mu\text{m}$  attributed to an isolated Fe complex. Both sets of lines have what appears to be a 9 meV phonon replica. No shift is observed in any of these phonon modes to less than 0.03 meV, while theory predicts shifts of at least 0.15 meV. Further isotope shift experiments on lines attributed to (Cu,Cu) pairs, which show a 7 meV phonon mode, do show a change in phonon energy of about 0.07 meV. In this case, theory predicts a change in phonon energy of 0.11 meV.

Experiments have suggested that certain luminescence features, which have been observed in silicon, are due to transition metal impurities. In some cases, these transition metal impurities are thought to form complexes with other dopants present in the silicon, and, in other cases, they are thought to complex on their own. These transition metals have been of interest in device applications, as they shorten carrier lifetimes. Also, the luminescence produced seems to be due to very few centers and have very long lifetimes. A particular case is the so-called P,Q,R luminescence seen in Si:In which has been attributed to (Fe,In) pairs.<sup>1-4</sup> In this case, for example, the lifetime of the P line is about 200  $\mu\text{sec}$ , and there may be as few as  $10^{12} - 10^{13}$  centers per centimeter cubed responsible for the luminescence.<sup>1</sup> This luminescence is seen to be enhanced upon the deliberate introduction of Fe. Other luminescence has been observed which has been attributed to (Fe,Tl), (Fe,B), (Cu,Cu), (Cr,B) pairs and an isolated Fe complex.<sup>2,5</sup> These luminescence features consist usually of one or two no-phonon lines followed by a number of phonon replicas. In the case of those features which have been related to Fe, there is seen what has been called a characteristic local phonon mode of approximately 9.0 meV.<sup>4,5</sup> This phonon is thought to be a vibrational mode of the Fe. To test this assertion and also to more conclusively identify these luminescence features, we have conducted isotope shift experiments on two systems, thought to involve Fe, to see if we can observe a shift in the position of the phonon replica as a function of the isotope of Fe introduced into the sample. The first was the P,Q,R luminescence in Si:In (see Fig. 1), the P line having been identified as the no-phonon line and the R line being the phonon replica.<sup>4,6</sup> The second system studied was the

luminescence attributed to an isolated Fe complex seen in both n- and p-type Si at about  $1.7\ \mu\text{m}$ , (see Fig. 2),<sup>5</sup> the line at  $1.687\ \mu\text{m}$  actually consisting of two no-phonon lines followed by phonon replicas at  $1.704\ \mu\text{m}$  and  $1.709\ \mu\text{m}$ .

Two isotopes of Fe,  $^{56}\text{Fe}$  (99.93%-enriched) and  $^{54}\text{Fe}$  (97.08%-enriched) were obtained as oxide ( $\text{Fe}_2\text{O}_3$ ) from Oak Ridge National Laboratories. The oxide was subsequently reduced at  $700^\circ\text{C}$  for one hour in an atmosphere consisting of 12%  $\text{H}_2$  with the balance made up of He. We used float-zone Si:In samples with In concentration of  $2.8 \times 10^{16}\ \text{cm}^{-3}$  and n-type Si samples with resistivities between  $7\ \Omega\text{-cm}$  and  $12\ \Omega\text{-cm}$  for the luminescence experiments. The iron was evaporated onto the surface of the samples and then diffused in at  $1100^\circ\text{C}$ . The samples were then quenched quickly in deionized water. The surface was then cleaned using a Si etch ( $3\text{HNO}_3:1\text{CH}_3\text{COOH}:0.4\text{HF}$ ). Care was taken during the diffusion and quench to prevent the introduction of iron from undesired sources.

All of the spectra presented here were obtained at 4.2 K, with the samples mounted in a Janis variable temperature dewar, and using a Spectra Physics model 166 argon ion laser for above band gap excitation with the laser spot focussed on the sample. The laser was operated in CW mode with a peak output power of 0.5 W. The luminescence was then collected from the edge of the sample and directed through the entrance slits of a Spex model 1269 spectrometer and measured with an RCA model 7102 photomultiplier tube cooled to liquid nitrogen temperature or with an InAs or Ge detector as indicated in the figures.

In Figure 3, we present the spectra of the P and R lines for  $^{56}\text{Fe}$  and  $^{54}\text{Fe}$ . The spectra are the result of extensive signal averaging, which has yielded a greater sensitivity in determining relative line positions. As can be seen, there is no shift in the position of the P or the R line to at least 0.3 meV. In Figure 4, we present the no-phonon and phonon replicas of those attributed to an isolated iron complex. Again, there is no shift in these lines to at least 0.3 meV. Theoretical calculations predict shifts of the order of 0.16 meV in the phonon energies (approximately  $1.5\ \text{\AA}$  for the P,Q,R lines and approximately  $3.0\ \text{\AA}$  in the case of the isolated iron lines). We see very slight changes in one or two places in the position or linewidth of these lines. These are of the order of two or three hundredths of an meV and do not appear to be completely reproducible. Since we use masking tape to mount our samples onto a sample holder in the dewar, it is possible that stress introduced into the samples, when cooling them to 4.2 K, produces these slight variations. To illustrate the magnitude that such effects can attain, we can describe the motion of the electronic levels, E, with strain  $\epsilon$ , by a simple deformation potential  $c$ . If the strain is produced by the difference in the thermal expansion coefficient of the masking tape and the Si, then

$$\Delta E \sim ac\beta\Delta T$$

where  $\beta$  is the volume expansivity,  $\Delta T$  is the temperature change, and  $a$  is a numerical coefficient describing the nonuniformity and difference in the thermal expansivity. If we take  $c$  to be 1 eV,  $\beta$  to be  $10^{-5} \text{ K}^{-1}$  and  $\Delta T$  to be 300 K, then  $c\beta\Delta T = 2 \text{ meV}$ . Hence, our shift of a few hundredths of an meV could be accounted for by a coefficient  $a$  as small as  $10^{-3}$ .

To ensure that our samples were not initially contaminated with iron, we carried out DLTS measurements on them before any treatment, after annealing them but without evaporating iron on the surface, and after iron evaporation and diffusion. We found that the as-grown samples and those that were annealed but which did have iron evaporated on the surface showed no iron related deep levels to a concentration of less than  $10^{13} \text{ cm}^{-3}$ . Samples that did have iron deliberately introduced did show iron related deep levels which have been previously identified.<sup>7</sup>

To further test our experimental technique, we carried these same sort of isotope-shift experiments on lines which have been identified as due to (Cu,Cu) pairs. These show a no-phonon line followed by a phonon replica of 7.0 meV. For this experiment, we used two isotopes of Cu,  $^{65}\text{Cu}$  (99.70%-enriched) and  $^{63}\text{Cu}$  (99.89%-enriched), which were obtained as oxide (CuO) from Oak Ridge National Laboratories and subsequently reduced at  $650^\circ\text{C}$  for one hour in 12%  $\text{H}_2$  atmosphere with the balance He. The results are presented in Figure 5. As can be seen, there is a substantial shift in both the no-phonon line (0.07 meV) and phonon replica (0.15 meV). This shift in the no-phonon line is not unexpected.<sup>8</sup> Thus, the phonon energies for  $^{65}\text{Cu}$  and  $^{63}\text{Cu}$  are 6.98 meV and 7.05 meV, respectively. These numbers are in good agreement with theory which predicts a shift in the phonon energy of 0.11 meV and also in good agreement with the numbers reported for this same experiment by Weber et al.<sup>9</sup>

It seems, therefore, that there is a fundamental problem with the understanding of those luminescence features that are supposed to involve iron. It could be that those lines identified as phonon modes are, in fact, excited electronic states of Fe in the final state of the transition, or that the P,Q,R lines are not due to the presence of Fe.

**Acknowledgement**—We would like to gratefully acknowledge the support of the Office of Naval Research and Defense Advanced Research Projects Agency under Contract No. N00014-81-C-0285. Further, one of us (T. E. S.) received financial assistance from the Natural Sciences and Engineering Research Council of Canada. The samples were provided by Hughes Research laboratories (J. P. Baukus and O. J. Marsh).

## REFERENCES

1. G.S. Mitchard, S.A. Lyon, K.R. Elliot, and T.C. McGill, *Solid State Commun.* **29**, 425 (1979).
2. R. Sauer and J. Weber, "Photoluminescence Characterization of Deep Defects in Silicon" in *Proceedings of the 12th International Conference on Defects in Semiconductors*, Amsterdam, August 31- September 3, 1982, and the references contained therein.
3. T. E. Schlesinger and T. C. McGill, *Phys. Rev.* **B25**, 7850 (1982).
4. J. Weber, R. Sauer, and P. Wagner, *J. of Lumin.* **24/25**, 155 (1981).
5. J. Weber and P. Wagner, *J. Phys. Soc. Jap.* **49**, 263 (1980).
6. M. L. W. Thewalt, U. O. Ziemelis, and R. R. Parsons, *Phys. Rev.* **B24**, 3655 (1981).
7. K. Wunstel and P. Wagner, *Solid State Commun.* **40**, 797 (1981).
8. V. Heine and C.H. Henry, *Phys. Rev.* **B25**, 3795 (1975).
9. J. Weber, H. Bauch, and R. Sauer, *Phys. Rev.* **B25**, 7688 (1982).

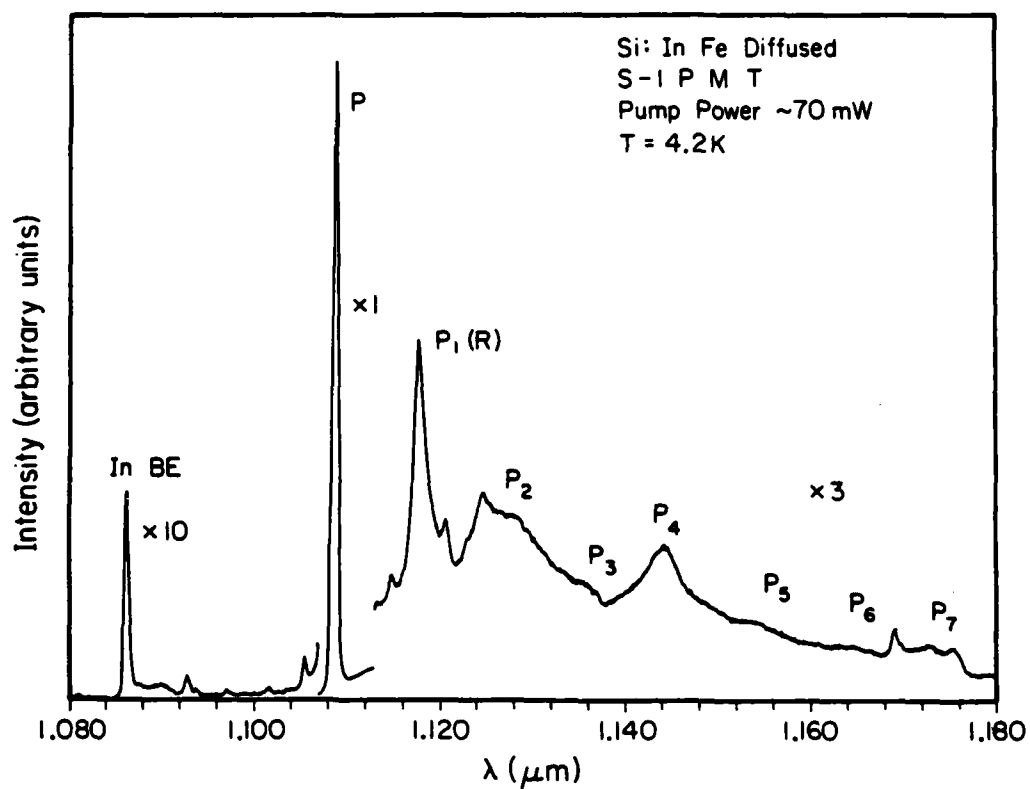


**Fig. 1.** The spectrum of Si:In after Fe diffusion. The P line being the no-phonon line and the R line the phonon replica of the P line. The Q line is seen only at higher temperatures.

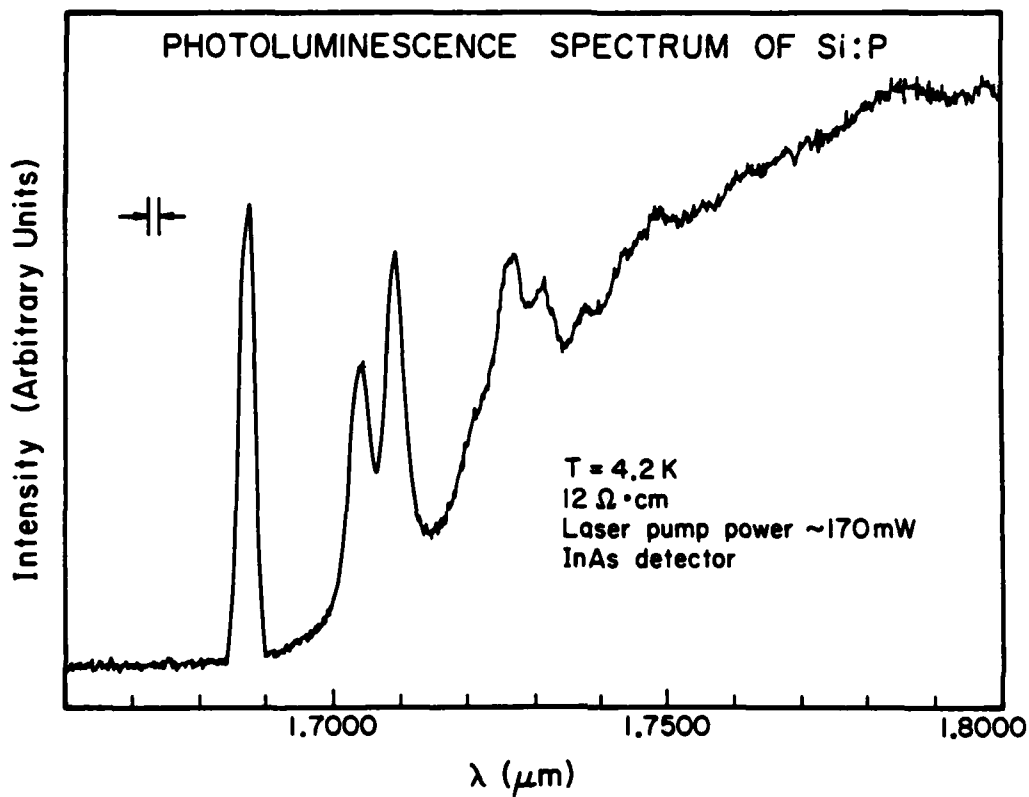


**Fig. 2.** The spectrum of Si:P after diffusion of natural Fe. The line at about  $1.687 \mu\text{m}$  actually consists of two no-phonon lines followed by phonon replicas at about  $1.704 \mu\text{m}$  and  $1.709 \mu\text{m}$ .

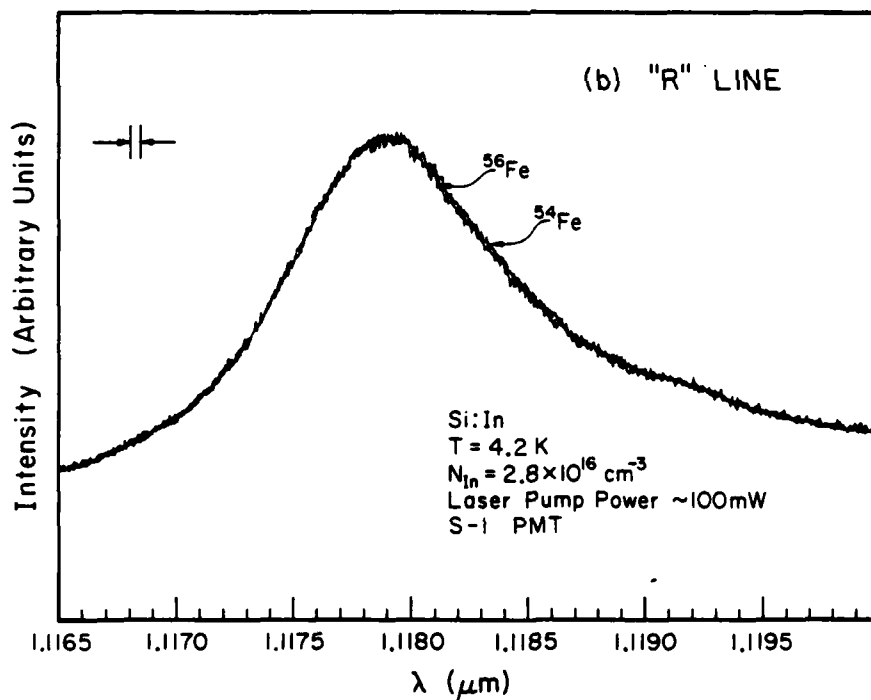
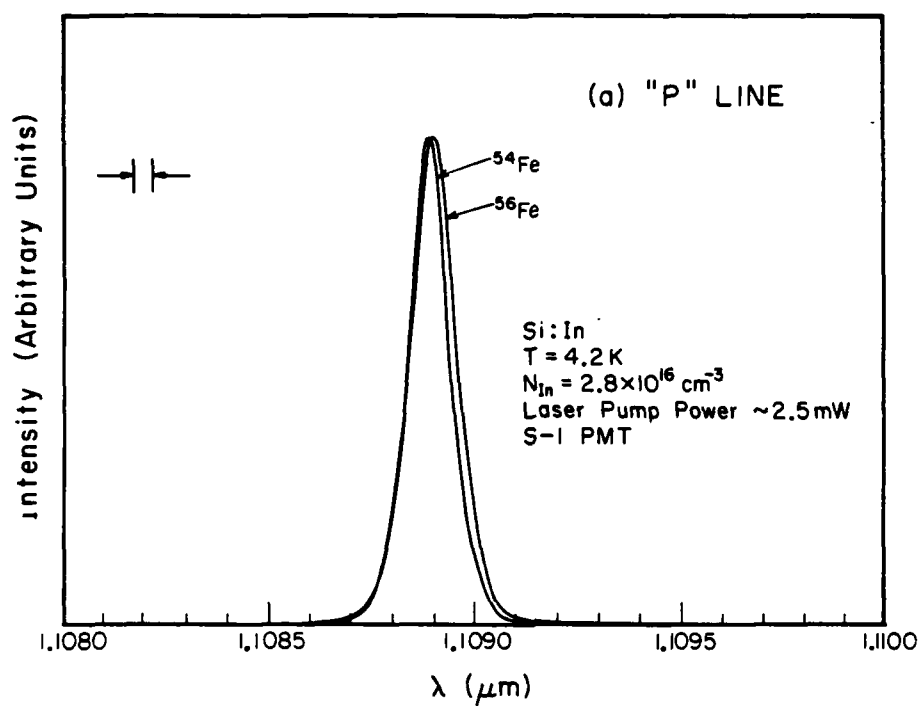


**Fig. 3.** The spectrum of Si:In after diffusion of  $^{56}\text{Fe}$  and  $^{54}\text{Fe}$ . (a) is the P line presented for both isotopes and (b) is the R line presented for both isotopes.

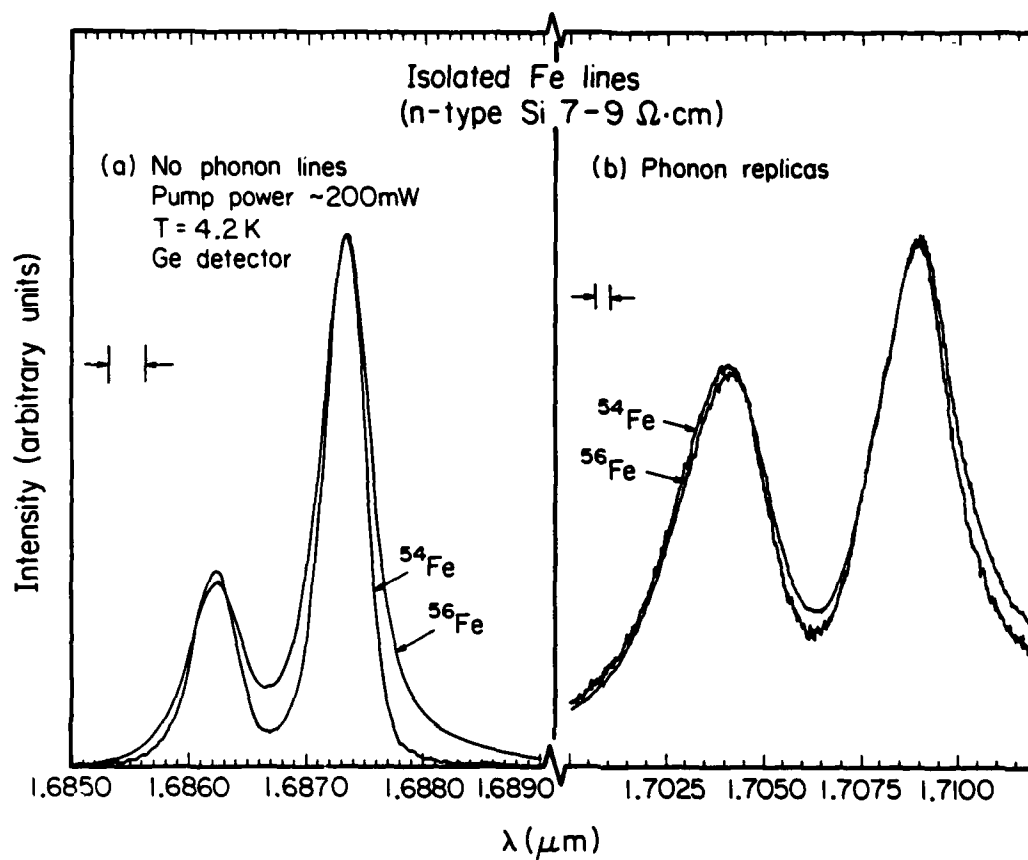


**Fig. 4.** The spectrum of the no-phonon lines and associated phonon replicas of the lines thought to be due to an isolated Fe complex. The results of the isotope shift experiments are presented here for both  $^{56}\text{Fe}$  and  $^{54}\text{Fe}$ .

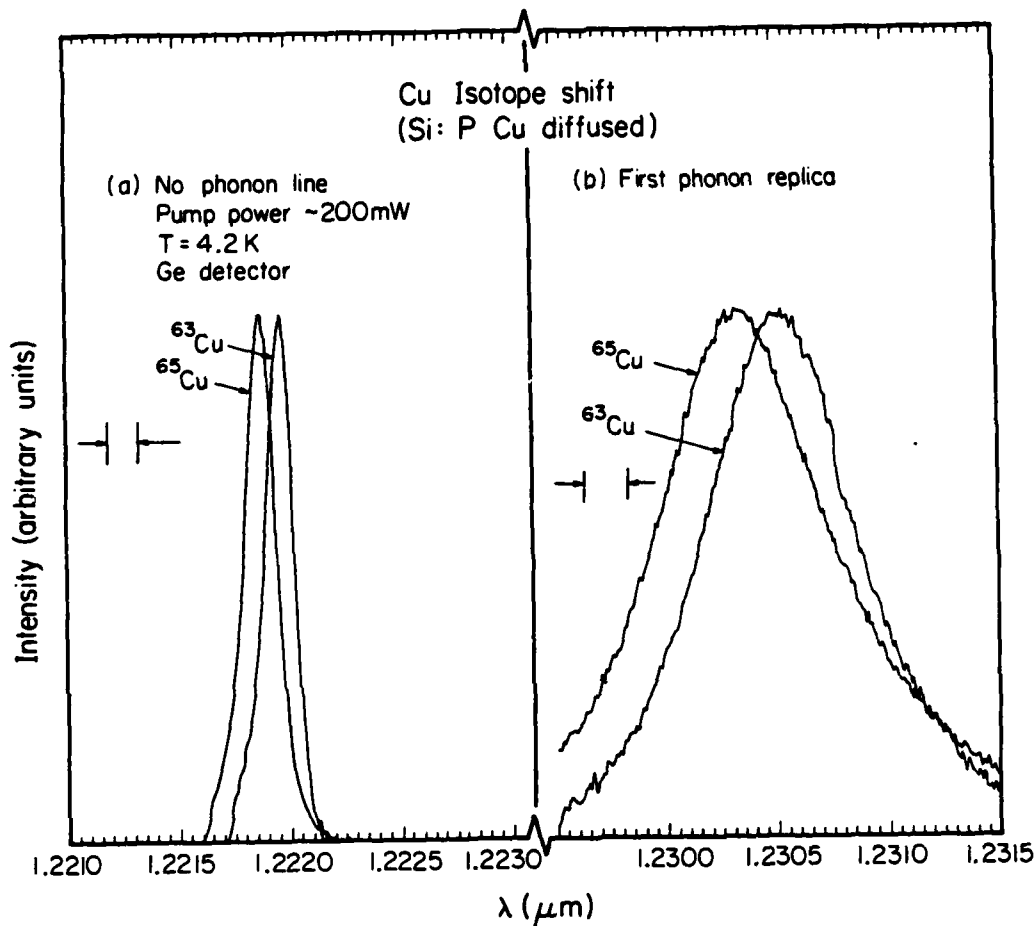
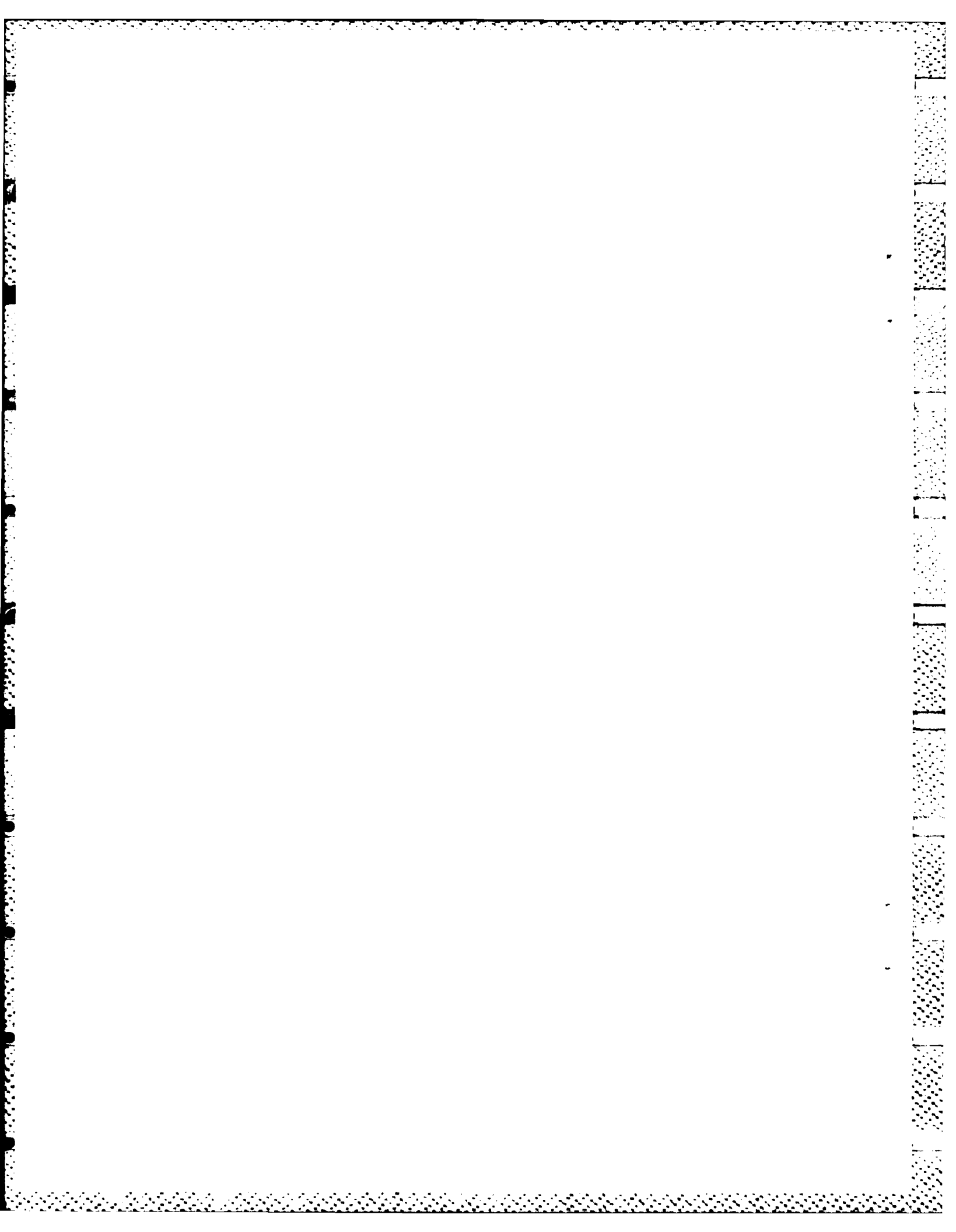


**Fig. 5.** The spectrum of the no-phonon and phonon replica of the lines thought to be due to (Cu,Cu) pairs. The results of the isotope shift experiment are presented here for both  $^{65}\text{Cu}$  and  $^{63}\text{Cu}$ . In this case an isotopic shift is clearly visible.



## Isotope-shift experiments on luminescence attributed to (Fe,B) pairs in silicon

T. E. Schlesinger and T. C. McGill

California Institute of Technology, Pasadena, California 91125

(Received 11 July 1983)

We present experimental results of isotope-shift experiments on luminescence features observed in silicon that have been attributed to (Fe,B) pairs. No change in phonon energy or shift in line positions is observed to at least 0.02 meV. This contradicts the expected change in phonon energy of 0.17 meV for an interstitial Fe impurity.

Luminescence features which have been attributed to the presence of iron in silicon have been observed. These features include luminescence interpreted as being due to (Fe,In), (Fe,Tl), (Fe,B) pairs and an isolated iron complex.<sup>1-4</sup> In a recent paper, we have presented the results of isotope-shift experiments performed on two of these systems.<sup>5</sup> In this Communication we present further results of isotope-shift experiments which we have performed on those luminescence features which have been attributed to (Fe,B) pairs. In Fig. 1 we present the spectrum of Si:B after Fe diffusion at 1100°C. We have used the labeling scheme of Sauer and Weber<sup>1</sup> to identify the prominent peaks at the high-energy end of the spectrum. The peak labeled  $\text{FeB}_1^0$  has been identified as a no-phonon line. The doublet labeled  $\text{FeB}_1^1$  and  $\text{FeB}_0^1$  has been identified as phonon replicas, with  $\text{FeB}_1^1$  being the replica of  $\text{FeB}_1^0$  and  $\text{FeB}_0^1$  being the replica of  $\text{FeB}_0^0$  (not visible in this spectrum at 4.2 K). This phonon mode is of about 9.6 meV and is thought to be a local vibrational mode of the iron.

We report here the results of an experiment to see if there were a change in this phonon energy as a function of the isotope of iron introduced into the sample. In fact, one would also expect, in general, a shift in the position of the no-phonon line as well since one might expect the spring constant binding the impurity to the lattice to be different for the initial and final electronic states. Thus the difference in the finite zero-point energy of the initial and final state will be different for a change in the impurity mass. A

complete discussion of this can be found in Ref. 6.

Two isotopes of Fe,  $^{56}\text{Fe}$  (99.93% enriched) and  $^{54}\text{Fe}$  (97.08% enriched), were used for this experiment. The Si:B samples had resistivities of 0.5 to 1.5  $\Omega\text{ cm}$ . The iron was evaporated onto the surface of the samples and then diffused in at 1100°C, following the method of Ref. 2. Care was taken during the diffusion and quench to prevent the introduction of Fe from uncontrolled sources. The spectra presented here were all obtained at 4.2 K with the samples mounted in a Janis variable temperature Dewar, with use of a Spectra Physics model 166 argon ion laser for above-band-gap excitation. The luminescence was collected from the edge of the sample and directed through the entrance slits of a Spex model 1269 spectrometer and detected with a North Coast Ge detector. The spectra showing the results of the isotope-shift experiments are the result of extensive signal averaging which has yielded a much improved signal-to-noise ratio.

In Fig. 2 we present the results of the isotope-shift experiment for the two isotopes. In the left-hand side of the figure we see the no-phonon line labeled  $\text{FeB}_1^0$  presented for both isotopes, and, in the right-hand side of the figure we see the phonon replicas labeled  $\text{FeB}_1^1$  and  $\text{FeB}_0^1$  presented for both isotopes. There is clearly no shift in either case to at least 0.3 Å. The very slight shift that may be visible in the no-phonon line of no more than 0.02 meV, we believe, may

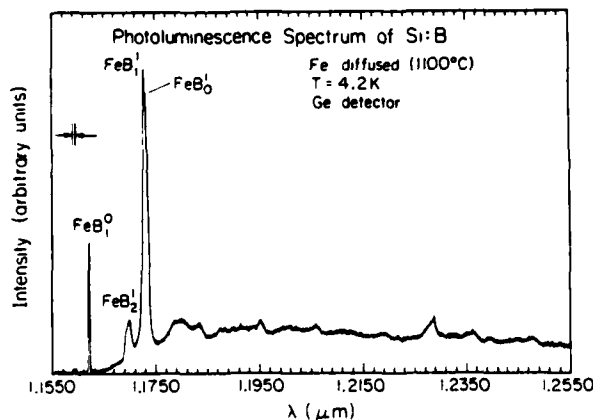


FIG. 1. Spectrum of Si:B after Fe diffusion at 1100°C. The line labeled  $\text{FeB}_1^0$  is the no-phonon line studied and the doublet labeled  $\text{FeB}_1^1$  and  $\text{FeB}_0^1$  is the phonon replica studied.

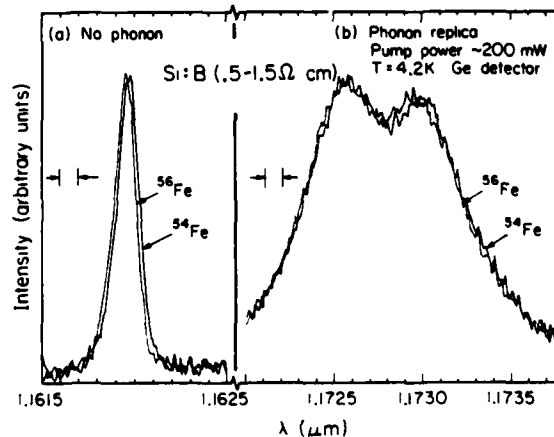


FIG. 2. Results of the isotope-shift experiment presented for both isotopes, the left-hand side of the figure showing the no-phonon line and the right-hand side of the figure showing the phonon replica.

be due to stress introduced into the sample when it is cooled to 4.2 K. A simple estimate based on a deformation potential and taking into account the thermal expansivity of silicon can easily account for small shifts such as this.<sup>7</sup>

Theoretical calculations predict a change in the phonon energy of 0.17 meV for an interstitial iron impurity.<sup>5</sup> This corresponds to a shift of at least 2.0 Å at these wavelengths for the position of the phonon replica. This lack of an isotopic shift is consistent with the results of the isotope-shift experiments performed on the other luminescence features that have been attributed to the presence of iron. It is however, incompatible with the present identification of this

center, and particularly, the identification of the phonon mode as a local vibrational mode of the iron.

#### ACKNOWLEDGMENTS

We would like to gratefully acknowledge the support of the Office of Naval Research and Defense Advanced Research Projects Agency under Contract No. N00014-81-C-0285. We would also like to acknowledge useful discussions with R. J. Hauenstein. Further, one of us (T. E. S.) received financial assistance from the Natural Sciences and Engineering Research Council of Canada.

<sup>1</sup>R. Sauer and J. Weber, in Proceedings of the 12th International Conference on Defects in Semiconductors, Amsterdam, 1982, (unpublished).

<sup>2</sup>T. E. Schlesinger and T. C. McGill, Phys. Rev. B **25**, 7850 (1982).

<sup>3</sup>J. Weber and P. Wagner, J. Phys. Soc. Jpn. **49**, 263 (1980).

<sup>4</sup>J. Weber, R. Sauer, and P. Wagner, J. Lumin. **24/25**, 155 (1981).

<sup>5</sup>T. E. Schlesinger, R. J. Hauenstein, R. M. Feenstra, and T. C. McGill, Solid State Commun. **46**, 321 (1983).

<sup>6</sup>V. Heine and C. H. Henry, Phys. Rev. B **11**, 3795 (1975).

<sup>7</sup>T. E. Schlesinger and T. C. McGill, in Proceedings of the 163rd Meeting of the Electrochemical Society, San Francisco, 1983 (unpublished).

## Photoluminescence of Si-rich Si-Ge alloys

G. S. Mitchard and T. C. McGill

*California Institute of Technology, Pasadena, California 91125*

(Received 27 July 1981)

A detailed study of the photoluminescence spectrum of  $\text{Si}_{1-x}\text{Ge}_x$  is presented for  $x \approx 0.1$ . Undoped and In-doped alloy samples are investigated. Spectral features are identified, and the effects of the disordered nature of the alloy on the luminescence spectrum are discussed. In particular, mechanisms for the observed broadening of bound-exciton luminescence are discussed, and the shift in alloy luminescence energy is obtained. At low temperatures a luminescence feature is observed which may result from recombination of excitons bound to local fluctuations in alloy composition.

## I. INTRODUCTION

The properties of alloy semiconductors have been of general interest for some time. Such alloys provide a convenient system with which to experimentally and theoretically study the effects of disorder, which can be varied with alloy composition. The band gap can also be varied with alloy composition, and for this reason considerable effort has been directed towards the development of intrinsic and extrinsic alloy optoelectronic devices. The study of the luminescence properties of alloy semiconductors can provide useful and relatively easily interpreted information regarding the properties of the alloys and the consequences of their disordered nature. Most attention has been directed towards the III-V ternary alloys, where luminescence processes have been studied extensively.<sup>1-3</sup> Luminescence of II-VI ternary alloys has also been studied, most notably  $\text{Hg}_{1-x}\text{Cd}_x\text{Te}$  (Ref. 4) where ir detector applications are particularly important.

Another alloy material of interest is the binary alloy  $\text{Si}_{1-x}\text{Ge}_x$ . The luminescence properties of  $\text{Si}_{1-x}\text{Ge}_x$  are not particularly well known, although free- and bound-exciton,<sup>5</sup> donor-acceptor,<sup>6</sup> and electron-hole droplet<sup>7</sup> recombination has been observed in Ge-rich alloys. In this paper we report the first detailed measurements of luminescence from Si-rich alloys, in particular alloys for which  $x \approx 0.1$ . Intrinsic and impurity-related luminescence is discussed, as well as certain properties of the luminescence which arise as a result of the compositional disorder of the alloy. In particular, we have been able to identify the luminescence features which result from free-exciton and bound-exciton recombination in the alloy. Also,

mechanisms for the observed bound-exciton luminescence broadening are discussed. Comparison of the luminescence energies from Si and the alloy samples results in values for the band-gap shift and free-exciton binding energy for the values of the composition parameter  $x$  which we were able to study. Finally, some evidence is presented which suggests that we observe at low temperatures luminescence which is the result of recombination of excitons bound to local fluctuations in alloy composition.

The remainder of this paper is organized in the following way. In Sec. II, we discuss the  $\text{Si}_{1-x}\text{Ge}_x$  alloy samples studied, and the general features of the experimental technique. In Sec. III, the results of measurements on the undoped  $\text{Si}_{1-x}\text{Ge}_x$  samples are presented and discussed. In Sec. IV, we consider the results obtained for one In-doped  $\text{Si}_{1-x}\text{Ge}_x$  sample. In Sec. V, we discuss the general mechanisms for luminescence line broadening in the alloy, compare the alloy luminescence energies with those observed in Si, and consider the evidence for excitons bound to composition fluctuations. Finally, in Sec. VI, the results are summarized.

## II. EXPERIMENTAL CONSIDERATIONS

## A. Si-Ge alloy samples

In this paper, we present measurements of the photoluminescence properties of three  $\text{Si}_{1-x}\text{Ge}_x$  samples, two of which were not intentionally doped and the third of which was doped with In. The crystals were grown by the Czochralski technique.

Impurity concentrations and alloy compositions were determined at Hughes Research Laboratories, where the crystals were grown. Impurity concentrations were established on the basis of Hall-effect measurements. These measurements show that residual concentrations of B and P impurities are present in all the samples. Alloy compositions were obtained from a variety of techniques; results of the electron microprobe, density, and x-ray diffraction measurements were in excellent agreement. The samples studied, their impurity concentrations, and their alloy compositions are given in Table I.

### B. Experimental technique

The Si-Ge alloy samples described above were mechanically etched, and then mounted in a Janis variable-temperature cryostat. The luminescence resulted from above band-gap optical excitation by a Spectra-Physics Model 166 Ar<sup>+</sup> laser, which could be operated in pulsed or cw mode. The luminescence was collected from the edge of the sample, wavelength-analyzed with a Spex Model 1269 spectrometer, and detected with an RCA 7102 S-1 photomultiplier cooled to liquid-nitrogen temperature. The photomultiplier output was processed with standard photon-counting electronics, acquired on a Nuclear Data ND-60 multichannel analyzer, and finally passed to a PDP 11/34 computer for analysis and storage.

## III. EXPERIMENTAL RESULTS AND DISCUSSION FOR UNDOPED Si<sub>1-x</sub>Ge<sub>x</sub>

In this section, the results of the application of the photoluminescence technique to the undoped samples are considered. Two undoped Si<sub>1-x</sub>Ge<sub>x</sub> samples were available, C077 ( $x=0.11$ ) and C021-3 ( $x=0.067$ ). As indicated in Table I, these samples

have low residual concentrations of B and P impurities, in spite of not being intentionally doped.

### A. Typical photoluminescence spectrum and identification of phonon replicas

A typical low-temperature photoluminescence spectrum of sample C077 is shown in Fig. 1. Two broad features are visible at the high-energy end of the spectrum and are labeled FE (free exciton) and BE<sub>p</sub> (bound exciton). Replicas of these lines, labeled FE(TO) and BE<sub>p</sub>(TO), are observed approximately 58 meV lower in energy. Since this is the transverse-optical (TO) phonon energy in Si, the low-energy lines are interpreted as being due to TO phonon replicas of the higher-energy lines.

### B. Identification of free-exciton luminescence

In this section we consider the effect of increasing the sample temperature on the photoluminescence spectrum of sample C077. In Fig. 2 we see that as the temperature is increased the line labeled BE<sub>p</sub> thermalizes with respect to the line labeled FE. Above 10 K (Fig. 3), the line labeled BE<sub>p</sub> is no longer visible, and the line labeled FE assumes a shape characteristic of free-exciton (FE) recombination in Si. In intrinsic Si, FE recombination luminescence has been fitted very accurately with a line shape,<sup>8</sup>

$$I(E) \propto \sqrt{E-E_0} \exp \left[ \frac{E-E_0}{k_B T} \right], \quad (1)$$

where  $I(E)$  is the luminescence intensity at photon energy  $E$ ,  $E_0$  is the FE threshold energy, and  $T$  is the temperature. In this expression we assume parabolic FE bands and a Boltzmann distribution of FE center-of-mass kinetic energies. The high-temperature luminescence from sample C077 can

TABLE I. Si<sub>1-x</sub>Ge<sub>x</sub> alloys studied using photoluminescence. The samples were grown and characterized at Hughes Research Laboratories.

Sample	$N_B$ (cm <sup>-3</sup> )	$N_P$ (cm <sup>-3</sup> )	$x$ $N_{In}$ (cm <sup>-3</sup> )	Electron microprobe	Density	X-ray diffraction
C077	$3.6 \times 10^{13}$	$2.8 \times 10^{13}$		0.1115	0.113	0.113
C021-3	$2.3 \times 10^{14}$	$4.1 \times 10^{14}$		0.0677	0.0685	
C093	$5.0 \times 10^{15}$	$5.3 \times 10^{14}$	$2.5 \times 10^{16}$			0.104

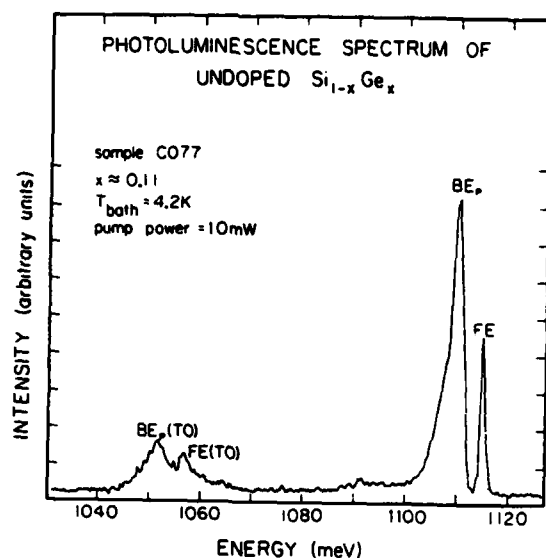


FIG. 1. Typical photoluminescence spectrum of undoped  $\text{Si}_{1-x}\text{Ge}_x$  sample C077. Refer to the text for an explanation of the line assignments.

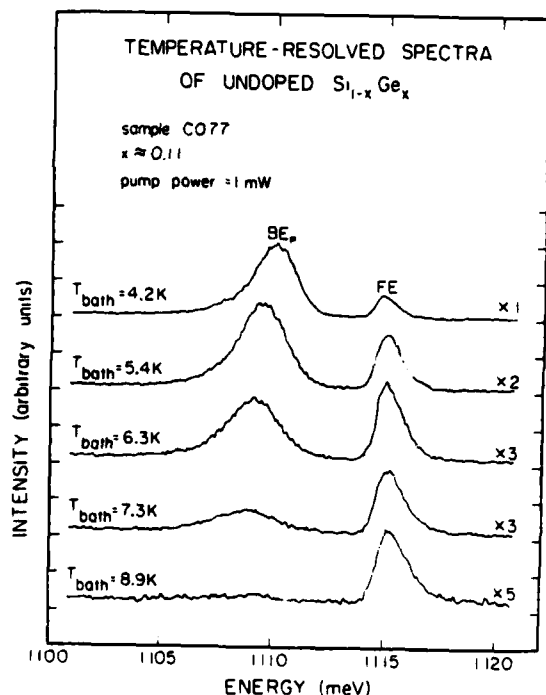


FIG. 2. Temperature-resolved spectra of undoped  $\text{Si}_{1-x}\text{Ge}_x$  sample C077 from 4.2 to 8.9 K. The scale factors (e.g.,  $\times 2$ ) give the relative intensity magnification. Note that thermalization of the line labeled  $\text{BE}_p$  is observed. In addition, the  $\text{BE}_p$  peak position shifts to lower energy as the temperature is increased. At high temperatures, the luminescence of the line labeled FE assumes a shape characteristic of free-exciton luminescence in Si.

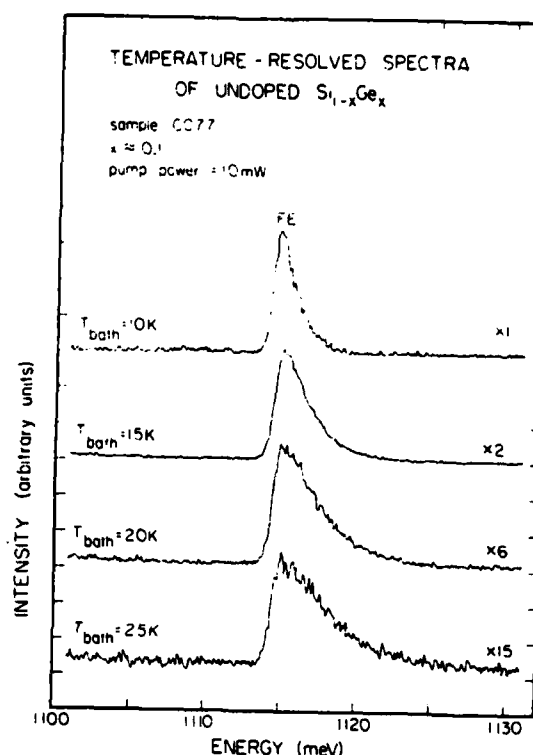


FIG. 3. Temperature-resolved spectra of undoped  $\text{Si}_{1-x}\text{Ge}_x$  sample C077 from 10 to 25 K. The scale factors (e.g.,  $\times 2$ ) give the relative intensity magnification. Note that, at these temperatures, the luminescence of the line labeled FE assumes a shape characteristic of free-exciton luminescence in Si.

also be fitted very well with the line shape described by Eq. (1). An example of this fit is shown in Fig. 4. In all cases, the fit temperature obtained in this manner was within 1 K of the measured bath temperature. Also, the threshold energy remained constant within 0.05 meV. On the basis of this analysis, the line labeled FE is identified as resulting from no-phonon (NP) FE recombination. Note that this intrinsic NP luminescence is greatly enhanced in the alloy, since the Ge atoms can act as momentum-conserving scattering centers.<sup>5</sup>

### C. Identification of bound-exciton luminescence

The identification of the FE line obtained in the preceding section, splitting between the FE threshold and the peak position of the line labeled  $\text{BE}_p$ , and the thermal behavior shown in Fig. 2, suggest that the line labeled  $\text{BE}_p$  is due to the NP recom-

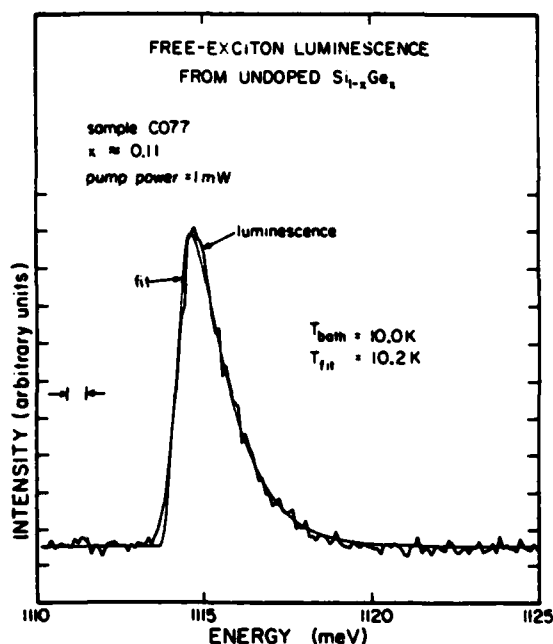


FIG. 4. Free-exciton luminescence from undoped  $\text{Si}_{1-x}\text{Ge}_x$  sample C077 and least-squares fit of the theoretical line shape [Eq. (1)]. The sample temperature obtained as a result of the fit  $T_{fit}$  is shown with the measured bath temperature  $T_{bath}$ .

bination of excitons bound by about 4 meV to a shallow level. The pump-power dependence at low power shown in Fig. 5 supports this proposal. As this figure demonstrates, the FE to  $\text{BE}_p$  luminescence intensity ratio is independent of pump power.

Candidates for such a level are clearly B and P, which have binding energies in the neighborhood of 4 meV in Si (3.9 and 4.7 meV, respectively<sup>8</sup>), and which are the most common shallow impurities in the undoped material. Photoluminescence measurements of Si containing approximately equal background concentrations of B and P show that P bound-exciton ( $\text{BE}_p$ ) luminescence is more intense than B bound-exciton ( $\text{BE}_B$ ) luminescence in the NP region by at least an order of magnitude. It seems reasonable to conclude, therefore, that the line labeled BE in the luminescence from sample C077 is primarily due to NP  $\text{BE}_p$  recombination.

The high-power pump-power dependence presented in Fig. 6 supports this conclusion. In undoped Si, low-energy lines due to bound-multiexciton complexes (BMEC) appear as the pump power is increased. The splitting between the  $\text{BE}_p$  line and the first BMEC line is 2.2 meV for B and 3.6 meV for P.<sup>9</sup> As shown in Fig. 6, in the luminescence spectrum of sample C077 the

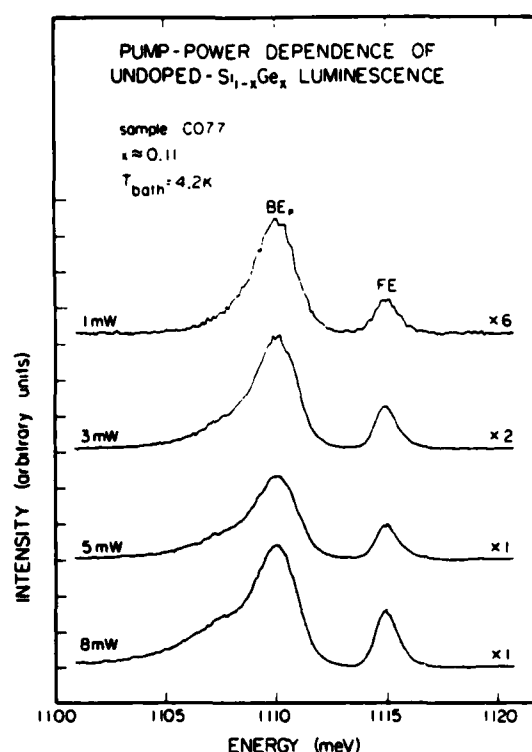


FIG. 5. Pump-power dependence of the luminescence from undoped  $\text{Si}_{1-x}\text{Ge}_x$  sample C077 at low pump powers. The scale factors (e.g.,  $\times 6$ ) give the relative intensity magnification. Note that the  $\text{BE}_p$  to FE luminescence intensity ratio is independent of pump power at these power levels.

$\text{BE}_p$  line develops a low-energy shoulder as the pump power is increased, which resolves into a separate line at high pump powers. The separation between this line and the  $\text{BE}_p$  line is about 3.8 meV, which is consistent with the splitting between the P BE and first BMEC in Si. Since no line is observed which would correspond to B BMEC luminescence, our conclusion regarding the origin of the  $\text{BE}_p$  line in the alloy seems justified.

#### D. Comparison of photoluminescence spectra

The interpretation of the photoluminescence spectrum of sample C077 developed in the previous sections is consistent with our investigation of the  $x=0.067$  sample, C021-3. In Fig. 7, the luminescence spectra of samples C077 and C021-3 are compared. We see that the ratio of  $\text{BE}_p$  to FE luminescence is considerably greater for sample C021-3. This is consistent with Table I, which in-

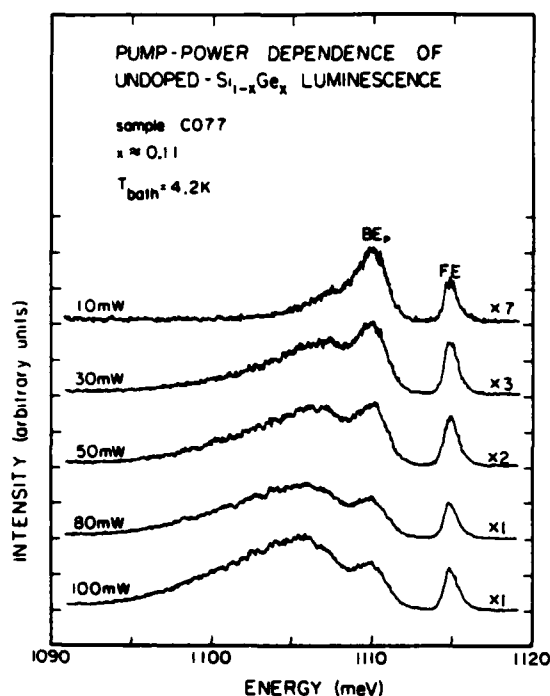


FIG. 6. Pump-power dependence of luminescence from undoped  $\text{Si}_{1-x}\text{Ge}_x$  sample C077 at high pump powers. The scale factors (e.g.,  $\times 7$ ) give the relative intensity magnification. Note the new feature which appears on the low-energy side of the  $\text{BE}_p$  line at high pump powers. This feature is discussed in the text.

icates that impurity concentrations in sample C021-3 are approximately an order of magnitude higher. In addition, we see that the luminescence spectrum of sample C021-3 is shifted to higher energy. This feature will be discussed in detail below.

#### IV. EXPERIMENTAL RESULTS AND DISCUSSION FOR In-DOPED $\text{Si}_{1-x}\text{Ge}_x$

The subject of the investigations reported in this section was the In-doped  $\text{Si}_{1-x}\text{Ge}_x$  sample C093, for which  $x = 0.10$ .

##### A. Typical photoluminescence spectra

Typical luminescence spectra obtained from  $\text{Si}_{1-x}\text{Ge}_x$  in sample C093 are shown in Fig. 8. Spectra measured at various temperatures are shown. Two features are prominent in the spectra. The higher-energy luminescence, labeled FE, be-

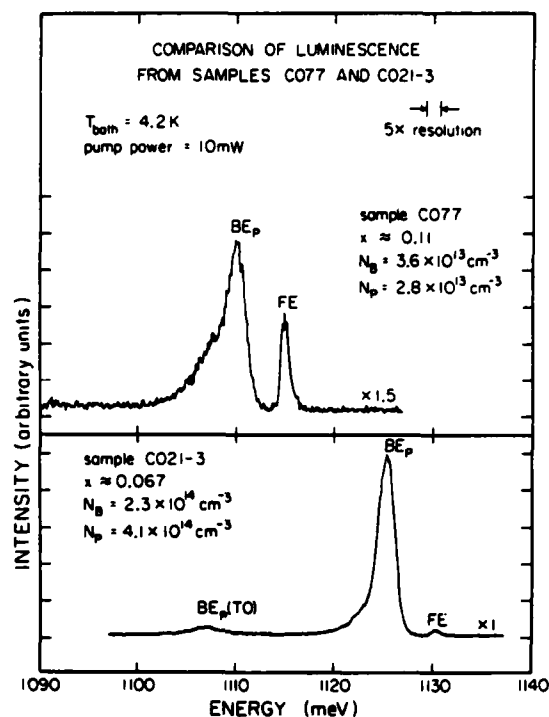


FIG. 7. Comparison of the luminescence spectra of samples C077 and C021-3. The scale factors (e.g.,  $\times 1.5$ ) give the relative intensity magnification. Note that  $\text{BE}_p$  luminescence is much more intense from sample C021-3 than from sample C077. Also, note that the luminescence from sample C021-3 is at higher energy than the luminescence from sample C077. These features are discussed in the text.

comes visible only at high temperatures. At somewhat lower energies a broad feature labeled  $L$  is visible, which moves to lower energy as the temperature is increased. The  $L$  luminescence develops a low-energy shoulder at high temperatures, which has been labeled  $\text{FE}(\text{TO})$ .

##### B. Identification of free-exciton luminescence

To begin with, we note that the luminescence labeled FE has a line shape and temperature dependence characteristic of NP FE recombination in Si, as described in detail in Sec. III. Equation (1), which describes the NP FE line shapes, can be fitted to the FE luminescence from sample C093 very accurately. The FE threshold energy obtained from such fits, 1115.8 meV, remained constant within about 0.3 meV. However, the fit temperatures  $T_{\text{fit}}$  were systematically higher than the mea-

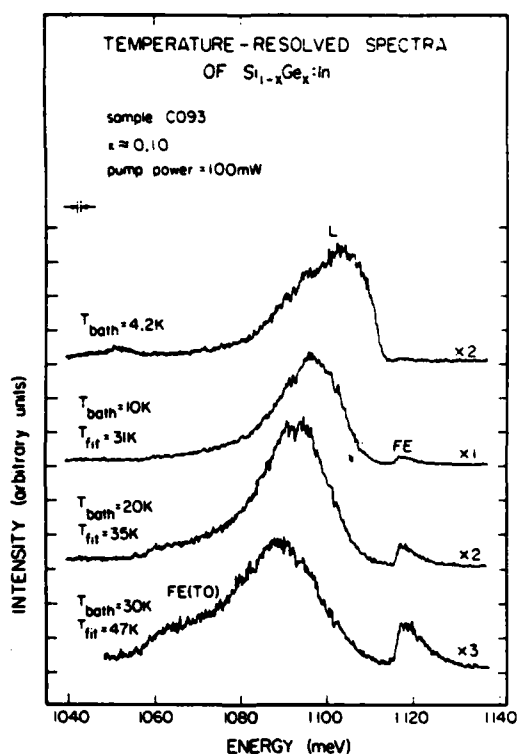


FIG. 8. Temperature-resolved spectra of  $\text{Si}_{1-x}\text{Ge}_x:\text{In}$  sample C093 from 4.2 to 30 K. The scale factors (e.g.,  $\times 2$ ) give the relative intensity magnification. Refer to the text for a discussion of the line assignments shown in the figure. Where FE luminescence is observed, the sample temperature obtained from a least-squares fit to the FE line shape,  $T_{\text{fit}}$ , is shown with the measured bath temperature  $T_{\text{bath}}$ . The discrepancy between these results is discussed in the text.

sured bath temperatures  $T_{\text{bath}}$ . These temperatures are indicated in Fig. 8. It seems, therefore, that either the FE luminescence is subject to some broadening as a result of the disordered nature of the alloy, or the sample is being locally heated by the laser pump. Of these two possibilities, the second seems most likely. First, one would expect some broadening mechanism to affect the FE threshold behavior as well as generally broaden the line. That is, we would expect to see the FE threshold "smear out" and become less abrupt. However, this behavior is not observed. As previously mentioned, the line shape is described by Eq. (1) very well. Second, as indicated in Table I sample C093 has impurity concentrations which are about 3 orders of magnitude higher than those in sample C077. As a result, much higher pump powers are needed to observe FE luminescence at all in sample C093. At these laser intensities, sam-

ple heating must be considered a very likely cause of the observed FE broadening.

If this explanation is accepted, the luminescence labeled FE can be interpreted as resulting from NP-FE recombination in the  $\text{Si}_{1-x}\text{Ge}_x:\text{In}$  alloy. Since the feature labeled FE(TO) is separated from the FE peak by approximately the Si TO phonon energy, we interpret this shoulder on  $L$  as being due to TO phonon-assisted FE recombination.

### C. Identification of bound-exciton luminescence

Our interpretation of the luminescence labeled  $L$  is necessarily considerably more complicated than that of the FE luminescence. There are a number of processes which are undoubtedly contributing to the  $L$  line. Primarily,  $\text{BE}_B$ ,  $\text{BE}_P$ , and  $\text{BE}_{\text{In}}$  luminescence must be considered. Indium, of course, is the majority dopant, and will dominate the NP-BE luminescence. The B concentration is about an order of magnitude greater than the P concentration. It follows from our discussion of BE luminescence from undoped  $\text{Si}_{1-x}\text{Ge}_x$  that B and P will probably contribute equally to the NP-BE luminescence. In addition, the  $L$  luminescence is sufficiently broad that transverse-acoustic (TA) phonon replicas of the FE and BE lines may contribute as well. It is unlikely that NP-BMEC or electron-hole-droplet (EHD) luminescence will have any significant influence on the spectra presented here. The impurity concentrations in sample C093 preclude the observation of such effects at the pump powers utilized in this study.

#### 1. Time-resolved spectra and isolation of B bound-exciton component

In an effort to separate the BE components which produce the  $L$  luminescence, the time evolution of the luminescence from sample C093 was measured at low pump power. The time-resolved spectra are shown in Fig. 9 for low-power laser excitation. As this figure demonstrates, the  $L$  luminescence is composed of a relatively sharp high-energy component with a long lifetime, and a broad low-energy component with a short lifetime. Consideration of the  $\text{BE}_B$ ,  $\text{BE}_P$  and  $\text{BE}_{\text{In}}$  decay times in Si (1055, 272, and 2.7 nsec, respectively<sup>10</sup>) leads to the suggestion that the sharp, long-lifetime component is primarily a result of  $\text{BE}_B$  recombination. The broad, short-lifetime, low-energy shoulder is therefore probably due to  $\text{BE}_{\text{In}}$  recombination.

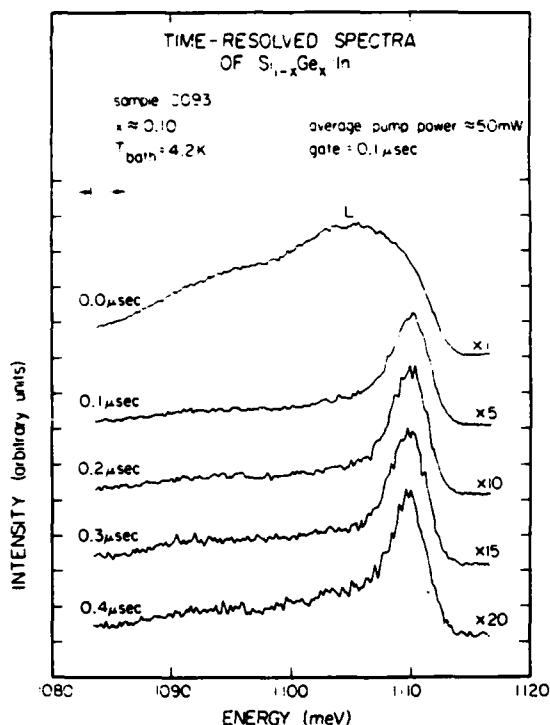


FIG. 9. Time-resolved spectra of  $\text{Si}_{1-x}\text{Ge}_x\text{In}$  sample C093. The scale factors (e.g.,  $\times 5$ ) give the relative intensity magnification. At long times, a sharp, long-lifetime component of  $L$  luminescence is isolated.

## 2. Temperature-resolved spectra and isolation of In bound-exciton component

A further separation of the BE components which produce the  $L$  luminescence can be accomplished by measuring the temperature dependence of the photoluminescence spectrum. This measurement is shown in Fig. 8. We see that the high-energy side of the  $L$  luminescence thermalizes as the temperature is increased. This observation is consistent with the interpretation of  $L$  luminescence presented in the previous section. At high temperatures, only the lower-energy  $\text{BE}_{\text{In}}$  component is observed. The higher-energy  $\text{BE}_{\text{B}}$  component has thermalized.

This effect is seen clearly in Fig. 10, which shows the temperature dependence of  $L$  luminescence which is gated in time. At low temperatures, the  $\text{BE}_{\text{B}}$  peak is reasonably well isolated. At the high pump powers used for this measurement, however, a low-energy shoulder is clearly observed. We interpret this shoulder as being due to a  $\text{BE}_{\text{In}}$  component which has not been eliminated by the time resolution. As the temperature is increased,

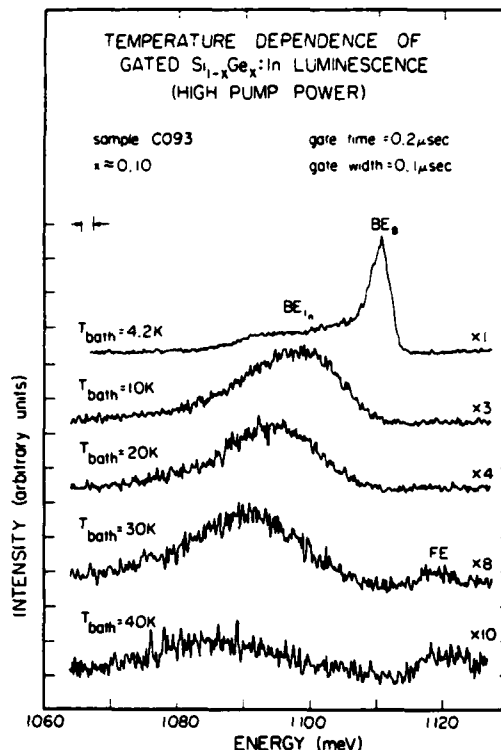


FIG. 10. Gated, temperature-resolved spectra of  $\text{Si}_{1-x}\text{Ge}_x\text{In}$  sample C093 at high pump power. The scale factors (e.g.,  $\times 3$ ) give the relative intensity magnification. At high temperature, the  $\text{BE}_{\text{B}}$  luminescence component thermalizes, and the  $\text{BE}_{\text{In}}$  component is isolated. At high temperatures, weak FE luminescence is also observed.

we see the  $\text{BE}_{\text{B}}$  component thermalize with respect to the  $\text{BE}_{\text{In}}$  component. Above 10 K, only the  $\text{BE}_{\text{In}}$  component remains.

There is one difficulty with this interpretation which should be mentioned. As the temperature is raised above 10 K, the  $\text{BE}_{\text{In}}$  component peak position moves to lower energy, as expected from the behavior of  $\text{BE}_{\text{P}}$  luminescence in undoped  $\text{Si}_{1-x}\text{Ge}_x$ . This effect is observed in Fig. 8 and Fig. 10. However, the  $\text{BE}_{\text{In}}$  peak moves too far; at 30 K, it is already approximately 25 meV below the FE threshold, while the  $\text{BE}_{\text{In}}$  binding energy in Si is only 13.7 meV.<sup>11</sup> In spite of this, the bulk of the experimental evidence supports the interpretation that this high-temperature luminescence is due to  $\text{BE}_{\text{In}}$  recombination in the alloy. It may be that contributions from FE and BE TA-assisted luminescence combine to produce the anomalously low high-temperature  $\text{BE}_{\text{In}}$  peak position. However, this seems unlikely when the relative intensities of TA and NP luminescence in Si are considered.

It is also possible that the high-temperature  $BE_{In}$  binding energy in the alloy is increased as a result of some complicated effect which may involve the unusually large radii of the Ge and In atoms relative to the Si-Si bond length. Of course, this mechanism is also unlikely, practically by definition. Unfortunately, all we can state at this point is that the anomalous temperature dependence of the  $BE_{In}$  luminescence remains unexplained.

## V. DISCUSSION

In the previous sections, we have presented the experimental photoluminescence data for the undoped and In-doped Si-Ge alloy samples, and have attempted to interpret the spectra qualitatively. In this section, we continue our qualitative discussion of the experimental results. In particular, we focus on some effects which result from the compositional disorder of the alloy.

### A. Bound-exciton line broadening

To begin with, we see that the BE line is considerably broadened in the alloy. In fact, the BE line in the undoped  $Si_{1-x}Ge_x$  samples is approximately ten times broader ( $\sim 3$  meV) than its counterpart in Si ( $\sim 0.4$  meV). In general, this broadening can be accounted for on the basis of the compositional inhomogeneity of the alloy material. The energy of the luminescence which results from the recombination of an exciton bound to a particular impurity will depend on the local configuration of Si and Ge atoms. This luminescence energy can be schematically written as

$$E_{PL}(\{c\}) = E_G(\{c\}) - E_{FE}(\{c\}) - E_{BE}(\{c\}), \quad (2)$$

where  $E_{PL}$  is the photon energy,  $E_G$  is the band-gap energy,  $E_{FE}$  is the free-exciton binding energy, and  $E_{BE}$  is the bound-exciton binding energy, and where  $\{c\}$  denotes the particular configuration for the impurity being considered.

We can consider two simple limits to the general expression, Eq. (2). First, we assume that the local configuration does not affect the free-exciton binding energy or bound-exciton binding energy. Then Eq. (2) indicates that the BE-line broadening is the result of variations in band-gap energy produced by local fluctuations in the alloy composition  $x$ . This limit was first discussed by Alferov *et al.*<sup>12</sup>

We can roughly estimate this effect on the basis of the following argument. Given a volume  $4\pi a^3/3$ , there will be  $4\pi a^3 \propto N/3$  atoms, where  $N$  is the density of lattice sites in the alloy, if the Ge atoms are distributed randomly the typical fluctuation in the number of Ge atoms in the volume will be  $(4/3\pi a^3 x N)^{1/2}$ . Therefore, the typical fluctuation in the composition parameter  $x$  will be

$$\Delta x \sim \frac{(\frac{4}{3}\pi a^3 x N)^{1/2}}{\frac{4}{3}\pi a^3 N} = \left[ \frac{x}{\frac{4}{3}\pi a^3 N} \right]^{1/2}. \quad (3)$$

If  $\Delta E = \alpha \Delta x$ , where  $\Delta E$  is the change in gap energy produced by a change in composition  $\Delta x$ , then Eq. (3) becomes

$$\Delta E \sim \alpha \left[ \frac{x}{\frac{4}{3}\pi a^3 N} \right]^{1/2}. \quad (4)$$

$N$  can be estimated for the alloy from the lattice-constant measurements of Dismukes *et al.*<sup>13</sup> For  $x=0.1$ , we find  $N \sim 6 \times 10^{21} \text{ cm}^{-3}$ . From the absorption measurements of Braunstein *et al.*,<sup>14</sup> we can estimate  $\alpha \sim 600$  meV. Assuming that  $a$  is approximately an exciton Bohr radius in Si, i.e., about 40 Å, we obtain  $\Delta E \sim 5$  meV, which is reasonable agreement for a crude calculation.

In spite of the agreement, this limit does not explain the temperature-dependence data presented in Figs. 2 and 8. The data clearly shows that the BE peak shifts to lower energy as the temperature increases. However, the band-gap fluctuation limit does not produce this behavior. In this limit, we expect that as the temperature increases excitons will thermalize to bound-exciton states in the regions where the band gap is larger, which produces a BE peak which moves to higher energy.

The second limit to Eq. (2) we will consider accounts for the observed temperature dependence. In this limit, we assume that the local configuration does not affect the band-gap energy or the FE binding energy. We assume that the gap energy and the FE binding energy are the bulk average values for the alloy. Then the BE line broadening is the result of variations in the BE binding energy caused by variations in the local configuration of Si and Ge atoms. It is possible, therefore, that the BE line is composed of several overlapping luminescence lines from BE's with slightly different binding energies. These binding energies will increase, in principle, from the BE binding energy in Ge to the BE binding energy in Si.

Qualitatively, this limit produces the temperature dependence observed in Figs. 2 and 8. At low

temperatures, we see luminescence from all BE's. As the temperature increases, though, we expect that luminescence from the most tightly bound BE's will dominate. As we have previously mentioned, these BE's will have the most Si-like local configuration. In addition to explaining the temperature-dependence data, this picture of BE-line broadening is consistent with time-resolved spectra of the alloy luminescence. An analysis of the relevant decay times shows that the decay of all components of BE luminescence is capture-limited in the cases studied here.<sup>15</sup> This is consistent with our observation that all components of the BE line decay at the same rate — the line shape does not change and the peak position remains fixed.

#### B. Comparison of Si and Si-Ge luminescence energies

If we assume that, at high temperatures, the BE luminescence is dominated by components which have the most Si-like local configuration, then a procedure for directly comparing Si and  $\text{Si}_{1-x}\text{Ge}_x$  luminescence energies presents itself. We propose that the difference in recombination energy between the high-temperature BE-peak position in the Si-Ge alloy and the corresponding BE-peak position in Si is just due to the shift in band gap of the alloy.

Figure 11 schematically illustrates the consequences of this proposal for the  $x=0.11$   $\text{Si}_{1-x}\text{Ge}_x$  sample, C077. The high-temperature  $\text{BE}_p$  luminescence line position, 1108.71 meV, was obtained from the 8.0-K spectrum. This was the highest temperature at which  $\text{BE}_p$  luminescence could be reliably observed, and it was assumed that the luminescence was dominated by recombination of  $\text{BE}_p$ 's in essentially a Si environment. The P luminescence line position in Si, 1150.11 meV, was obtained from direct measurement of lightly doped Si:P. If this change in line position is attributed solely to a change in gap energy, these measurements imply a band-gap decrease of 41.4 meV for  $x=0.11$ . This value fluctuated by about 0.6 meV due to large-scale inhomogeneities in the crystals being examined. If a rough graphical extrapolation of the absorption data published by Braunstein *et al.*<sup>14</sup> is attempted, we obtain an alloy band-gap shift of approximately 60 meV for  $x=0.11$ , which is in reasonable agreement with the luminescence data.

#### SCHEMATIC COMPARISON OF UNDOPED-Si AND UNDOPED- $\text{Si}_{1-x}\text{Ge}_x$ LUMINESCENCE ENERGIES

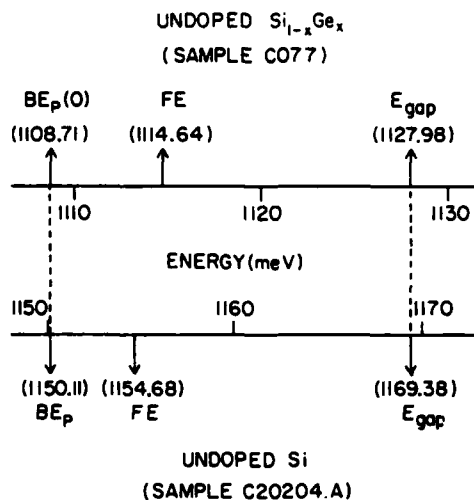


FIG. 11. Schematic line-position comparison between Si and  $\text{Si}_{1-x}\text{Ge}_x$  sample C077. This comparison is based on the assumption that the difference between the energy of high-temperature  $\text{BE}_p$  alloy luminescence is equal to the difference in band-gap energies for Si and  $\text{Si}_{1-x}\text{Ge}_x$  sample C077. This fixes the alloy gap energy. The spectra are then compared by lining up the Si and  $\text{Si}_{1-x}\text{Ge}_x$  gap energies.

In addition to the high-temperature  $\text{Si}_{1-x}\text{Ge}_x$   $\text{BE}_p$  line position and the Si  $\text{BE}_p$  line position, Fig. 11 also shows the FE threshold and  $E_{\text{gap}}$  positions for Si and the  $x=0.11$  alloy. The FE threshold position in the alloy, 1114.64 meV, was obtained by fitting Eq. (1) to the high-temperature FE luminescence spectra (Fig. 3), as illustrated in Fig. 4. The NP-FE threshold position in Si, 1154.68 meV, was obtained by fitting Eq. (1) directly to NP-FE luminescence from pure Si. The Si gap energy, 1169.38 meV, was determined from the NP-FE threshold energy by adding the FE binding energy, which is 14.7 meV. Then the alloy gap energy, 1127.98 meV, was obtained by subtracting the band-gap shift, 41.4 meV, from the Si gap energy.

As indicated in Fig. 11, this method implies that the FE dissociation energy in the  $x=0.11$  alloy has decreased by 1.36 meV from its value in Si, to 13.34 meV. This compares favorably with a rough estimate based on a linear interpolation between the FE dissociation energies in Si and Ge, which are 14.7 and 4.15 meV, respectively. The linear in-

terpolation results in an estimate of 13.54 meV for the FE dissociation energy in the  $x=0.11$  alloy.

A similar analysis has been applied to the  $x=0.067$  sample, C021-3. As shown in Fig. 7, compared to sample C077 the luminescence from sample C021-3 is shifted to higher energy by 15.5 meV. This implies a band-gap decrease of 25.9 meV for the  $x=0.067$  alloy. This result and the result previously obtained for sample C077 are consistent with the alloy-composition measurements presented in Table I if a linear relationship between the alloy composition and change in band gap is assumed. The composition ratio between the two samples is 0.609 while the ratio of the measured band-gap shifts is 0.626.

To compare the Si and  $\text{Si}_{1-x}\text{Ge}_x$  luminescence energies for the In-doped sample, C093, we note that samples C077 and C093 differ in composition by only about 1%. We therefore assume that the FE binding energies in the two samples are the same. This leads to the comparison schematically illustrated in Fig. 12. The gap energy for sample C093, 1129.14 meV, was determined by adding the assumed FE binding energy, 13.34 meV, to the FE

threshold energy, 1115.8 meV. This results in a measured band-gap shift of 40.2 meV for the  $x=0.104$  alloy. The band-gap shifts and alloy-composition measurements are reasonably consistent, assuming a linear relationship between the alloy composition and change in band gap. The composition ratio between samples C077 and C093 is 0.920 while the ratio of measured band-gap shifts is 0.971. Samples C021-3 and C093 agree exactly — the composition ratio and the ratio of measured band-gap shifts are both 0.644.

### C. Excitons bound to composition fluctuations

One feature in the luminescence spectrum of sample C077 remains to be discussed. At high temperatures (Fig. 3), the FE line assumes a shape characteristic of FE recombination in Si and is well described by Eq. (1), as previously discussed. The FE threshold energy obtained by fitting Eq. (1) is independent of temperature, as expected. However, at low temperatures this is no longer the case. Spectra taken at various temperatures below 6 K are shown in Fig. 13. We see that as the temperature decreases, the line shifts to lower energy and assumes a shape which is no longer characteristic of FE recombination.

These measurements of low-temperature FE luminescence suggest that a low-energy shoulder appears on the FE luminescence at low temperatures. This shoulder may be due to the recombination of excitons bound by only about 0.1 meV to a very shallow level. This interpretation is supported by the temperature-resolved spectra, which show that the shoulder has completely thermalized by 6 K. Above 6 K, Eq. (1) correctly describes the line shape, and the threshold energy is independent of temperature. This behavior is consistent with a binding energy of tenths of meV. Also, the pump-power dependence at 1.6 K (Fig. 14) shows that the FE to  $\text{BE}_p$  intensity ratio is independent of pump power, as expected for independent exciton-binding centers in the absence of saturation.

These features, and the fact that there is no known defect or impurity in Si which binds an exciton by only 0.1 meV, leads us to suggest that the new feature may be due to the recombination of excitons weakly bound to local fluctuations in the alloy composition ( $\text{BE}_F$ ). The possibility of such a state was first pointed out by Baranovskii and Éfros,<sup>16</sup> who extended the bulk fluctuation theory of Alferov *et al.*<sup>12</sup> to include excitons. A line

SCHEMATIC COMPARISON OF  
Si:In AND  $\text{Si}_{1-x}\text{Ge}_x$ :In  
LUMINESCENCE ENERGIES

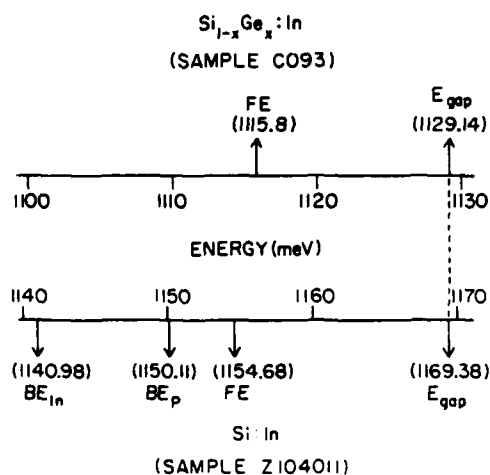


FIG. 12. Schematic line-position comparison between Si and  $\text{Si}_{1-x}\text{Ge}_x$ :In sample C093. This comparison is based on the assumption that the FE binding energy in sample C093 and sample C077 is identical. This fixes the alloy gap energy. The spectra are then compared by lining up the Si and  $\text{Si}_{1-x}\text{Ge}_x$ :In gap energies.

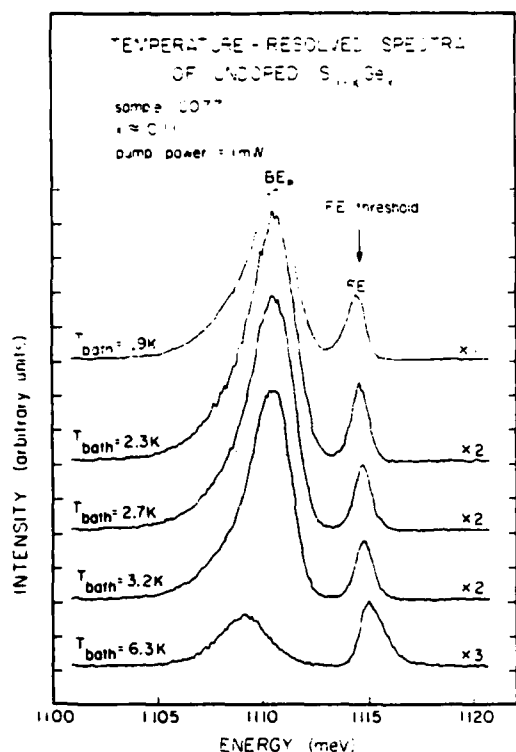


FIG. 13. Temperature-resolved spectra of undoped  $\text{Si}_{1-x}\text{Ge}_x$  sample C077 at low temperatures. The scale factors (e.g.,  $\times 2$ ) give the relative intensity magnification. Note that the free-exciton line shifts and broadens as the temperature is decreased. For reference, the free-exciton threshold energy measured at high temperature is shown.

which may be due to fluctuation bound excitons has just recently been reported in  $\text{GaAs}_{1-x}\text{P}_x$ ,<sup>17</sup> and has characteristics which are similar to those of the line reported here.

One of the most important features of this model is the prediction that  $\text{BE}_F$  luminescence should have a very long lifetime. As indicated during the discussion of  $\text{BE}_P$  decay, the dominant decay mechanism for donor or acceptor BE's in Si is the Auger process. This results in observed decay rates which can be orders of magnitude larger than the radiative rates obtained from measured oscillator strengths.<sup>10,18</sup> For instance, the  $\text{BE}_P$  radiative decay rate is estimated to be  $5 \times 10^2 \text{ sec}^{-1}$ , whereas the observed Auger decay rate is  $3.7 \times 10^6 \text{ sec}^{-1}$ .<sup>10</sup> When an exciton is bound to a local composition fluctuation, however, the Auger

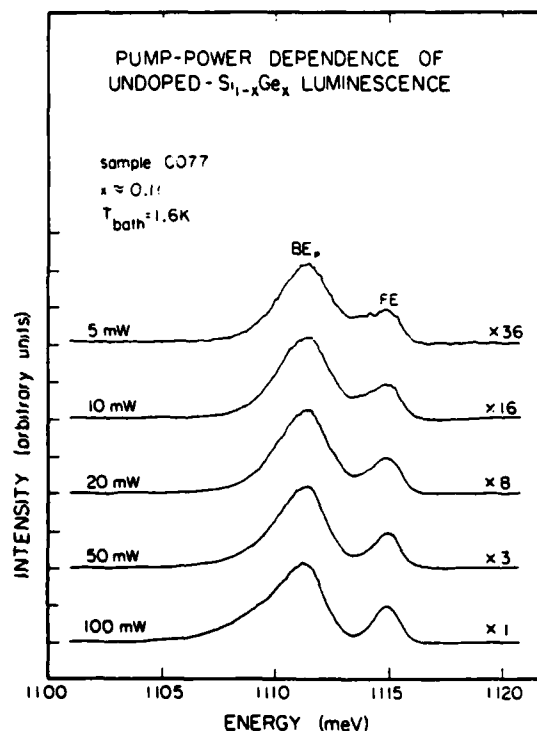


FIG. 14. Pump-power dependence of luminescence from undoped  $\text{Si}_{1-x}\text{Ge}_x$  sample C077 at 1.6 K. The scale factors (e.g.,  $\times 36$ ) give the relative intensity magnification. Note that the  $\text{BE}_P$ -FE intensity ratio is independent of pump power.

process is not possible and long-lifetime luminescence is expected. Indeed, this was the case for the luminescence feature observed in  $\text{GaAs}_{1-x}\text{P}_x$ .<sup>16</sup>

Figure 15 presents the best low-temperature time-resolved spectra available for the  $\text{Si}_{0.9}\text{Ge}_{0.1}$  alloy. Although the spectra are somewhat noisy, we see that the  $\text{BE}_F$  luminescence does not appear to have a particularly long lifetime compared to the  $\text{BE}_P$  luminescence line. This apparent discrepancy can be investigated by estimating the relevant decay times. These estimates show that in this case we are in a regime where the decays are capture limited,<sup>13</sup> which explains why all components in the spectrum appear to decay with the same rate. Hence, while the low-temperature time-resolved spectra do not show long lifetimes for the  $\text{BE}_F$  luminescence, the data are not inconsistent with the model proposed above.

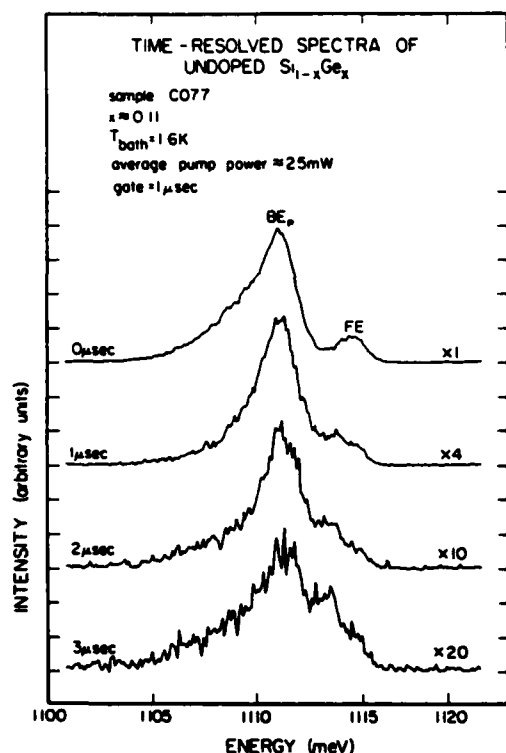


FIG. 15. Time-resolved spectra of undoped  $\text{Si}_{1-x}\text{Ge}_x$  sample C077 at 1.6 K. The scale factors (e.g.,  $\times 4$ ) give the relative intensity magnification. Note that FE luminescence does not dominate the long-time spectrum.

## VI. SUMMARY AND CONCLUSION

In this paper, we have presented the results of a study of the photoluminescence spectra of Si-rich  $\text{Si}_{1-x}\text{Ge}_x$  alloy materials. Undoped and In-doped samples were considered in the range  $0.067 \leq x$

$\leq 0.11$ . The luminescence features observed in the spectra were identified as free-exciton and bound-exciton luminescence. The free-exciton luminescence is described very accurately by the Si no-phonon free-exciton line shape, Eq. (1). As a result, a no-phonon free-exciton threshold energy was obtained for each sample.

In addition to this identification of the luminescence features, mechanisms for the observed bound-exciton—luminescence broadening were discussed. On the basis of this discussion, the Si-Ge luminescence energies were compared with those from Si, and values for the alloy band-gap shift and change in free-exciton binding energy were obtained. Finally, evidence was presented which may indicate that luminescence from excitons bound to local composition fluctuations is observed in the low-temperature luminescence spectra.

## ACKNOWLEDGMENTS

The authors would like to thank R. Baron, J. Baukus, O. J. Marsh, and H. Kimura of Hughes Research Laboratories for growing and characterizing the Si-Ge alloy samples. Also, we have appreciated valuable discussions with Y. C. Chang, A. T. Hunter, and R. M. Feensira. Finally, we acknowledge the financial support of the Office of Naval Research under Contract No. N00014-81-C-0285, and the National Sciences and Engineering Research Council of Canada.

- <sup>1</sup>A. Onton, *J. Lumin.* **7**, 95 (1973), and references therein.
- <sup>2</sup>D. J. Wolford, R. E. Anderson, and B. G. Streetman, *J. Appl. Phys.* **48**, 2442 (1977), and references therein.
- <sup>3</sup>Zh. I. Alferov, V. I. Amosov, D. Z. Garbuzov, Yu. V. Zhilyaev, S. G. Konnikov, P. S. Kop'ev, and V. G. Trofim, *Fiz. Tekh. Poluprovodn.* **6**, 1879 (1972) [*Sov. Phys.—Semicond.* **6**, 1620 (1973)], and references therein.
- <sup>4</sup>A. T. Hunter, D. L. Smith, and T. C. McGill, *Appl. Phys. Lett.* **37**, 200 (1980), and references therein.
- <sup>5</sup>See, for example, E. F. Gross, N. S. Sokolov, and A. N. Titkov, *Fiz. Tverd. Tela (Leningrad)* **14**, 2004 (1972) [*Sov. Phys.—Solid State* **14**, 1732 (1973)].
- <sup>6</sup>R. Rentzsch and I. S. Shlimak, *Fiz. Tekh. Poluprovodn.*

- 12**, 713 (1978) [*Sov. Phys.—Semicond.* **12**, 416 (1978)].
- <sup>7</sup>C. Benoit à la Guillaume and M. Voos, *Phys. Rev. B* **10**, 4995 (1974).
- <sup>8</sup>S. A. Lyon, D. L. Smith, and T. C. McGill, *Phys. Rev. Lett.* **41**, 56 (1978).
- <sup>9</sup>R. B. Hammond, D. L. Smith, and T. C. McGill, *Phys. Rev. Lett.* **35**, 1535 (1975).
- <sup>10</sup>W. Schmid, *Phys. Status Solidi B* **84**, 529 (1977).
- <sup>11</sup>S. A. Lyon, D. L. Smith, and T. C. McGill, *Phys. Rev. B* **17**, 2620 (1978).
- <sup>12</sup>Zh. I. Alferov, E. L. Portnoi, and A. A. Rogazhev, *Fiz. Tekh. Poluprovodn.* **2**, 1194 (1968) [*Sov. Phys.—Semicond.* **2**, 1001 (1969)].
- <sup>13</sup>J. P. Dismukes, L. Ekstrom, and R. J. Paff, *J. Phys.*

Chem. 68, 3021 (1964).

<sup>14</sup>R. Braunstein, A. R. Moore, and F. Herman, Phys. Rev. 109, 695 (1958).

<sup>15</sup>G. S. Mitchard, Ph. D. thesis, California Institute of Technology, 1981 (unpublished).

<sup>16</sup>S. D. Baranovskii and A. L. Éfros, Fiz. Tekh. Poluprovdn. 12, 2233 (1978) [Sov. Phys.—Semicond. 12,

1328 (1978)].

<sup>17</sup>S. Lai and M. V. Klein, Phys. Rev. Lett. 44, 1087 (1980).

<sup>18</sup>G. C. Osbourn, S. A. Lyon, K. R. Elliott, D. L. Smith, and T. C. McGill, Solid State Electron. 21, 1339 (1978).

# Platinum diffusion into silicon from PtSi

A. Prabhakar, T. C. McGill, and M-A. Nicolet  
California Institute of Technology, Pasadena, California 91125

(Received 4 August 1983; accepted for publication 26 September 1983)

We have observed platinum diffusion into the silicon underlying a PtSi film. Silicon substrates covered with platinum films were annealed at temperatures from 300 to 800 °C to form the silicide. Backscattering spectrometry spectra show no degradation of the silicide in the samples treated below 700 °C. Deep level transient spectroscopy (DLTS) was used to measure diffused platinum electron traps. Electron trap concentrations in samples treated below 700 °C are below the DLTS detection limit of  $5 \times 10^{11}/\text{cm}^3$ . Trap concentration profiles for the samples annealed at higher temperatures were obtained. These profiles cannot in general be explained by simple diffusion from an infinite source of platinum at the surface.

PACS numbers: 66.30.Jt, 71.55.Fr, 61.70.Wp, 81.40.Ef

Transition metal silicides have received a great deal of attention recently due to their applications in a number of devices.<sup>1,2</sup> One example is platinum silicide which has application in large scale integrated circuits<sup>1</sup> and in infrared detection schemes.<sup>3</sup> A difficulty with using transition metals in silicon systems is the possibility of poisoning the silicon with metal impurities during processing, since a large number of transition metals form deep traps in silicon. Platinum traps in silicon in particular have been studied because of their application as lifetime killers.<sup>4</sup> Thus, a knowledge of the effects of annealing on the metal diffusion into silicon is important in considering any silicide for use in a device.

In this letter we describe the observation of diffusion of platinum and its related deep levels into silicon from PtSi on the surface. Deep level transient spectroscopy (DLTS) and backscattering spectrometry (BS) were used to measure metal contaminants. DLTS observes traps in the depletion region of the reverse-biased Schottky barrier formed by the silicide-silicon structure, i.e.,  $\sim 0.5\text{--}7\text{ }\mu\text{m}$  from the interface. For our samples, trap concentrations above  $5 \times 10^{11}/\text{cm}^3$  can be detected by DLTS. BS can detect atom impurity concentrations greater than about 0.1 at. % ( $5 \times 10^{19}$  atoms/ $\text{cm}^3$  in silicon) within  $\sim 0.3\text{ }\mu\text{m}$  of the interface of the structure. The two techniques measure what may be physically different configurations of platinum impurities, since BS measures total atomic concentration and DLTS measures only the electron traps, and the regions of the structure in which the measurements are made are different. Both these experiments offer little spatial resolution in the plane of the interface.

The samples used in this study were fabricated from 7–10- $\Omega$  cm *n*-type (100) silicon wafers which were cleaned and dipped in an HF solution before loading into an ion-pumped vacuum system. A 500-Å-thick platinum film was electron beam evaporated onto each wafer at a pressure less than  $3 \times 10^{-7}$  Torr. Regions of each wafer were masked to make 0.75-mm-diam diodes for the DLTS studies. The wafers were diced, and diodes as well as pieces with broad-area platinum coverage were annealed together at pressures less than  $10^{-6}$  Torr at temperatures ranging from 300 to 800 °C. The pieces which were completely covered with the silicide were used for the backscattering analysis. The diodes, with

In-Ga ohmic contacts on the backs, were mounted on headers and wire bonded to prepare them for DLTS profiling.

Backscattering spectrometry using 2-MeV  $^4\text{He}^+$  ions was carried out on these samples. Figure 1 shows three of the resulting spectra. Analysis of the spectra using the ratio of the Pt signal leading-edge height to the Si signal leading-edge height yields compositions consistent with Pt<sub>3</sub>Si for the 300 °C sample and PtSi for all higher temperature samples. The film thickness for each of the PtSi samples is approximately 1000 Å. The solid line in Fig. 1 shows the spectrum for the PtSi sample which was annealed at 600 °C for 30 min. This and all samples treated at lower temperatures exhibit Pt signals which fall off sharply on the low energy end, indicating abrupt silicide-silicon interfaces and smooth silicide surfaces. These Pt signals fall off as sharply as do Pt signals in the case of unannealed samples (Pt on Si).

Samples annealed at 700 and 750 °C (not shown in the figure) exhibit very small tails at the low energy end of the Pt signal. However, a significant platinum tail is seen in the 800 °C samples. Inspection of the surface with an optical microscope reveals a smooth topology, while scanning elec-

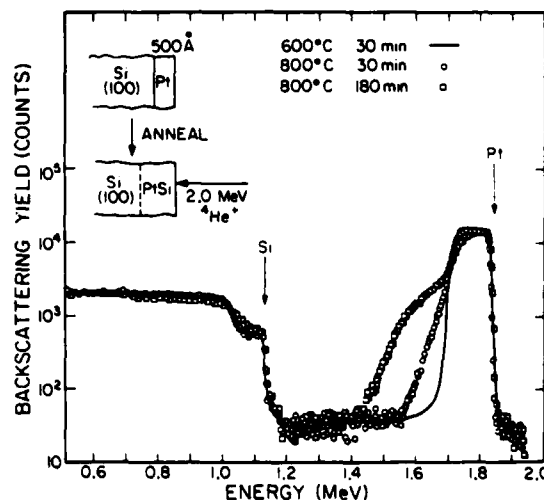


FIG. 1. BS spectra for PtSi-Si structures. These spectra were taken with the beam of 2-MeV  $^4\text{He}^+$  ions incident normal to the sample and with the detector at 170° from the normal.

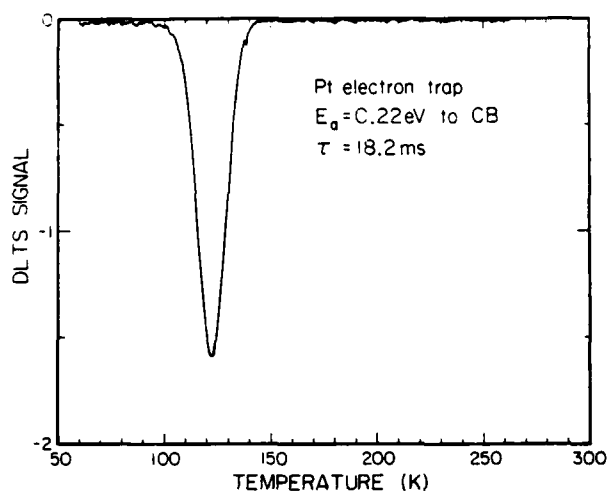


FIG. 2. Platinum electron trap seen in DLTS spectrum taken with time constant of 18.2 ms.  $E_a$  is the trap activation energy measured relative to the conduction band (CB).

tron microscopy images reveal features approximately one micron wide. Thus the tail could correspond to a nonabrupt interface between the silicide layer and the substrate, or it could be a result of the surface roughness. The circles in Fig. 1 show the BS spectrum for PtSi annealed at 800 °C for 30 min. The tail at the low energy end of the Pt signal for this case is almost a straight line on this semilog plot. If we assume that it results from a nonabrupt interface, the slope of the tail corresponds to a decrease in the Pt atomic concentration of approximately one order of magnitude for every 0.2  $\mu\text{m}$  from the interface, with a Pt concentration of  $\sim 3\%$  at a distance of 500 Å from the interface. The squares in Fig. 1 show the spectrum for the sample treated at 800 °C for 180 min. In this final case, the low energy end of the platinum signal exhibits a large tail which is not a straight line. Here, the onset of the disintegration of the PtSi film is evident, as the number of counts at the peak of the platinum signal is approximately 10% less than in the samples which were treated for a shorter time.

The DLTS trap measurements were made using a Boonton model 72 BD capacitance meter. A double boxcar gating scheme<sup>3</sup> was used to analyze the capacitance transients of the Schottky barrier diode, which were caused by the emission of electrons by deep levels. A typical DLTS spectrum for a sample with a detectable concentration of platinum traps is shown in Fig. 2. For a scanning time constant of 18.2 ms, no other traps were observed in the samples up to 350 K. The trap observed was found to have an activation energy of  $0.22 \pm 0.015$  eV, which is in good agreement with the value given by Brotherton *et al.*<sup>6</sup> for the platinum electron trap in silicon.

By applying reverse bias voltages from 2 to 25 V and changing the amplitude of the trap-filling pulses, we are able to observe electron emission from platinum traps in a region from 0.5–7  $\mu\text{m}$  from the interface. The trap concentration profiles obtained by this method are shown in Fig. 3 for the samples which had detectable platinum trap concentrations. In the sample annealed at 700 °C for 30 min, we measure trap concentrations of  $\sim 5 \times 10^{11}/\text{cm}^3$  which are just within our

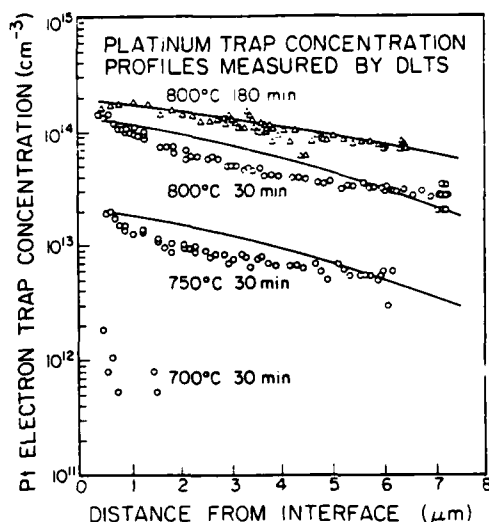


FIG. 3. Platinum electron trap concentration profiles obtained by DLTS. The solid lines are representative erfc's.

detection limit. Trap concentrations are approximately  $10^{13}$  and  $10^{14}$  for samples treated at 750 and 800 °C, respectively. The concentration profile for the sample which was annealed at 800 °C for 180 min falls off more slowly with distance from the interface than that for the sample annealed at the same temperature for 30 min, but the concentrations 0.5  $\mu\text{m}$  from the interface are relatively close.

For simple diffusion of platinum from an infinite source at the surface, the concentration distribution at any temperature would be described by a complementary error function (erfc). The profiles we have measured are not in general described by complementary error functions, as our DLTS profiles bend in the opposite direction from erfc's. Thus, the distribution of platinum traps which we have observed is not due to simple diffusion. However, our profiles are similar in shape to the diffusion profile of gold in silicon, measured in Ref. 7 by radiotracer experiments. The profile in that case is thought to be a result of the interaction among Au atoms in substitutional sites, and silicon self-interstitials.<sup>8</sup> A similar theory could explain our platinum trap diffusion profiles.

To date, few attempts have been made to measure transition metal diffusion into silicon from a silicide at the surface. Ishiwaru *et al.*<sup>9</sup> have reported the observation of platinum diffusion by backscattering spectrometry for PtSi on (100) and (111) oriented silicon wafers. Our BS spectra for (100) wafers show significantly less motion of the platinum atoms than theirs. In our sample which was annealed at 800 °C for 3 h, we measure 22% platinum diffusion in contrast to 53% for a 2-h 800 °C treatment reported by Ishiwaru. Here, the percentage of diffused metal atoms is defined as the ratio of the area under the Pt tail to the total area under the Pt signal, and we have assumed, as they did, that the tails correspond to diffusion of platinum. Their samples were prepared in a manner very similar to ours, except that their evaporations were carried out at pressures about an order of magnitude lower. The doping level in their substrates may also have been different, as the only information given about their substrates is the orientation. These differ-

ences may account for the disparity in the results.

Our DLTS studies of platinum diffusion into (100) silicon substrates from PtSi have shown that there is no observable diffusion at temperatures below 700 °C for our samples. BS spectra show that the PtSi phase is maintained at the surface at 800 °C for annealing times less than 3 h. The electron trap concentration measured by DLTS ranges from  $2.0\text{--}0.5 \times 10^{13}/\text{cm}^3$  in the region from 0.5–7  $\mu\text{m}$  from the interface for the sample treated at 750 °C for 30 min. In the 800 °C samples, the concentration range is  $1.8\text{--}0.3 \times 10^{14}/\text{cm}^3$ . Thus, we conclude that 700 °C is a safe temperature below which the silicon is not poisoned by the diffusion of platinum electron traps.

We would like to thank M. Finetti for her assistance. This work was supported in part by the Office of Naval Re-

search under contract No. N00014-81-C-0285.

<sup>1</sup>F. Mohammadi, *Solid State Technol.* **24**, 65 (1981).

<sup>2</sup>M.-A. Nicolet and S. S. Lau, in *VLSI Electronics: Microstructure Science*, edited by N. Einspruch (Academic, New York, 1983), Vol. 6, Chap. 6.

<sup>3</sup>W. F. Kosonocky, H. G. Erhardt, G. Meray, F. V. Shallcross, H. Elabd, M. J. Cantella, J. Klein, L. H. Skolnik, B. R. Capone, R. W. Taylor, W. Ewing, F. D. Shepherd, and S. A. Roosild, *Soc. Photo-Opt. Instrum. Eng.* **225**, 69 (1980).

<sup>4</sup>M. D. Miller, H. Schade, and C. J. Nuese, *J. Appl. Phys.* **47**, 2569 (1976).

<sup>5</sup>D. V. Lang, *J. Appl. Phys.* **45**, 3023 (1974).

<sup>6</sup>S. D. Brotherton, P. Bradley, and J. Bicknell, *J. Appl. Phys.* **50**, 3396 (1979).

<sup>7</sup>W. R. Wilcox and T. J. LaChapelle, *J. Appl. Phys.* **35**, 240 (1964).

<sup>8</sup>U. Gösele, F. Morehead, W. Frank, and A. Seeger, *Appl. Phys. Lett.* **38**, 157 (1981).

<sup>9</sup>H. Ishiwara, K. Hikosaka, and S. Furukawa, *J. Appl. Phys.* **50**, 5302 (1979).

## APPENDIX J

*Thin Solid Films*, 108 (1983) 69-78

PREPARATION AND CHARACTERIZATION

69

### SPUTTER-INITIATED RESONANCE IONIZATION SPECTROSCOPY\*

J. E. PARKS, H. W. SCHMITT, G. S. HURST† AND W. M. FAIRBANK, JR.‡

*Atom Sciences Inc., 114 Ridgeway Center, P.O. Box 138, Oak Ridge, TN 37830 (U.S.A.)*

(Received March 24, 1983; accepted April 21, 1983)

A new technique, sputter-initiated resonance ionization spectroscopy (SIRIS), which provides an ultrasensitive analysis of solid samples for all elements except helium and neon is described in this paper. Sensitivities down to 1 part in  $10^{12}$  should be available in routine SIRIS analysis, and greater sensitivities should be available for special cases.

The basic concepts of this technology and early results in the development of the new SIRIS process and apparatus are presented.

#### 1. INTRODUCTION

Sputter-initiated resonance ionization spectroscopy (SIRIS) is a new ultrasensitive and ultrasensitive technique for the analysis of the elemental composition of solids. This new technique combines two established and well-understood technologies, ion beam sputtering and resonance ionization spectroscopy (RIS), to make analysis of impurities in solids at concentration levels several orders of magnitude lower than has been possible previously with other techniques. SIRIS is being developed commercially by Atom Sciences Inc. in Oak Ridge, TN.

The concept for SIRIS in its simplest form is illustrated in Fig. 1. An energetic ion beam is used to sputter the constituents of a solid sample so that a vapor cloud of ions and neutral atoms is formed above the sample located in a vacuum. An RIS laser beam then probes the vapor cloud to ionize these atoms of a given element selectively. Ionized atoms of the selected element are then directed to an ion detector and counted. In a more practical form a mass spectrometer is added to the detection system to confirm the elemental identity of the ionized atom and/or to add isotopic identification.

SIRIS provides ultrasensitive analysis of solid samples for all the elements except helium and neon. Sensitivities down to 1 part in  $10^{12}$  will be possible in routine SIRIS analysis, and greater sensitivities will be possible for special cases.

\* Paper presented at the International Conference on Metallurgical Coatings, San Diego, CA, U.S.A., April 18-22, 1983.

† Consultant from the Oak Ridge National Laboratory, Oak Ridge, TN, U.S.A.

‡ Visiting scientist on sabbatical leave from Colorado State University, Fort Collins, CO, U.S.A.

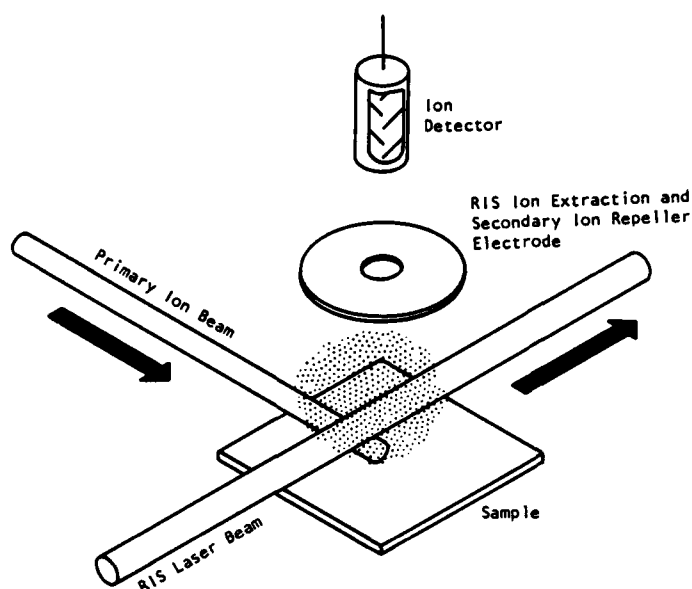


Fig. 1. SIRIS concept.

## 2. BACKGROUND TECHNOLOGY FOR SPUTTER-INITIATED RESONANCE IONIZATION SPECTROSCOPY

### 2.1. Resonance ionization spectroscopy

RIS is a relatively new technology developed at Oak Ridge National Laboratory by Hurst and coworkers in 1975<sup>1</sup>. This new technology has been reported<sup>2</sup> as a means of providing a new ultrasensitive analytical technique for the counting of single atoms of a selected element in a background sea of atoms of other elements. Comprehensive reviews of RIS technology have been published by Hurst and coworkers<sup>3</sup>. RIS technology forms the basis for new innovative ultrasensitive analysis techniques being developed at Atom Sciences Inc. and is the basis for the work being reported here.

In the resonance ionization process a laser is tuned precisely to the wavelength required to excite an atom from its ground state to a particular excited state which is unique to the element being measured. In the simplest RIS scheme (Fig. 2) a second photon of the same wavelength then interacts with the excited state and causes an electron to be released from the atom, thus producing a positive ion and a free electron. This RIS process, therefore, is a two-step process, first involving excitation of the atom to a specific quantum state (resonance) and second involving removal of an electron from the selected excited state (ionization). A charged particle detector is used to detect and count the ions or electrons produced to achieve the ultrasensitive ultraselective measurement.

This simple RIS scheme, or a variation of it involving frequency doubling, can be used for many but not all elements. A second laser (with or without frequency doubling) in combination with the first laser provides the ability to excite two states

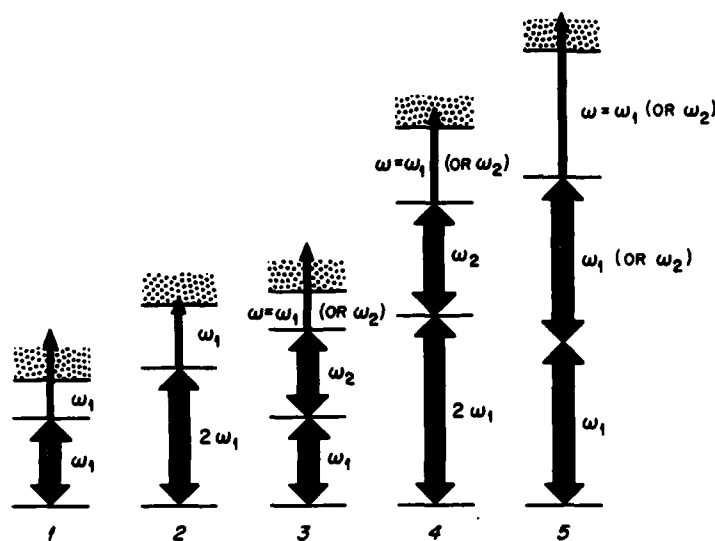


Fig. 2. Five basic schemes for RIS.

sequentially prior to ionization. Still another RIS process involves a two-photon transition to an intermediate state prior to ionization. These five RIS schemes, applied appropriately, permit the detection and analysis of every element in the periodic table, except helium and neon.

The uniqueness of resonance ionization is that it is extremely *selective* and extremely *efficient*. It is uniquely selective in that only those atoms of a given element are ionized, since the selected intermediate excited states through which the process proceeds are unique to the selected element. It is uniquely efficient in that all atoms of the selected element which are present in the laser beam are ionized. In contrast, the more familiar methods of ionization of matter (such as ionization by  $\alpha$  particles,  $\beta$  rays etc.) are inefficient and non-selective.

While the RIS process is completely selective as to element, it has no, or only moderate, selectivity as to isotope, except for the very light elements (of atomic number less than about 5). To identify and detect isotopes of any given element, a mass analyzer is incorporated in the RIS apparatus. This can be a magnetic sector, r.f. quadrupole or time-of-flight analyzer. Recycling and enrichment procedures can also be incorporated into the process when especially high isotopic abundance ratio requirements must be met.

Resonance ionization is predictable because the physical process can be calculated from data that have been compiled for many years. Energy levels of all atoms in the periodic table have been compiled together with tabulations of the transition probabilities. The RIS technique itself is beginning to supplement the available information. For example, RIS can be used to measure photo-ionization cross sections of particular excited states. In summary, data exist, both theoretical and experimental, which permit good approximations of the intensities required to achieve saturation.

## 2.2. Sputtering

Sputtering of surfaces by energetic ion beams has formed the basis for several analytical techniques for the analysis of impurities in solid materials. Most notable among these are secondary ion mass spectrometry (SIMS), ion microprobe mass spectrometry and ion scattering spectrometry.

SIMS heretofore has been the most sensitive and widely used technique for analyzing semiconductor and other materials for low concentrations of impurities. In the SIMS technique an energetic ion beam is used to sputter ions and neutral atoms from a solid matrix material. Typically a primary ion beam of 5–20 keV argon,  $O_2$  or cesium ions is used to do the sputtering. The secondary ions generated in the process are generally passed first through an energy analyzer and then through a mass analyzer. The better instruments use a double-focusing mass spectrometer consisting of an electrostatic sector for energy analysis and a magnetic sector for mass analysis. The sputtering process is used to liberate atoms from the matrix and to generate secondary ions, while the mass spectrometer is used to select out the impurity atoms from the matrix atoms. The sensitivity and selectivity of the technique depend entirely on the resolution and abundance sensitivity of the mass spectrometer.

There are problems which limit the effectiveness of the SIMS technique, the most serious of which is the strong dependence of the secondary ion yield from a given matrix on the element being sputtered. In addition, the secondary ion yield is very small compared with the yield of neutral atoms. The dependence of the secondary ion yield on the presence of other atoms in the matrix material, coupled with the low yield of secondary ions, increases the uncertainty of the measurements and limits the sensitivity and reliability of the measurements.

Sputtering, however, is an established technique which has been well characterized both experimentally and theoretically. Since the yield of neutral atoms from a sample material is much greater and less dependent on extraneous matrix effects, compared with secondary ions, it is preferable to analyze the neutral sputtered material. RIS is well suited to ionizing neutrals and, when combined with sputtering, provides an ultrasensitive technique for the analysis of solids. This technique, being developed by Atom Sciences Inc., is referred to as sputter-initiated resonance ionization spectroscopy and is now described.

## 3. THE SPUTTER-INITIATED RESONANCE IONIZATION SPECTROSCOPY APPARATUS

A schematic diagram of the SIRIS apparatus that has been designed and built by Atom Sciences Inc. is shown in Fig. 3. The primary ion beam is generated with a duoplasmatron ion source and is mass analyzed by the analyzing magnet to ensure beam purity. A set of deflection plates is used to sweep the beam across a pair of chopping slits. Focusing is achieved magnetically, with quadrupole magnets as well as the analyzing magnet itself. Through most of its travel the ion beam density is kept small to prevent the beam transport from being space charge limited. A final  $4^\circ$  bending magnet is placed in the ion beam just prior to its reaching the target to prevent any beam contaminants or line-of-sight ions generated by scattering from the walls from hitting the target.

Typically, a 1 mA argon beam is generated and ion pulses of about 2  $\mu$ s

duration are directed to the target sample. The energy of the ions can be varied from 5 to 30 keV. Generally, the frequency with which the ion pulses are directed to the target is equal to the frequency of the laser used as the RIS probe, typically 30 Hz. However, the frequency of pulses can be increased up to a duty cycle of 100% (direct current mode) to sputter away substantial amounts of material so that depth profiling can be performed.

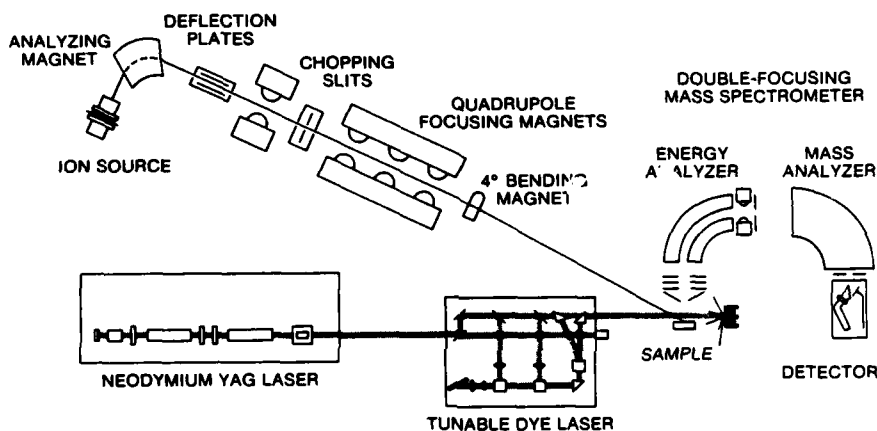


Fig. 3. Schematic diagram of SIRIS apparatus.

The ion beam intersects the sample plane at  $60^\circ$  with respect to the normal and is focused to a  $2.6 \text{ mm} \times 3.3 \text{ mm}$  spot. The resulting puff of sputtered material from the sample contains both secondary ions and neutral atoms characteristic of the sample itself. Secondary ions are formed indiscriminately and could interfere with subsequent analysis except that in the SIRIS apparatus they are repelled back to the sample, leaving only the neutrals to be probed by the RIS process.

Ions of the selected elemental species which are created by the RIS process are verified and their isotopic mass is measured with a mass spectrometer. The mass spectrometer used in SIRIS is a double-focusing type consisting of an electrostatic sector which acts as an energy analyzer and a magnetic sector which determines the mass of the ion. Neutral atoms sputtered from a solid sample, and therefore the ions produced by RIS, have an energy distribution that extends to several hundred electronvolts. Fortunately, the distribution is sharply peaked and most of the ions are centered about an average energy of about 10 eV. The electrostatic sector is adjusted to allow ions to be transmitted with energies ranging from 0 to about 100 eV. Ions having higher energies are rejected, thus ensuring that the input to the magnetic sector is such that mass analysis can be performed with the required high resolution and abundance sensitivity. The resolution of the mass spectrometer is 440 at 300 a.m.u. but, more importantly, its abundance sensitivity is greater than  $10^6$ .

After the RIS selected ions are verified as to element and their mass is measured with the mass spectrometer, they are detected with a channel electron multiplier equipped with a special conversion electrode. Since SIRIS is a pulsed technique, the background is reduced to a minimum by time gating the electronics. The ion-

counting system is set to accept pulses only during the time period when an ion is expected to arrive. Typically, noise factors for single-ion detectors are reduced by more than a million using this technique.

The RIS process is achieved by using a Nd:YAG laser to pump one, two or more tunable dye lasers. Each dye laser consists of three sections: an oscillator, a preamplifier and an amplifier. These sections can be used in various combinations to optimize the production of light of the desired wavelength and intensity. The dye laser produces tunable light of the desired wavelength throughout the visible spectrum. In addition to visible light, UV light down to about 2000 Å can be generated by additional non-linear processes consisting of second harmonic generation and mixing.

The target chamber of the SIRIS apparatus has been designed to have versatility in its sample-handling capability. Sample sizes can be accommodated which are as small as 5 mm × 5 mm and as large as 3 in in diameter. *x*, *y* and *z* rastering at a rate of 0.16 mm s<sup>-1</sup> can be done. Sputtering for depth profiling can be performed at a rate of 0.03 Å cm<sup>-2</sup> or 0.065 μm s<sup>-1</sup> (silicon).

Other features of the SIRIS apparatus incorporate special ultrahigh vacuum

TABLE I  
SPECIFICATIONS OF DESIGN AIMS FOR SPUTTER-INITIATED RESONANCE IONIZATION SPECTROSCOPY APPARATUS

<i>Ion beam</i>	
Ions	Ar (others available)
Mass resolution	1:40 (Ar)
Energy	5–30 keV
d.c.	1 mA
Focusing	all magnetic
Beam spot size on target	2.6 mm × 3.3 mm
Vacuum	1 × 10 <sup>-7</sup> Torr or less (static)
Pulse repetition rate	0–10000 Hz
Pulse width	0.25–10.0 μs
<i>Mass analysis section</i>	
Type	double-focusing, electrostatic and magnetic sectors
Abundance sensitivity	10 <sup>6</sup>
Transmission efficiency	90%
Resolution	440
Mass range	1–300 a.m.u.
Vacuum	1 × 10 <sup>-8</sup> Torr or less
<i>Target chamber</i>	
Precision sample manipulation	
Specimen dimensions	5 mm × 5 mm to 2 cm × 2 cm
Vacuum	1 × 10 <sup>-9</sup> Torr or less
<i>x</i> – <i>y</i> – <i>z</i> rastering	
Depth profiling	0.065 μm s <sup>-1</sup> (silicon) or 0.03 Å cm <sup>-2</sup>
<i>Other features</i>	
Ultraclean ultrahigh vacuum system with cryogenic, sorption and ion pumping	
Vacuum lock and bake-out for sample introduction	
Automated multiple-sample handling capability	
Microprocessor controlled	
Computer-based data acquisition system	

techniques and computer control. The SIRIS apparatus is entirely microprocessor controlled and a minicomputer is programmed to control the microprocessor. The minicomputer also functions as a computer-based data acquisition system. The system is designed to collect data in a variety of ways, *e.g.* in a single-ion counting mode or in an analog current mode.

The design of the SIRIS apparatus has taken advantage of available information to optimize the performance of the instrument. Ion transport computer programs have been used to determine both the transport of ions of the primary sputtering beam and the transport of ions analyzed by the mass spectrometer. With the supporting theoretical and experimental information, calibration of the SIRIS apparatus can be achieved from first principles as well as from standard calibration samples.

The specifications of the design aims of the SIRIS apparatus being developed by Atom Sciences Inc. are summarized in Table I.

#### 4. PRELIMINARY RESULTS AND DATA

The initial phase of the construction of the SIRIS apparatus has been completed and testing began in early 1983. The double-focusing magnetic mass spectrometer has been adjusted to achieve the double-focusing condition; however, the final optimum conditions have not yet been reached. The results show that the mass resolution specifications have been met easily, and the abundance sensitivity specification of  $10^6$  will be achieved when the ultimate vacuum conditions are obtained. Pulsing of the ion beam has just recently been included, and this will improve the dynamic vacuum conditions of the target chamber. Measurements at present indicate that the abundance sensitivity is greater than  $10^5$  and, when the

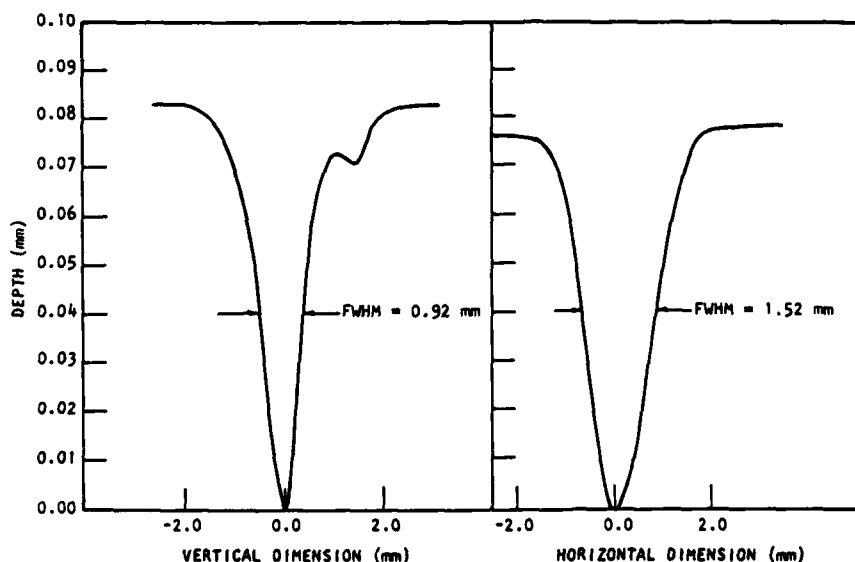


Fig. 4. Surface profile of a sample of GaAs.

system is properly baked out and the proper vacuum specifications are met under the pulsed ion beam mode of operation, the  $10^6$  value will be obtained.

The size of the ion beam as it is focused onto the target is important. Measurements indicate that the horizontal and vertical dimensions of the present beam are well within the design aims. Figure 4 shows a surface profile of a sample of GaAs sputtered with a d.c. beam. The depth of the sputtered crater was measured as a function of the horizontal and vertical dimensions with a Sloan Dektak surface profile measuring system. The full width at half maximum (FWHM) measurements of the horizontal and vertical dimensions are 1.52 mm and 0.92 mm respectively, and therefore the beam spot size is well within the design specifications of  $2.6 \text{ mm} \times 3.3 \text{ mm}$ .

For an initial experiment a sample of silicon was obtained from Hughes Research Laboratories containing gallium in the bulk at a concentration of 1 part in

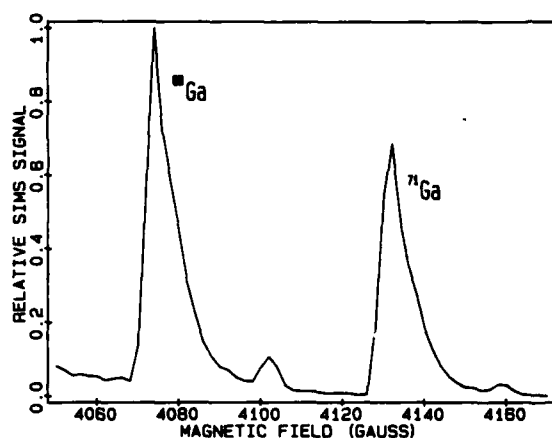


Fig. 5. SIMS mass spectrum of gallium in silicon (bulk concentration of gallium, 1 part in  $10^4$ ).

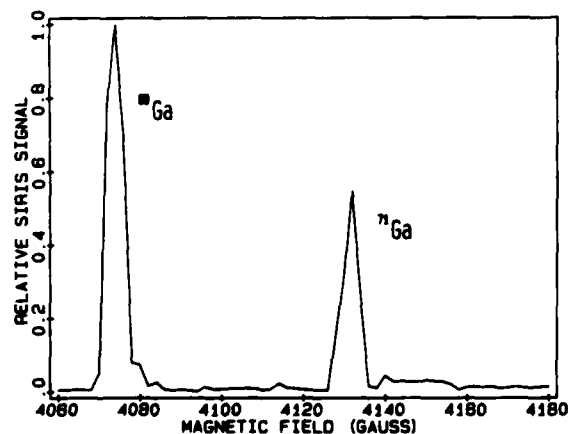


Fig. 6. SIRIS mass spectrum of gallium in silicon (bulk concentration of gallium, 1 part in  $10^4$ ).

$10^4$ . The mass analyzer was tuned to the  $^{69}\text{Ga}$  and  $^{71}\text{Ga}$  isotopes using the apparatus in the SIMS mode of operation. The results of this SIMS experiment are shown in Fig. 5 where the SIMS signal is measured as a function of the magnetic field. The apparatus was then adjusted for the RIS mode of operation and the results of that experiment are shown in Fig. 6. There are two notable differences between the SIMS and the SIRIS results. The SIMS spectra have a tail on the high mass side of each peak and have two additional peaks at the mass 70 and 72 positions. The tails in the SIMS spectra probably result from the high energy ions sputtered from the sample and not rejected by the energy analyzer. The peaks at masses 70 and 72 may be due to hydrides of gallium,  $\text{GaH}^+$ . These additional mass peaks are not displayed in the SIRIS spectrum. If the hydrides are formed at the surface during the sputtering process, then the SIRIS process would reject them and they would not be further ionized by the RIS process.

To illustrate the selectivity of the RIS process, a wavelength spectrum of gallium was measured while the mass spectrometer was kept tuned to the  $^{69}\text{Ga}$  peak.

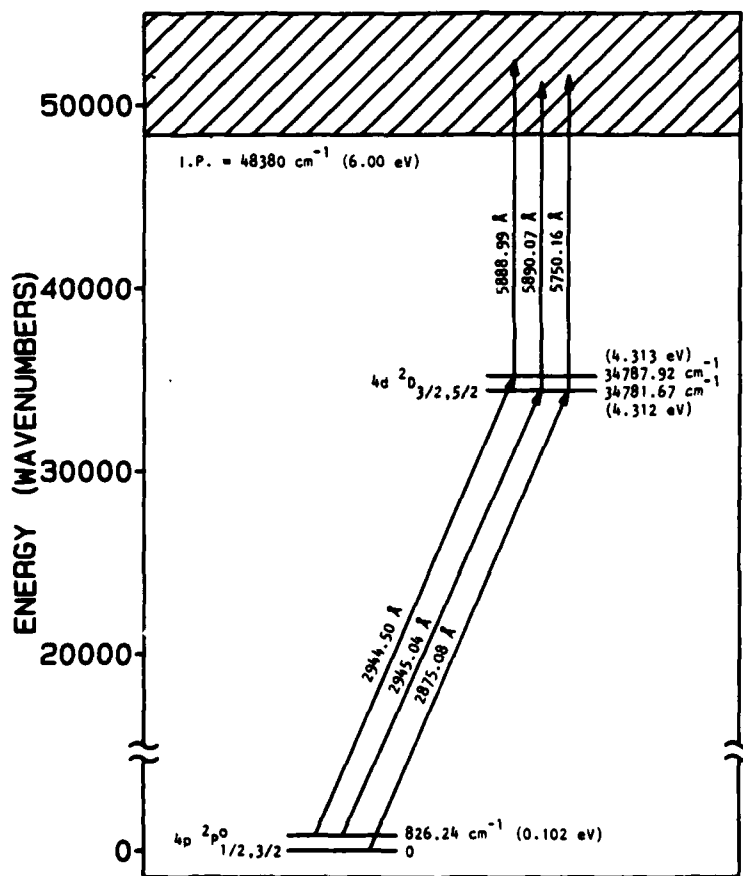


Fig. 7. Grotrian diagram of gallium.

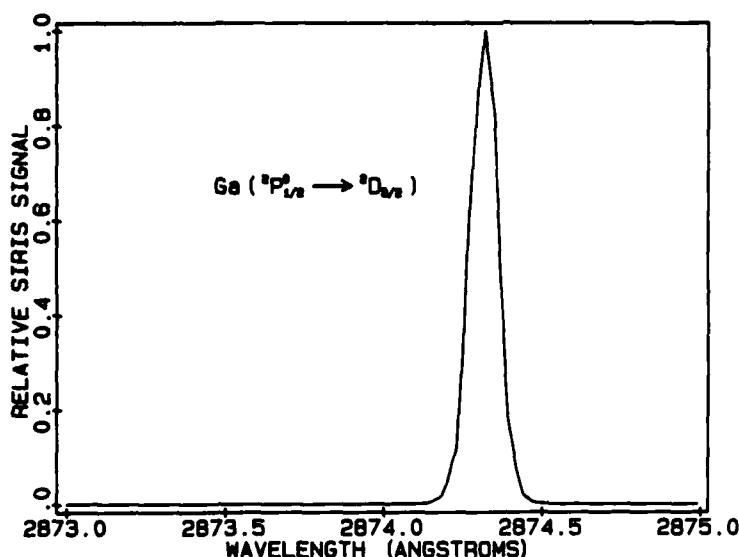


Fig. 8. SIRIS wavelength spectrum of gallium in silicon for excitations from the  $^2P_{1/2}^0$  state (bulk concentration of gallium, 1 part in  $10^4$ ).

The dye laser was tuned to produce yellow light at 5750 Å and then was frequency doubled to produce UV light at 2875 Å. A grotrian diagram for gallium is shown in Fig. 7. The UV light was used for the resonant excitation step and the more intense yellow light was used for the photo-ionization step. This produced a resonant transition in gallium from the  $Ga\ ^2P_{1/2}^0$  state to the  $Ga\ ^2D_{3/2}$  state. The excited gallium atoms were then photo-ionized by the absorption of a photon of visible light. A wavelength spectrum of the results is shown in Fig. 8.

##### 5. SUMMARIZING REMARKS

The results reported here are preliminary and qualitative in nature. In the gallium experiments, quantitative measurements were not accurate enough for making precise comparisons. The results thus far are encouraging, and the addition of a pulsed ion beam at 20 times the present output and single-ion counting should allow detection of gallium at sensitivities down to 1 part in at least  $10^9$ . With planned increases in the efficiency of the SIRIS apparatus, we should be able to reach the desired sensitivity of 1 part in  $10^{12}$ .

##### REFERENCES

- 1 G. S. Hurst, M. G. Payne, M. H. Nayfeh, J. P. Judish and E. B. Wagner, *Phys. Rev. Lett.*, **35** (1975) 82.
- 2 G. S. Hurst, M. H. Nayfeh and J. P. Young, *Appl. Phys. Lett.*, **30** (1977) 229.
- 3 G. S. Hurst, M. G. Payne, S. D. Kramer and J. P. Young, *Rev. Mod. Phys.*, **51** (1979) 767.  
G. S. Hurst, M. G. Payne, S. D. Kramer and C. H. Chen, *Phys. Today*, **33** (1980) 24.

APPENDIX K

Invited Talk entitled

Ultrasensitive Elemental Analysis of Solids by  
Sputter Initiated Resonance Ionization Spectroscopy

presented by

J. E. Parks, H. W. Schmitt, G. S. Hurst\*, and W. M. Fairbank, Jr.\*\*  
Atom Sciences, Inc.  
Post Office Box 138  
114 Ridgeway Center  
Oak Ridge, Tennessee 37830

at

SPIE - The International Society for Optical Engineering Conference 426  
"Laser-based Ultrasensitive Spectroscopy and Detection V"

during

SPIE's 27th Annual International Technical Symposium and Instrument Display

held

August 21-26, 1983  
San Diego, California

\*Consultant from the Oak Ridge National Laboratory

\*\*Visiting Scientist on Sabbatical Leave from Colorado State University

Ultrasensitive elemental analysis of solids by  
sputter initiated resonance ionization spectroscopy

J. E. Parks, H. W. Schmitt, G. S. Hurst\*, and W. M. Fairbank, Jr.\*\*

Atom Sciences, Inc.  
114 Ridgeway Center, Oak Ridge, Tennessee 37830

Abstract

This paper describes a new technique, Sputter-Initiated Resonance Ionization Spectroscopy (SIRIS)<sup>†</sup>, for ultrasensitive elemental analysis of solid samples. SIRIS combines resonance ionization spectroscopy and ion beam sputtering to provide analyses for all the elements except helium and neon with predicted sensitivities down to 1 part in  $10^{12}$  in routine analysis, and greater for special uses. Basic concepts of this technology and new results in the development of the new SIRIS process and apparatus are presented.

Introduction

Sputter-Initiated Resonance Ionization Spectroscopy (SIRIS) is a new analytical procedure being developed commercially by Atom Sciences. The principal technology in SIRIS is Resonance Ionization Spectroscopy (RIS) which was conceived and developed by G. S. Hurst at Oak Ridge National Laboratory<sup>1-4</sup>. RIS is an ultra-sensitive analytical technique for trace element or isotope analysis. In the simplest RIS process (see Figure 1), a tunable laser is adjusted so that it emits precisely the correct wavelength to excite an electron in an atom from its original state to a higher state. Another photon of the same wavelength then interacts with the excited state and causes the electron to be released from the atom, thereby producing a positive ion and a free electron. RIS, therefore, is an ionization process which occurs in two steps, the first involving excitation of the atom to a specific excited state (resonance) and the second involving removal of the electron from the atom (ionization).

We note that the simplest RIS scheme just described, in which both steps are produced by the same laser, can be used for relatively few elements. Other RIS processes may involve a second resonance step (requiring another laser) such that two excited bound states are sequentially populated prior to ionization; or, in rare cases, a two-photon resonant intermediate state may be produced by the simultaneous absorption of two photons from the same laser. These techniques, applied appropriately, permit every element in the periodic table, except helium and neon, to be analyzed and detected by an RIS process.

With commercial lasers it is possible to saturate all of these processes. That is, an atom in the initial state (usually the ground state) before the laser pulse arrives will be excited through the resonant intermediate state(s) and into the ionization continuum with unit probability during a single laser pulse.

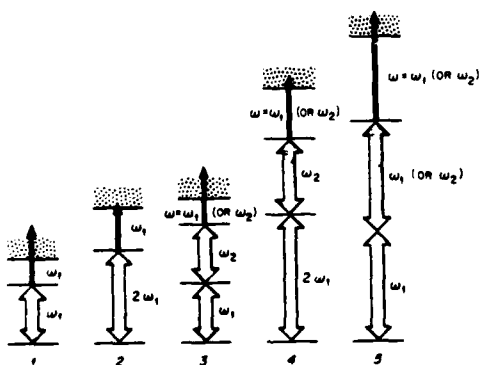


Figure 1. Five basic RIS schemes

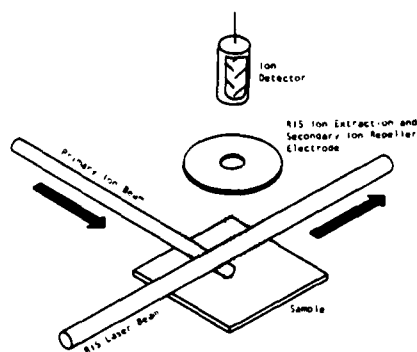


Figure 2. SIRIS concept

\*Consultant from the Oak Ridge National Laboratory

\*\*Visiting scientist on sabbatical leave from Colorado State University

†Patent pending

The uniqueness of RIS is that it is an extremely selective and sensitive process. It is selective in that only atoms of a given element are ionized, since the intermediate excited states through which the ionization proceeds may be chosen such that they are uniquely characteristic of that element. RIS is extremely efficient in that all atoms of the selected element which are in the laser beam are ionized, provided only that the laser power is sufficient.

An inherent condition of almost all RIS techniques is that the sample must be in the gas phase. In a few cases, the sample is initially a gas, but most samples of interest are either solid or liquid. SIRIS uses sputtering to accomplish this.

Sputtering is a well established technique for vaporizing solids and is very reproducible. The basic concept for SIRIS is illustrated in its simplest form in Figure 2. In SIRIS a pulsed ion beam (usually argon) is focused onto a solid sample, thus producing a cloud of vapor immediately above the target. RIS lasers then selectively ionize atoms in the vapor cloud of the chosen element which are subsequently accelerated through a mass filter for detection at an electron multiplier. Secondary ions, produced by the impact of the ion beam, can be rejected by electrostatic fields, electrostatic energy analysis, the relative timing between the ion beam pulse and RIS laser pulse, or a combination of all the above.

SIRIS has several important advantages over Secondary Ion Mass Spectrometry (SIMS), a technique which also uses a primary ion beam to sputter a solid for mass analysis. The secondary ion yield (the quantity measured in SIMS) varies greatly depending on the composition of the surface of the sample. Also, the ratio of secondary ions to neutrals is usually on the order of  $10^{-3}$  to  $10^{-4}$ . This means that SIRIS should be more sensitive than SIMS by several orders of magnitude and should not be susceptible to variations in signal magnitude caused by matrix effects.

SIRIS provides ultrasensitive analysis of solid samples for all the elements except helium and neon. Sensitivities down to 1 part in  $10^{12}$  will be possible in routine SIRIS analysis, and greater sensitivities will be possible for special cases.

#### The SIRIS apparatus

A schematic diagram of the SIRIS apparatus that has been designed and built by Atom Sciences is shown in Figure 3. The primary ion beam is generated with a duoplasmatron ion source and is mass analyzed by the analyzing magnet to insure beam purity. A set of deflection plates is used to sweep the beam across a pair of chopping slits. Focusing is achieved magnetically, with quadrupole focusing magnets as well as the analyzing magnet itself. A final 4° bending magnet is placed in the ion beam just prior to its reaching the target to prevent any beam contaminants or line-of-sight ions generated by scattering from the walls from hitting the target.

For this work, a 50 uamp argon beam was generated and ion pulses of about .75 microseconds duration were directed to the target sample. Ion beam currents of 1 milliamp or greater can be obtained. The energy of the ions can be varied from 5 to 30 keV. Generally, the frequency with which the ion pulses are directed to the target is equal to the frequency of the laser used as the RIS probe, typically 30 Hz. However, the frequency of pulses can be increased up to a duty cycle of 100% (direct current mode) to sputter away substantial amounts of material from the top surface.

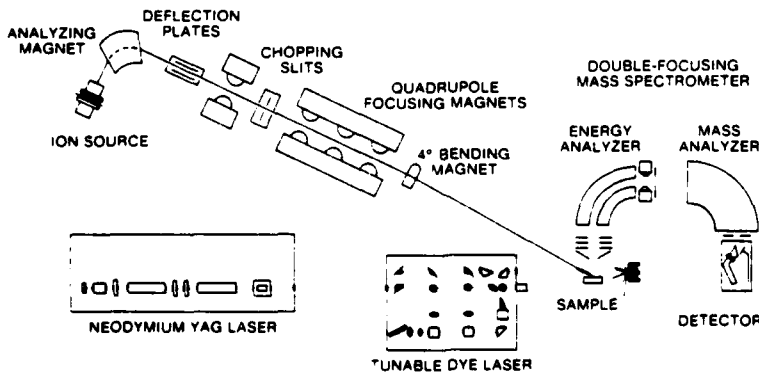


Figure 3. Diagram of SIRIS apparatus

The ion beam intersects the sample plane at 60° with respect to the normal and is focused to a 2.6 x 3.3 mm spot. The resulting puff of sputtered material from the sample contains both secondary ions and neutral atoms characteristic of the sample itself. Secondary ions are formed indiscriminately and could interfere with subsequent analysis except that in the SIRIS apparatus they are rejected by energy analysis and time discrimination. RIS produced ions are created in a different region of space and are accelerated a shorter distance than the SIMS ions. The RIS ions are given less energy and are allowed to pass through the energy analyzer while the SIMS ions are rejected. By delaying the laser pulse, the RIS ions are created at a different time than the SIMS ions and this allows the data acquisition system to time discriminate against the SIMS ions.

Ions of the selected elemental species which are created by the RIS process are verified and their isotopic mass is measured with a mass spectrometer. The mass spectrometer used in SIRIS is a double focusing type consisting of an electrostatic sector which acts as the energy analyzer and a magnetic sector which determines the mass of the ion. Neutral atoms sputtered from a solid sample, and therefore the ions produced by RIS, have an energy distribution that extends to several hundred eV. Fortunately, the distribution is sharply peaked and most of the ions are centered about an average energy of a few eV. The electrostatic sector is adjusted to allow these ions to be transmitted.

Ions having higher energies are rejected, thus insuring that the input to the magnetic sector is such that mass analysis can be performed with the required high resolution and abundance sensitivity. The resolution of the mass spectrometer is designed to be 440 at 300 amu. More importantly, its abundance sensitivity is designed to be greater than  $10^6$ .

After the RIS selected ions are verified as to element and their mass is measured with the mass spectrometer, they are detected with a channel electron multiplier equipped with a special conversion electrode. Since SIRIS is a pulsed technique, background is reduced to a minimum by time gating the electronics of the data acquisition system. The ion counting system is set to accept pulses only during the time period when an ion is expected to arrive. Typically, noise factors for single ion detectors are reduced by more than a million using this technique.

The RIS process is achieved by using a neodymium YAG laser to pump one, two, or more tunable dye lasers. Each dye laser consists of three sections: an oscillator, a preamplifier, and an amplifier. These sections can be used in various combinations to optimize the production of light of the desired wavelength and intensity. The dye laser produces tunable light of the desired wavelength throughout the visible spectrum. In addition to visible light, ultraviolet light down to about 2000 Å can be generated by additional non-linear processes consisting of second harmonic generation and mixing.

The target chamber of the SIRIS apparatus has been designed to have versatility in its sample handling capability. Sample sizes can be accommodated which are as small as 5 x 5 mm and as large as 2 inches in diameter. X, Y, and Z rastering at a rate of 0.16 mm/sec can be done. Sputtering for depth profiling can be performed at a rate of 0.03 amps/cm<sup>2</sup> or 0.065 μm/sec (Si).

Other features of the SIRIS apparatus incorporate special ultrahigh vacuum techniques and computer control. The SIRIS apparatus is entirely microprocessor controlled and a minicomputer is programmed to control the microprocessor. The minicomputer also functions as a computer-based data acquisition system. The system is designed to collect data in a variety of ways, e. g., in a single ion counting mode or in an analog current mode.

The design of the SIRIS apparatus has taken advantage of available information to optimize the performance of the instrument. Ion transport computer programs have been used to determine both the transport of ions of the primary sputtering beam and the transport of ions analyzed by the mass spectrometer. With the supporting theoretical and experimental information, calibration of the SIRIS apparatus can be achieved from first principles as well as from standard calibration samples.

#### Data and results

The initial phase of the construction of the SIRIS apparatus has been completed and testing began in early 1983. The double-focusing magnetic mass spectrometer has been adjusted to achieve the double focusing condition, however the final optimum conditions have not yet been reached. The results show that the mass resolution specifications have been met easily, and the abundance sensitivity specifications of  $10^6$  will be achieved when the ultimate vacuum conditions are obtained. Pulsing of the ion beam has just recently been included, and this has improved the dynamic vacuum conditions of the target chamber. Measurements at present indicate that the abundance sensitivity is greater than  $10^5$ , and when the system is properly baked out and the proper vacuum specifications are met under the pulsed ion beam mode of operation, the  $10^6$  figure will be obtained.

The size of the ion beam as it is focused on the target is important. Measurements indicate that the horizontal and vertical dimensions of the present beam are well within the design aims. Figure 4 shows a surface profile of a sample of GaAs sputtered with a DC beam. The depth of the sputtered crater was measured as a function of the horizontal and vertical dimensions with a Sloan Dektak surface profile measuring system. The FWHM measurements of the horizontal and vertical dimensions are 1.52 mm and 0.92 mm respectively, and therefore the beam spot size is well with the design specifications of  $2.6 \times 3.3$  mm.

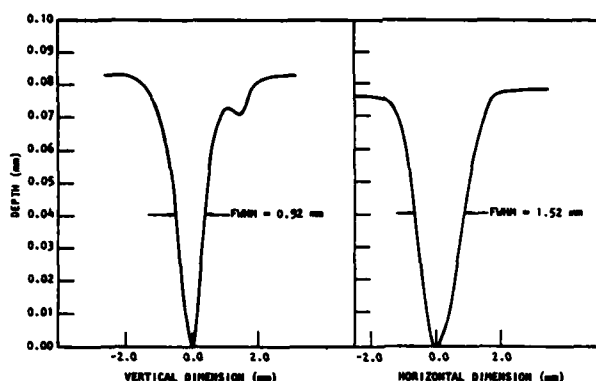
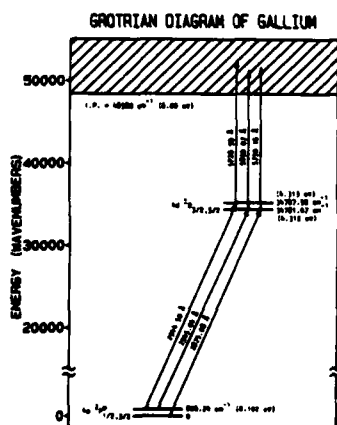


Figure 4. Sputter profile of gallium arsenide sample

To illustrate the selectivity of the RIS process, a wavelength spectrum of gallium was measured while the mass spectrometer was kept tuned to the  $\text{Ga}^{69}$  peak. The dye laser was tuned to produce yellow light at  $5750 \text{ \AA}$  and then was frequency doubled to produce uv light at  $2875 \text{ \AA}$ . A Grotrian diagram for gallium is shown in Figure 5. The uv light was used for the resonant excitation step and the more intense yellow light was used for the photoionization step. This produced a resonant transition in gallium from the  $\text{Ga}(^2P^{\circ}_{1/2})$  state to the  $\text{Ga}(^2D_{3/2})$  state. The excited gallium atoms were then photoionized by the absorption of a photon of visible light. A wavelength spectrum of the results are shown in Figure 6.



Data were taken to demonstrate the validity of the SIRIS technique by scanning the magnetic field of the mass analyzer over a range that would include several isotopes of the impurity atoms of interest and other adjacent masses. The computer based data acquisition system was programmed to set the magnetic field at a specified value while SIRIS signals were measured for a specified number of laser pulses, typically 300 (at 30 hertz, for a time of 10 seconds). Two modes of signal processing were used, single ion counting with pulse height discrimination and analog pulse averaging. In the single ion counting mode, count rates were less than one ion per laser pulse. Ideally, the rate should be kept at less than one out of ten, but in order to extend the dynamic counting range higher rates (but less than one out of one) were allowed. The data was then corrected using Poisson statistics and the corrected data was used as the representative measurement of SIRIS ions arriving at the detector. Single ions produced a voltage pulse of about one volt and a discrimination level of 0.3 volts was set to reject noise pulses. The single ion counting mode was used for impurity levels of a few ppm and lower.

In the analog pulse averaging mode, more than one ion arrives at the detector for each laser pulse and the pulse height of the signal is proportional to the number of ions and the electronic gain. The pulse height of each laser generated event was measured and the average taken for the number of laser pulses used. Due to a dc voltage offset in the electronics, a small background noise level occurs in the spectra.

Well characterized silicon samples doped with gallium were supplied by Hughes Research Laboratories of Malibu, California and were used for the first demonstration experiments. A typical spectrum is shown in Figure 7. The spectrum shows two isotopes of gallium, gallium-69 and gallium-71, for a sample of silicon doped at the 58 ppm level. The relative natural abundance of gallium 69 and 71 is 60.5% and 39.5% respectively and the data agrees with that fact. Data points are seen as inflection points on the graph where the points have been connected with straight lines. The data was collected using the analog pulse averaging mode. A similar sample of silicon containing 0.5 ppm gallium was measured using the single ion counting mode. Those results are shown in Figure 8. It is clear that the single ion counting mode has essentially no background noise. The data indicates that 26 gallium-69 ions were counted in 10 seconds, 300 laser pulses at 30 hertz. In a 5 minute counting time more than 45,000 ions would have been counted. If the background could be kept relatively small, 100 ions could be counted in 5 minutes for a 0.001 ppm sample.

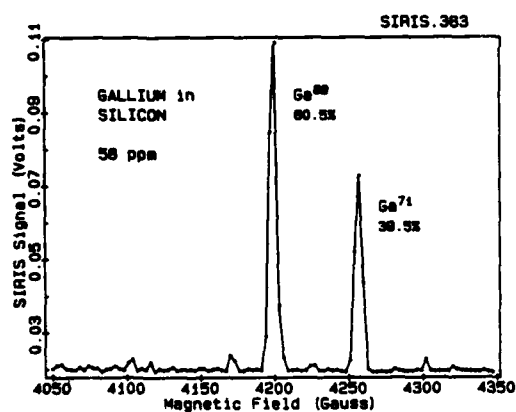


Figure 7. Mass spectrum of 58 ppm gallium in silicon

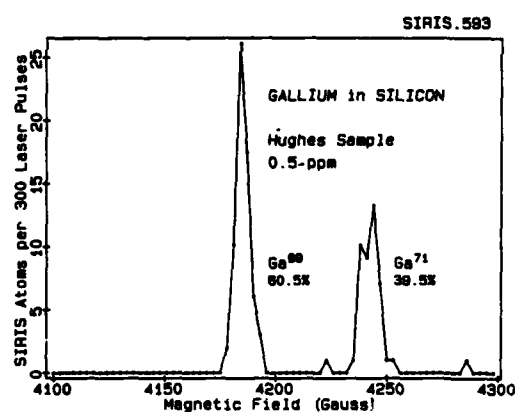


Figure 8. Mass spectrum of 0.5 ppm gallium in silicon

A series of gallium in silicon samples containing 58, 25, 2, 0.5, and 0.05 ppm were measured for their gallium-69 content. A composite plot of those results are shown in Figure 9. The gallium-69 peaks were integrated and background was subtracted for each of the samples and the measured values were correlated with the values supplied with the Hughes samples. The results are shown as points in the log-log correlation plot in Figure 10. The straight line indicates the one to one correlation. The 0.05 ppm sample shows an anomalous result where the SIRIS measured value is approximately 100 times higher than that specified by Hughes.

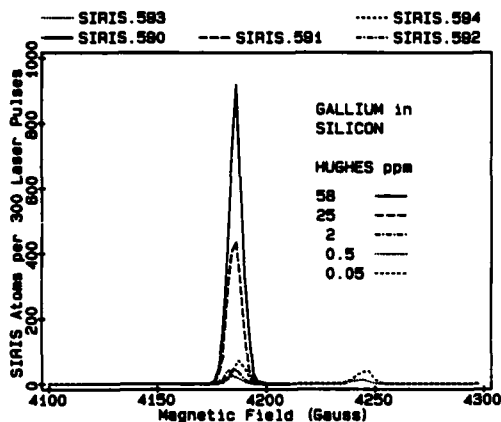


Figure 9. Composite of SIRIS spectra of gallium in silicon samples

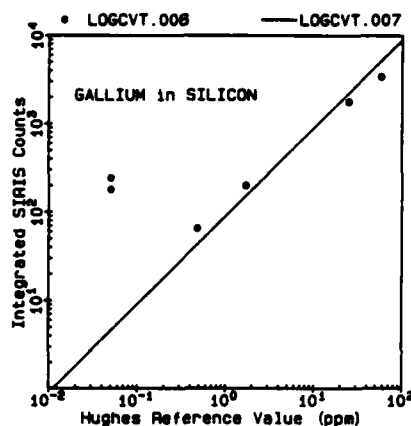


Figure 10. Comparison of SIRIS measurements with Hughes reference values

A set of five stainless steel samples with certified analyses of various impurity elements were obtained from the National Bureau of Standards. These samples were analyzed by SIRIS to determine the aluminum concentration. The spectra obtained in those measurements are shown in Figure 11 and a log-log plot of the SIRIS results versus the NBS values is shown in Figure 12. The measurements were made using the SIRIS apparatus in the analog pulse averaging mode since the concentrations of aluminum were well above the 1 ppm level. The data were analyzed as with the gallium in silicon data, by integrating the peaks and subtracting the background. The measurements were repeated a second day and were found to be reproducible. The SIRIS value for NBS sample #1265 was found to be slightly higher than the NBS reference value. By sputtering the surface, the samples were cleaned, and the repeated results of the second day were in good agreement with the NBS values. Surface contamination was particularly noticeable with the 7 ppm aluminum in stainless steel sample, as indicated by the somewhat high first-day run. Note that in Figure 12 the first day's results are shown as o's and the second day's results are shown as x's. NBS samples #'s 1264 and 1265 were not certified as to their aluminum content, and the values were obtained from direct measurements by NBS.

The same samples were measured for their vanadium content and were compared with the vanadium concentrations as measured and certified by NBS. The results of those measurements are shown in the composite spectrum plot of Figure 13 and in the log-log plot of Figure 14. Those results are in good agreement with the NBS certified values as shown in the correlation plot of Figure 14.

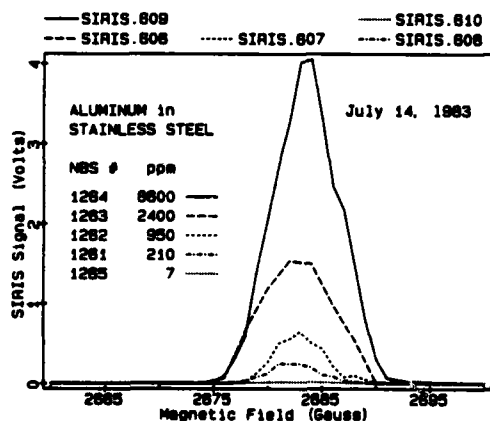


Figure 11. Composite of SIRIS spectra of aluminum in stainless steel

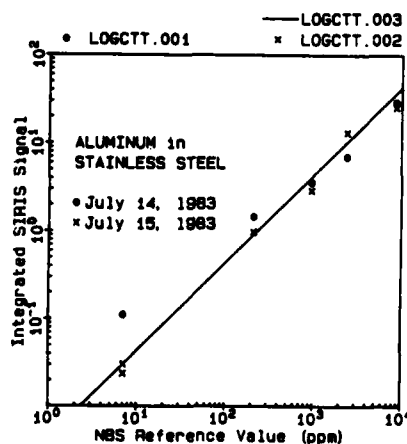


Figure 12. Comparison of SIRIS measurements of aluminum with NBS reference values

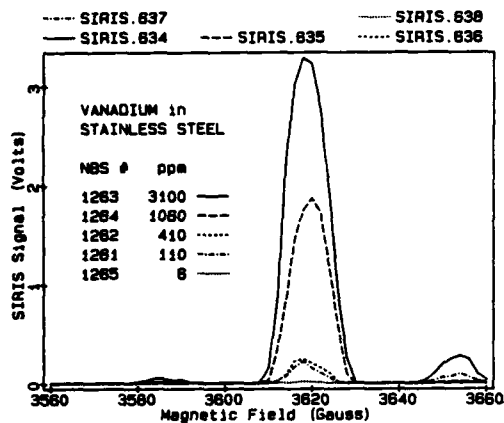


Figure 13. Composite of SIRIS spectra of vanadium in stainless steel

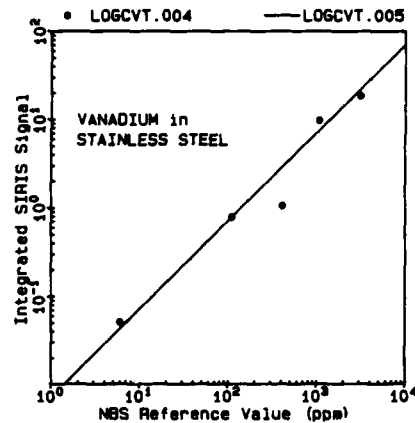


Figure 14. Comparison of SIRIS measurements of vanadium with NBS reference values

A set of indium doped silicon samples were obtained from Hughes Research Laboratories and measured with the SIRIS technique. The results of these measurements are shown in the composite graph in Figure 15. These samples were characterized by Hughes and their indium content had been determined to be 7.8, 4.1, 0.40, and 0.036 ppm. The SIRIS results were analyzed as the previously described samples and compared with the Hughes values. That comparison, shown in the correlation plot of Figure 16, shows good agreement, however, the uncertainty of the results of the 0.036 ppm sample are quite large since the signal was at the background noise level.

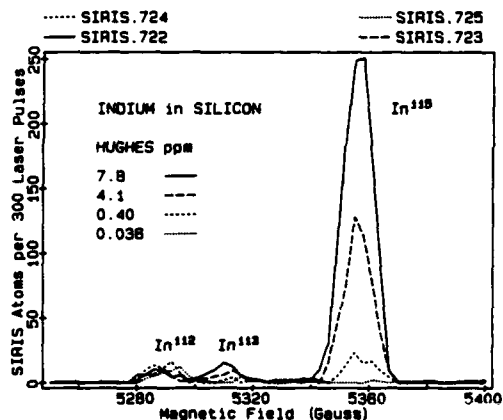


Figure 15. Composite SIRIS spectra of indium in silicon

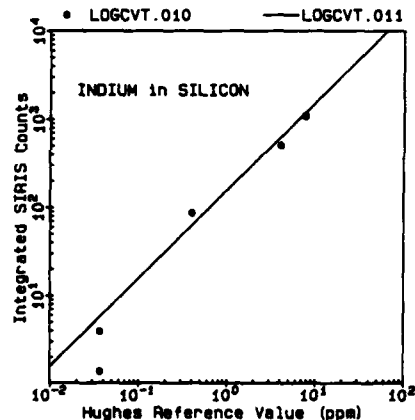


Figure 16. Comparison of SIRIS measurements with Hughes reference values

### Summary

The results presented here are the early results of the Sputter-initiated resonance ionization spectroscopy technique after having the SIRIS apparatus for approximately six months. Improvements in the ion optics of both the ion beam and mass analyzer sections of the apparatus are in progress. The desired sensitivity of 1 part in  $10^{10}$  for a five minute counting period (with statistical uncertainty of  $\pm 10\%$ ) should be reached in the near future.

The SIRIS apparatus can also be operated as a SIMS instrument and it is frequently convenient to do so. While it was not designed as a SIMS instrument and although its operators are not SIMS experts, it is obvious that the SIRIS technique has many advantages over the SIMS technique. The SIMS signal is observed to decrease while the SIRIS signal increases when the surface of a sample is cleaned by the sputtering process. The selectivity of the RIS process causes the spectra of the SIRIS measurements to be singularly representative of the element being measured while the SIMS spectra have multiple representations of other elements and molecules. The SIRIS spectra are free of other elements, isobars, and molecular species, both single and double charged species.

This new measurement technique, Sputter Initiated Resonance Ionization Spectroscopy (SIRIS), which is free of interferences and provides high sensitivity will revolutionize surface analysis and the material sciences.

#### Acknowledgements

The authors gratefully acknowledge discussions with, and preparation of samples by, O. J. Marsh and J. P. Baukus, Hughes Research Laboratories.

The partial support of this work by the Defense Advanced Research Projects Agency is gratefully acknowledged.

#### References

1. G. S. Hurst, M. G. Payne, M. H. Nayfeh, J. P. Judish, and E. B. Wagner, Phys. Rev. Lett. 35, (1975) 82.
2. G. S. Hurst, M. H. Nayfeh, and J. P. Young, Appl. Phys. Lett. 30, (1977) 229.
3. G. S. Hurst, M. G. Payne, S. D. Kramer, and J. P. Young, Rev. Mod. Phys. 51, (1979) 767.
4. G. S. Hurst, M. G. Payne, S. D. Kramer, and C. H. Chen, Phys. Today 33, (1980) 24.

ENCLOSURE 3

CONTRACT DATA REQUIREMENTS LIST  
INSTRUCTIONS FOR DISTRIBUTION  
ARPA/ONR

Minimum Distribution of Technical Reports

Addressee	DODAAD Code	<u>Number of Copies</u>	
		Unclassified/ Unlimited	Unclassified/ Limited and Classified
Director, Advanced Research Projects Agency 1400 Wilson Blvd. Arlington, VA 22209 Attn: Program Management	HX1241	2	2
Scientific Officer	N00014	3	
Administrative Contracting Officer	FY1767	1	1
Director, Naval Research Laboratory, Attn: Code 2627 Washington, D.C. 20375	N00173	6	1
Defense Technical Information Ctr. Bldg. 5, Cameron Sta. Alexandria, VA 22314	S47031	12	2
Office of Naval Research Western Regional Office 1030 E. Green Street Pasadena, CA 91106	N62887	1	1

CONTRACT NUMBER: N00014-81-C-0285